Morphological Development and Taxonomy of Cortical Neurons in Mouse Barrel Cortex: The Effect of Sensory Deprivation During the Critical Period

by

Chia-Chien Chen

Dissertation submitted to the Graduate Faculty in Psychology (Neuropsychology Subprogram) in partial fulfillment of the requirement for the degree of Doctor of Philosophy. The Graduate Center, City University of New York

2013

This manuscript has been read and accepted for the Graduate Faculty in Psychology (Neuropsychology Subprogram) in satisfaction of the dissertation requirement for the degree of Doctor of Philosophy

Joshua C. Brumberg, PhD

_____	_____
Date	Chair of Examining Committee

Maureen O'Connor, PhD

_____	_____
Date	Executive Officer

Members of the Supervisory Committee

Carolyn Pytte, PhD

Jonathan Levitt, PhD

George Huntley, PhD

Randy Bruno, PhD

The City University of New York

Abstract

Morphological Development and Taxonomy of Cortical Neurons in Mouse Barrel Cortex: The Effect of Sensory Deprivation During the Critical Period

by

Chia-Chien Chen

Advisor: Joshua C. Brumberg, PhD

Neurons are the basic processing units and the fundamental building blocks of the nervous system, and understanding neuronal morphology provides a necessary first step towards comprehending the composition of the cortical microcircuits that perform cognitive computations within the cerebral cortex. Utilizing a histological impregnation technique that labels neurons in their entirety, detailed morphologies of barrel cortical neurons were investigated and the effect of chronic sensory deprivation explored. This research produced a number of key findings: 1) neurons in layer VI of the barrel cortex, which receives inputs from the contralateral facial whiskers, are composed of six geometrically distinct and morphologically heterogeneous populations; 2) chronic sensory deprivation of whisker-related input spanning across early neonatal development can considerably influence neurons' geometric properties, with structural alterations observed in somatic, apical and basilar dendritic features in layer VI of barrel cortex; 3)

cortical response to disruption and restoration of sensation, as assessed by quantifying and categorizing dendritic protrusions, is cortex-layer specific and age-dependent, and a key protein regulating the content of extracellular matrix is upregulated following disruption of sensory experience. The main conclusions drawn from this research were that the composition within cerebral cortex is definable yet highly complex, and neurons respond to the ever-updating sensory environment by modifying their morphology and molecular content within the cerebral cortex. Characterizing neuronal elements provides a framework for better understanding of structure-function relationships within neocortical circuits in general, and how the sensory input provides the essential mechanisms for the appropriate development of cerebral cortex, an important prerequisite for proper perceptual functioning.

Key Words: Barrel Cortex, Neocortex Layer VI, Golgi Stain, Neuronal Morphology, Sensory Deprivation, Dendrites, Cortical Development, Dendritic Spines and Filopodia, Glutamatergic Transmission, Tissue-Type Plasminogen Activator, Extracellular Matrix

Words in Abstract: 254
Figures: 31
Tables: 6

Dedications and Acknowledgement

First and foremost, I would like to thank my grandparents, particularly my grandmother, who is afflicted with Parkinson's disease. The original motivating factor for me wanting to know more about the brain came from seeing her combating this debilitating disorder. It is from then I knew I wanted to gain more knowledge about the nervous system so I may better contribute to humankind regarding how consciousness and cognition work in general. This powerful desire led me to my wonderful advisor, Dr. Joshua Brumberg, who has been supportive and enthusiastic every single step of my academic journey. I feel extremely blessed and privileged to have worked alongside him, and the only feeling that I have is my absolute gratitude for him. Along this academic quest, I have also met some great people who made this journey a much more interesting and intellectually stimulating one. For that reason I would like to acknowledge my appreciation of them: Drs. Carolyn Pytte, Areti Tsiola, Raddy Ramos, Mary Rocco Donovan, & Qizong Yang. I am thankful for all of the scientific discussions as well as emotional support that they have freely offered me due to their generosity. Next, I am exceedingly grateful for my dissertation committee members (Drs. Joshua Brumberg, Carolyn Pytte, Jonathan Levitt, George Huntley, & Randy Bruno) who took their time from their busy schedules to be a part of my dissertation experience. I am also grateful for my undergraduate laboratory assistants who helped me in collecting the data necessary for the completion of this dissertation. Last, but also most importantly, I would like to offer my absolute appreciation and love to my family and friends who have been so understanding and supportive of the lengthy completion of my dissertation. It is because of all these people

mentioned here, that this academic (and also emotional) journey was satisfying and worthwhile.

From the bottom of my heart,

Chia-Chien Chen

This research is supported by two DSC grants to C-C Chen and NS75875 to JC Brumberg.

Table of Contents

List of Tables

List of Figures

Chapter One: Literature and Background Review

General Introduction

Neocortex, phylogenetically the newest region of the cerebral cortex, has been proposed to play key roles in the processing of sensation, perception, motor, attention, language, memory, and consciousness. Within this heterogeneity of functional compartmentalization, the primary sensory cortices (e.g., Primary Visual Cortex, Primary Somatosensory Cortex, & Primary Auditory Cortex) receive and manage environmental signals from peripheral receptors mediated through thalamic relay nuclei, and subsequently project this processed cortical information to "higher-order" association areas (Martin, 2003). In addition, these primary sensory cortices also originate the reciprocal connections with the thalamus (Tombol, 1986; Brumberg et al., 2003; Kumar & Ohana, 2008), which gate/filter the information that ultimately ascends to the cerebral cortex. These primary sensory cortices, therefore, serve as an important bridge between the external world and our internal perception.

Because of the crucial role that primary sensory cortices play in sensation and perception, normal functioning of these cortical areas is a prerequisite for neurocognitive processes. A myriad of scientific literature has shown that proper development of the sensory cortices is dependent on adequate/normal sensory experience (see Feldman & Brecht, 2005; Fox & Wong, 2007), in which significant changes in sensation (e.g., deprivation or enrichment) during certain developmental "critical periods" can cause alterations in anatomical arrangement and physiological properties of the neocortex. For

example, the classic studies of Hubel & Wiesel (Wiesel & Hubel, 1963; Hubel et al., 1977) have demonstrated that monocular deprivation by means of suturing one eye dramatically influences the topographical organization of the ocular dominance columns within the primary visual cortex. Similarly, other peripheral manipulations such as finger amputation (Merzenich et al., 1984) and dark rearing (Blakemore, 1975) can also affect many features of neocortical neuronal structure and function. Within the somatosensory cortex (S1) of rodents, it has been shown that ablating a whisker follicle at birth disrupts proper formation of the corresponding cortical barrel (Woolsey & Van Der Loos, 1973). These data highlight the paramount importance of peripheral input on the appropriate development of primary sensory cortices.

This portion of the dissertation will emphasize the role sensory activity has on cortical areal patterning and organization, along with the effects of sensory deprivation on development and processing of information by the sensory systems. We first review what is already known about the primary sensory cortical areas, specifically their basic anatomical and physiological features. Next, the development of the neocortex is briefly discussed. The main focus, however, is given to the mechanisms involved for activity-dependent plasticity during developmental critical periods. In particular, we discuss the neuronal substrates that are known to be involved in the process of triggering and expressing neuroplasticity.

1. Background: Fundamentals of Neocortical Organization

1.1. From environmental input to the cerebral cortex: flow of information.

The perceptual process starts from attended environmental stimuli which are transduced by peripheral receptors into electrical signals. These electrical signals carrying sensory information are subsequently transmitted to the brainstem and thalamus. Many thalamic nuclei are responsible for information processing of a specific sensory modality. For example, the lateral geniculate nucleus (LGN) and medial geniculate nucleus (MGN) are responsible for the thalamic relay and processing of vision and audition, respectively. Similarly, the lateral and medial portions of the ventral-posterior nucleus of the thalamus (VPL and VPM) are devoted to the processing of somatosensory information. VPL is responsible for processing tactile information from below the neck, while VPM, along with medial portion of the posterior thalamic nucleus (POm), are the thalamic nuclei designated to process facial somatosensory information (Diamond, 1992).

Each primary sensory cortex receives thalamocortical afferents (TCA) from its corresponding thalamic counterpart. After sensory information is registered and processed at the primary cortical areas, the signals are subsequently transmitted to the corresponding association cortical areas, where further cortical processing takes place. This means that the sensory information has gone "upstream" in a feed-forward manner. In the visual system, for example, sensory information after leaving V1 is processed by multiple visual association areas such as the secondary visual area (V2), visual area V4, middle temporal area (MT or V5), inferior temporal area (IT), fusiform face area (FFA),

mesial side of superior temporal lobe (MST), anterior intraparietal area (AIP), etc. (see Goldstein, 2005). Within S1 barrel cortex, the corticocortical feed-forward connections predominantly target three areas: primary motor cortex (M1), secondary somatosensory cortex (S2), and the contralateral barrel field (Chakrabarti & Alloway, 2006; Rocco & Brumberg, 2007; Ramos et al., 2008).

1.2. Laminar organization and function of the cerebral cortex

The mammalian neocortex itself is organized into six cytoarchitectural layers and several sub-layers, with each layer/sub-layer presumably subserving a specific role. In the primary sensory cortices, the granular layer (layer IV) and multiform layer (layer VI) of the sensory cortices are the main TCA recipient zones (see White, 1989; Davis & Sterling, 1979), while the multiform layer solely gives rise to the specific corticothalamic feedback (Tombol, 1986; Brumberg et al., 2003; Kumar & Ohana, 2008). In the barrel system, VPM nucleus projects to layers IV and VI, while the POm projects to layer V and the upper portion of the multiform layer (layer VI_a). By contrast, the pyramidal neurons of the supragranular (layers II/III) and infragranular (layer V & VI) layers originate the majority of cortico-cortical, corticotectal, corticopontine, and corticospinal efferent fibers (see Molyneaux et al., 2007; Killackey et al., 1989; Leergaard et al., 2004; Ramos et al., 2008). The molecular layer (layer I) is located directly underneath the pia mater, and its function has been poorly understood until recently. It was reported that the axons of the Martinotti cells make synapses with the apical dendrites of the pyramidal neurons from layer III and V in this most superficial layer of the cerebral cortex (Fanselow et al., 2008; Xu & Callaway, 2009) thereby modulating their activity.

1.3. Receptive field and columnar organization of the neocortex.

The receptive field (RF) of a sensory neuron refers to a regional space in the periphery that, when stimulated, alters the electrophysiological properties of the corresponding sensory neuron. These electrophysiological alterations may be excitatory or inhibitory. For example, a typical simple cell in V1 simultaneously exhibits on- and off-zones (Hubel & Wiesel, 1959). When a bar of light, oriented in a specific tilt, is positioned on the on-zone, this particular V1 simple cell's firing rate increased. By contrast, when the same bar of light is positioned on the off-zone, the same V1 simple cell's firing rate decreased (or ceased to fire altogether). Receptive field properties have been observed across sensory modalities (vision, audition, & somatic senses). In general, the receptive fields in the lower-order sensory neurons (e.g., retinal ganglion cells and mechanoreceptors in the dermis) are considerably smaller than upper-order sensory neurons (e.g., cortical neurons in V1 and S1). This change of RF size is primarily due to the massive synaptic convergence from the lower-order sensory neurons to their afferent higher-order counterparts (see Goldstein, 2007).

The receptive field properties in the somatosensory cortex were initially documented by Mountcastle (1957), who first demonstrated that the neocortex is organized in a columnar fashion. A cortical column refers to a group of neurons, which when penetrated in succession by a recording electrode perpendicular to the cortical plate, display nearly identical receptive field and stimuli predilection across multiple laminae. Hubel and Wiesel followed Mountcastle's discovery by investigating the functional

modularity in V1, and found that the primary visual cortex is also organized into narrow columns of cells, with two main distinct features: *ocular dominance* and *orientation-selective* columns (Hubel & Wiesel, 1972; Hubel, Wiesel, & Stryker, 1978), which lead to the proposal of the famous iceberg cortical organization in V1. Similar functional organization was observed in the primary auditory cortex, where cortical columns share similar characteristic frequencies and are organized in isofrequency bands (Tunturi, 1950, Merzenich et al., 1975), and summation (binaural) / suppression (monaural) interaction blocks (Imig & Adrian, 1977, Middlebrooks et al., 1980). In the barrel cortical field, functional columnarity in the representation of the rodent mystacial vibrissae is clearly observed (Kossut et al., 1988), where two main types of columns exist: barrel columns, which receive strong and direct input from the VPM nucleus of the thalamus, , and septal columns, which receive direct input from POm nucleus of the thalamus, and indirect input from VPM nucleus of the thalamus (Lu & Lin, 1992; Brumberg et al., 1999).

1.4. Functional mapping of the cerebral cortex

Primary sensory cortices are arranged in a topographic fashion. In primates, the somatosensory cortical regions are organized into four distinct yet intercorrelated areas: 3a, 3b, 1, & 2 (Kaas et al., 1979). Each area is somatotopically arranged similarly to the location of the skin, and is often referred to as the homunculus. However, the distribution of the neuronal density does not necessarily reflect spatial topography in a proportional manner, due to the cortical magnification factor. The cortical areal representations of lips and the index fingers, for examples, are substantially exaggerated due to their significantly more important roles in tactile perception. These tactile areas, in need of

high spatial resolution, require higher density of cortical neurons. In rodents, the barrel cortex in S1 precisely represents the spatial organizations of the mystacial vibrissae, and, since rodents use their whiskers to actively explore their environment, the cortical magnification phenomenon is also observed in the barrel cortex. Interestingly, increased usage of whiskers (i.e., enrichment of sensory environment) leads to refinement of RFs in the barrel cortex, which correlates with enhanced sensitivity and tactile recognition ability in the somatosensory system. By contrast, decreased usage of whiskers (e.g., sensory deprivation via whisker trimming) has the opposite effect and leads to the broadening of RFs in the barrel field (see Feldman and Brecht, 2005).

1.5. Classification of neurons in the cerebral cortex

Due to the complexity of the microcircuitry in the neocortex, classification of cortical neurons has been a field of ongoing research for decades. Ever since Cajal and Lorente de No's era, neuroscientists have been attempting to taxonomize cortical neurons using a variety of approaches. Morphologically, neurons can be separated into two main categories: pyramidal and non-pyramidal neurons. Pyramidal neurons exhibit triangular somata, along with apical dendrites that typically project towards the pial surface. Non-pyramidal neurons, in contrast, lack apical dendritic features (see White, 1989). A variety of subclasses of non-pyramidal neurons include basket cells (Somogyi et al., 1983), Chandelier cells (Lewis & Lund, 1990), double bouquet cells (Somogyi & Cowey, 1981), Martinotti cells (Fanselow et al., 2008; Xu & Callaway, 2009), neurogliaform (Ferrer et al., 1986), and spiny stellate cells (Jones, 1973). Interestingly, morphological heterogeneity of cortical neurons can be found even within a single cortical lamina

(Tsiola et al., 2003; Chen et al., 2009). Functionally, pyramidal and spiny stellate cells are the excitatory glutamatergic regular-spiking units (RSUs) in the neocortex (Simons 1978; McCormick et al., 1985). By contrast, the basket, Chandelier, double bouquet, Martinotti cells are inhibitory GABAergic neurons. Histochemically, neocortical neurons exhibit a wide range of protein expression, including parvalbumin, somatostatin, 5HT-3a, Neuropeptide Y (NPY), vasoactive intestinal polypeptide (VIP), cholecystokinin (CCK), calretinin, and calbindinD28K (Cauli et al., 1997; Lee et al., 2011; also see Hof et al., 2008).

Recent research has attempted to use a combinational approach to classify neurons (Cauli et al., 1997; Lee et al., 2011, Karagiannis et al., 2009), but due to the complexity and diversity of the cortical neuronal population, a lot has yet to be elucidated. However, it has been documented that although the majority of the non-pyramidal neurons are inhibitory and GABAergic, not all non-pyramidal neurons are fast-spiking units (FSU). Similarly, not all pyramidal neurons are RSUs, as some exhibit high-frequency rhythmic bursting (chattering) spiking patterns that are associated with intrinsic gamma-oscillations during suprathreshold activations (Brumberg et al., 2000; Cardin et al., 2005). In addition, it was found that calretinin-positive cells, despite their non-pyramidal morphological features, do not have fast-spiking firing rates (Cauli et al., 1997). Most of the basket, double-bouquet (which are calbindin^{+}), and Chandelier cells are parvalbumin-positive (see Hof et al., 2008). Last, a recent discovery suggested that the non-pyramidal neurons which exhibit spiking adaptations are strongly associated with NPY, somatostatin, and/or VIP (Karagiannis et al., 2009). Despite the plethora of information regarding specific cortical interneurons, it remains elusive how these

different phenotypes of neurons respond to sensory input and what their exact roles are in the cerebral cortex.

2. Development of the Neocortex

2.1. Corticogenesis & neuronal migration

Cell proliferation starts as the neural tube undergoes rapid mitosis. Here, the cleavage plane is critical: for the progenitor cells that are cleaved vertically during mitosis, their daughter cells will undergo repetitive cell proliferation, while the daughter cells produced from horizontal cleavage are unlikely to divide again. Two transcription factors, *Notch-1* and *Numb*, are in part responsible for differentiating the two types of cleavage planes. Vertical cleavage is associated with symmetrical partitioning of *Notch-1* and *Numb*, and horizontal cleavage is associated with nonsymmetrical partitioning of these two key transcription factors (Zhong et al., 1996; Soleck et al., 2001; also see Verdi et al., 2002). Interestingly, when *Notch-1* is not inhibited by *Numb* (in the case of horizontal cleavage), it activates the cellular blueprint to cease neuronal proliferation, and directs the cells to migrate outside of the ventricular zone.

In the early stage of cortical development, the telencephalic vesicle has two zones: the ventricular zone (VZ, facing the inner lining of the neural tube) and the preplate (PP). The ventricular zone contains the progenitors which will eventually differentiate into neurons and glia. The preplate separates into the marginal zone (MZ) and the subplate (SP), with the cortico plate (CP) sandwiched in the middle. The Cajal-Retzius cells in the

marginal zone express the extracellular matrix glycoprotein *reelin*, which is important for the guidance of radial migration of cells (Rice and Curran, 2001). The primitive neurons (neuroblasts) migrate away from ventricular border toward the external border of the thickening neural tube vesicle (telencephalon). This is accomplished by following and climbing the fibers derived from specialized radial glial cells (see O'Leary and Nakagawa, 2002). The very first cells to move in will become part of the subplate, as the subsequent cells to cross the subplate will become the deepest and the most superficial layers of the neocortex, layer VI_b & 1, while the other layers of the neocortex grows within, as evidenced by the presence of Martinotti cells that can be only found in deepest part of the multiform layer as well as the molecular layer of the neocortex. This process of starting from the deepest layer and filling in all other neocortical layers in between is sometimes referred as inside-out development (see Casanova and Trippe, 2006). Interestingly, the *reeler* mice that do not express *reelin*, the opposite cortical arrangement (i.e., outside-in) is observed (Caviness, 1982).

While the glutamatergic projection neurons are born from the VZ directly underneath the cortical plate, the surprising finding is that most GABAergic interneurons are born near the lateral and medial ganglionic eminences away from the cortical VZ, and later migrate tangentially into their final destinations within the cortical plate (Zhu et al., 1999; Marin & Rubenstein, 2002). These extracortical tangential migrating routes of the GABAergic neurons are in part mediated by the guidance molecules from the *Slit* and *Semaphorin* families (Marin et al., 2001). Marin and colleagues demonstrated that the semaphorin receptor *neuropilin* is responsible for the cellular fate of these interneurons.

The neuropilin negative neurons enter the striatum, while the neuropilin positive neurons are guided by the semaphorins to enter the neocortex.

2.2. Patterning of the cortex

2.2.1 Molecular regulation of cortical regionalization

Cortex (pallium) develops from a morphologically uniform ventricular zone located in the dorso-caudal part of the telencephalic vesicles, with the dorsal pallium eventually differentiating into the neocortex. Functional differentiation of the pallium is directed in part by focal signaling centers that secrete a variety of molecules. These signaling centers are located along the edges and midline of the neural plate and (later) at the midline of the telencephalic vesicles (see Sur and Rubenstein, 2005). There are several key regional centers that orchestrate the areal patterning events of the cerebral cortex in this early stage of development, each with its specific protein expression: Sonic hedgehog (Shh), fibroblast growth factor-8 (FGF8), WNTs, and bone morphogenic proteins (BMPs) (see O'Leary and Nakagawa, 2002). A number of transcription factors such as *Emx2* and *Pax6* are induced by these regional centers, with their expression levels varying in a gradient fashion based on the anatomical positioning of the cortex. Specifically, *Emx2* is expressed more strongly in the caudal pole of the cerebral cortex and less in the rostral pole. By contrast, *Pax6* is expressed more strongly in the rostral pole and less in the caudal pole. Using a combinational approach consisting of genetic

expression analyses and areal targeting of TCA projections, it was demonstrated that *Emx2*$^{-/-}$ mice exhibited exaggerated and augmented S1 area, while *Pax6*$^{-/-}$ mice exhibited exaggerated and augmented V1 area (Bishop et al., 2000; Mallamaci et al., 2000). These findings implicate that both *Emx2* and *Pax6* are expressed in graded yet opposite fashion, and their expressions are responsible for the conferment of areal patterning, cortical size, and regionalization of cortical identity.

2.2.2. Areal patterning of the barrel cortex

Ever since its characterization by Woolsey and Van Der Loos (1970), the barrel cortex has been widely used as a model for the investigation of cortical areal patterning. The barrels, specifically, are clusters of layer IV neurons that topographically represent the distribution of vibrissae on the rodent mystacial pad. These topographic patterns are also observed in the brainstem trigeminal nucleus principalis (i.e., *barrelettes*) and the VPM nucleus of the thalamus (i.e., *barreloids*). The barrel's cortical differentiation and arealization seem to be dictated by the activity of thalamic afferent fibers. It has been suggested that in rats by embryonic day (E)17, the thalamocortical fibers have begun their radial growth into cortex and their arbors span the cell-sparse zone between layer VI_b and the bottom of the cortical plate (Catalano et al., 1991). Schlaggar and O'Leary (1991) replaced the parietal lobe (S1 barrel region) with a piece of striate cortex (V1) in the S1 area and found that thalamic connection took on and formed the striate cortical matter into barrels, the hallmark of rodent somatosensory cortex. This suggests that thalamic afferents are important for specifying the pattern of cortical areas, and that

barrel cortex formation is relatively resistant to genetic pre-programming in the cortical plate. It is postulated that the areal-specific thalamic axons initially innervate the subplate cells, and when the overlying cortical plate is mature, the thalamic fibers invade the cortical plate and execute the blueprint of the neocortical cytoarchitecture.

It has been demonstrated that peripheral manipulation of the whisker follicles in the very early postnatal stage (i.e., before PND4) can greatly influence barrel formation (Van Der Loos and Woolsey, 1973). Following this seminal finding, neuroscientists have been seeking a variety of neurochemical underpinnings that may be responsible for barrel cortex patterning. Due to the glutamatergic nature of the TCA, studies have looked at the roles of glutamatergic transmission and its effect on barrel formation. For example, it was found that blocking all glutamatergic receptors post-synaptically by means of pharmacological manipulations significantly disrupts the topographic refinement and functional representations of individual whiskers in the barrel cortex (Fox et al., 1996). It was also found that through the utilization of transgenic mice, cortex-specific deletion of the NR1 subunit of the NMDA receptors prevents the barrel cortex forming into clearly defined clusters (Iwasato et al., 2000). Similarly, mice that lack mGluR5 or its associated downstream GPCR cascade components PKARIIβ5 or PLC-β15 also exhibit the absence of or a delay in barrel formation in S1 (Hannan et al., 2001; Inan et al., 2006, She et al., 2009., Ballester-Rosado et al., 2010). These data implicate the importance of glutamatergic TCA transmission in the activation of the postsynaptic cortical blueprint, which eventually results in the formation of barrel clusters in layer IV.

2.3. Development of dendritic processes

2.3.1. Dendritogenesis

Recent evidence has strongly suggested that dendritogenesis is regulated by extracellular signals. For example, growth of the apical dendrite in pyramidal neurons seems to be regulated by the molecular guidance cue Semaphorin 3A (Polleux and Gosh, 2000). In particular, Semaphorin 3A is abundant in the marginal zone and acts as chemorepellent for axons and as chemoattractant for apical dendrites, even in the case of grafted neuroblasts from other donor brain regions. Furthermore, soluble guanylate cyclase (SGC) and one of its subsequently affected molecule, cGMP-dependent protein kinase (PKG), both assist Semaphorin 3A in the choreography of the orchestrated event of attracting apical dendrites (Polleux and Gosh, 2000).

In addition to guidance molecules, neurotrophins also act as extracellular signals which can significantly influence dendritic development. The effects of a variety of neurotrophic factors on dendritic fanning formation have been intensively studied over the past several years. It has been documented that by transfecting cortical neurons with growth factors such as Neural Growth Factor (NGF), Brain-Derived Neurotrophic Factor (BDNF), neurotrophin-3 and 4 (NT3 and 4), the treated neurons gain significantly more proximal dendrites than their untreated counterparts (McAllister et al., 1995, 1996). Interestingly, these dendrites also seem to have laminar-specific predilections to the growth effects of these neurotrophins. For instance, layer II/III pyramidal neurons showed dramatic basilar dendritic growth in response to NT3 (Niblock et al., 2000).

Similarly, layer IV pyramidal neurons respond more favorably to BDNF, whereas layer V/VI pyramidal neurons showed more dendritic growth by responding more favorably to NT4 (McAllister et al., 1995). This suggests that it is possible the dendrites respond in different manners depending on the location of the cortical lamina. Other non-conventional neurotrophic factors such as insulin-like growth factors (IGFs) and osteogeneic proteins (OP-1s) have also been shown to impact dendritic fanning pattern of cortical neurons (Le Roux et al., 1999; Niblock et al., 2000).

Out of all the subfields that investigate dendritic growth/patterning, none can compare to the rich literature and the intense efforts that neuroscientists have invested in understanding the phenomenon of experience (or activity)-dependent plasticity and the role of glutamatergic inputs on dendritic development. As early as 1973, Volkmar & Greenough showed that environmental enrichment leads to a considerable increase in the dendritic length, resulting in more elaborate dendritic fanning patterns of the spiny stellate neurons in layer IV of the primary visual cortex. In the barrel system, it has been well documented that within layer IV the spiny stellate neurons have a strong affinity with lemniscal thalamocortical afferent (TCA) inputs by polarizing their dendrites towards the center of barrels where the TCAs ramify (see Fox and Wong, 2005) while avoiding the TCA sparse septa. This particular dendritic fanning pattern is believed to be mediated by the activity of NMDA receptors, as cortex-specific NR1 subunit knockout mice showed very little bias in their dendritic fanning pattern (Datwani et al., 2002). In addition to the NMDA receptor's role in determining this directionally-oriented dendritic morphogenesis of spiny stellate cells, it has been recently documented that mGluR5, a subclass of metabotropic glutamatergic receptors, also play a significant role. It was

demonstrated that in both global and cortex-specific mGluR5 knockout animals, there were significantly decreased percentages of polarized spiny stellate cells in the layer IV of barrel cortex (She et al., 2009; Ballester-Rosado et al., 2010). Surprisingly, even though mGluR5 is thought to play important roles in the polarization of spiny stellate cells, it does not, however, influence the overall length of dendrites (Wijetunge et al., 2008). Taken together, the data suggest that polarization and growth of dendrites are two distinct processes in the cerebral cortex.

Regardless of the rich literature that exists in this area of research, the idea and the findings of activity-dependent regulation of dendritic arborization remain controversial, and is an ongoing topic of debate amongst developmental neuroscientists. For instance, one group of studies suggests that blocking synaptic transmission and/or depriving sensation during development leads to decreased dendritic fanning (Wiesel and Hubel, 1963; Lund et al., 1991, Kalb, 1994). Others have shown the exact opposite effect, that blocking/knocking out NMDA receptors leads to a more exuberant dendritic fanning pattern (Rocha and Sur, 1995; McAllister, 1996; Datwani et al., 2002). Evidence from other anatomical areas such as LGN (Dalva et al., 1994) and hippocampus (Kossel et al., 1997) do not provide any further consensus, as these studies showed that sensory activity and/or manipulation of glutamatergic receptor activities do not significantly impact dendritic arborization patterning. It is most likely that these inconsistencies of findings may be influenced by the bipolar plasticity-inducing properties of NMDA receptors, as activation of NMDA receptors can induce either long term potentiation (LTP) or long term depression (LTD), depending on the frequency of the excitation and the amount of calcium-ion influx into the postsynaptic dendrite. Since scientists do not use the same

means of manipulating sensory activity or standardize the methodology of blocking synaptic transmission, the level of NMDA receptor activation may be highly discrepant between studies, hence inconsistent findings result. Recently it has been demonstrated that apical dendritic features and basilar dendritic features respond in an opposite manner to chronic sensory deprivation (Chen et al., 2011). Moreover, such manipulation did not impact the overall (apical + basilar) dendritic features, suggesting that the dendrites of cortical neurons have a tendency to retain morphological homeostasis.

2.3.2. Spinogenesis

Dendritic spines, tiny protrusions extending from the dendritic shafts, have long been thought to be the morphological markers for structural indicators of learning and memory. In general, dendritic spines form shortly after the genesis of their parent dendritic shaft. Since the majority of the excitatory presynaptic inputs are made onto the heads of the dendritic spines (see Bhatt et al., 2009), spines serve as a means for the dendrites to compartmentalize an array of biochemical substrates (for details, see Sala et al. 2008). In addition, similar to growth cones, dendritic spines are highly dynamic structures, able to retract or extend their cytoskeletons within hours following changes in their cellular environment (Oray et al., 2004). Therefore, dendritic spines provide the anatomical evidence that rewiring of the cortical circuitry exists as a function of alterations in the cellular environment and accompanied changes in cellular structure, which is usually induced by natural developmental maturation and/or perturbations in the incoming sensory activity.

Density of dendritic spines varies as a function of developmental age. For example, it has been shown that in the visual system, shortly after eye opening, spine density in the binocular zone of V1 increases dramatically, coinciding with increased peripheral activity, and later reaches stabilization in density (Mataga et al., 2004). Furthermore, spines also change their morphological features by rearranging the polymerization patterns of their cytoskeletal proteins (i.e., F-actin and in some cases, tubulin). Traditionally, dendritic protrusions have been morphologically classified into five broad categories: branched, filopodia, stubby, thin (lollipops), and mushrooms (Fiala & Harris, 2000). Typically, small stubby (sessile spines) are more frequently observed in young, developing animals than mushrooms. By contrast, mushroom-spines are more frequently seen in mature, adult animals (Miller and Peters, 1981). Filopodia, on the other hand, are thought to be the potential precursors of thin spines; it is known that many, if not most, filopodia do not have a presynaptic bouton partners (Arellano et al., 2007). Currently, filopodia are viewed as the potential "probes" for the cellular environment, and are actively seeking for presynaptic axonal partner(s) (see Bhatt et al., 2009). This notion has been supported by recent findings which suggested that out of all the morphological types of spines, filopodia have the highest probability of not partnering with a presynaptic axonal bouton (Fiala et al., 1998; Arellano et al., 2007). For the filopodia that were successful at attracting a presynaptic axonal terminal, the end result is the formation of either a thin or mushroom spine. At the same time, the motility of these thin or mushroom spines is greatly decreased. In the case that a filopodium fails to connect with a presynaptic bouton, the lack of the proper presynaptic input would make the filopodium retract back into the parent dendritic shaft.

Once a dendritic spine is paired with its presynaptic axonal partner, one crucial step happens: the sealing of the bond by cell-adhesion molecules (CAM) and the condensation of the extracellular matrix (ECM) (see Sala et al., 2008, and Feldman, 2009). This results in the increased stabilization of dendritic spines. In support of this view, administration of the recombinant form of tissue plasminogen activator (tPA), a serine protease which cleaves the CAM bond, re-induces spine motility in adult rodents (Oray et al., 2004; Mataga et al., 2004). Interestingly, tPA protein level is greatly expressed during the critical period shortly after eye-opening in the visual system, and diminishes in adulthood (Zheng et al., 2008). The protein expression profile of tPA and the level of dendritic spine motility, therefore, coincides with one another and the current view is that tPA provides the permissive means for dendritic spines to be dynamic by removing the bond between the presynaptic bouton and the postsynaptic dendritic spine head. Similarly to the effect of tPA, the degradation of extracellular matrix by administrating chondroitin sulfate proteoglycans (CSPGs) was able to re-activate synaptic plasticity in adults, which was observed by increased level of dendritic spine motility and density (see Feldman, 2009). So far, the roles of tPA, CSPGs, and their extracellular matrix proteins and how they work together to affect dendritic spine dynamics have not been explored in other non-visual sensory modalities, and therefore may be particularly rewarding if their developmental profiles and the activity-dependent phenomenon are revealed.

2.3.3. Dendritic spine pruning and stabilization

Following the developmental peak of synaptogenesis and dendritic spine formation, dendritic spine pruning occurs. In primates, the peak of dendritic spine formation is approximately 3½ months of age, and is observed across functional hierarchies (i.e., prefrontal, visual association area, and V1) (Elston et al., 2009). Even though the timescales of synaptogenesis and spinogenesis coincide across functional hierarchies, the timing of dendritic spine pruning differs. It was found that, out of the three cortical areas investigated, spine pruning occurs first in V1 (by 28 months of age), followed by the visual association area. The prefrontal lobe, presumably the highest order in terms of cognitive hierarchy, finishes dendritic spine pruning last and does not reach stable level of dendritic spine density until 4½ years of age in monkeys (Elston et al., 2009). Since synapse and dendritic spine elimination are hallmarks of the maturation and reorganization of cortical areas (Pan and Gan, 2008), Elston et al.'s (2009) important findings support the notion that proper development of sensory cortex serves as a prerequisite for other higher order of neurocognitive functioning.

Recently with the advancement in microscopy imaging techniques, specifically with the innovative development of the two-photon microscopy and GFP/YFP (green/yellow fluorescence protein) transgenic mice, it was possible to visualize and inspect the event of dendritic spine formation and pruning *in vivo* for the first time. In rodents, it was found that there was 23% spine elimination in P30 animals (observed for one month from birth) and only 5% spine elimination when animals were P120 (observed for one month from P90) in the layer 5 apical pyramidal neurons located in the barrel cortex. The rate of dendritic spine formation, however, did not show a difference between the two sampled time periods (P30 vs. P120) (Zuo et al., 2005). Another study

showed similar results in V1, A1, and S1 (Majewska et al., 2006). These findings are consistent with prior studies in brain tissues observed *in vitro* and in fix (for more, see Pan and Gan, 2008), suggesting that the dynamics of synaptic/dendritic spine reorganization based on developmental age is a fundamental process for the maturation of cerebral functioning.

Despite the highly dynamic nature of dendritic spine motility during early developmental stages, the majority of dendritic spines seemed to be stable in adulthood. In fact, a study suggested that the rate of spine turnover (formation/elimination) in mice is approximately 5% per month, and a projected 74% of total dendritic spines are stable and maintained throughout the lifespan of the animal (Zuo et al., 2005). However, two other studies (Trachtenberg et al., 2002; Holtmaat, 2005) yielded very different conclusions, demonstrating that the rate of spine turnover can be as high as a projected 40% per week, thus suggesting that even in adulthood, dendritic spines are still highly motile. The disparity of results may be attributed to the choices of the cranial imaging window (Xu et al., 2007). It was demonstrated that the rate of dendritic spine turnover in adult animals is very stable with minimally invasive preparations (i.e., thinned skull). By contrast, the rate of spine turnover in adult animals is very high with an open-skull preparation. This "inflated" occurrence of spine turnover is mediated by increased microglial and astrocytic activities, which are similar to the mechanisms of injury-induced plasticity. Consistent with this view, the rate of spine turnover is substantially reduced following a one-month waiting period after the open-skull surgery, correlating with subsided GFAP (Glial fibrillary acidic protein) expression (Xu et al., 2007). This important finding indicated that there is a dramatic decline of spine turnover in adulthood

from prior developmental stages, and that dendritic spines are most likely very stable across the lifespan. It also suggests that when studying dendritic spine motility *in vivo*, it is more ideal to use a minimally invasive procedure such as thinning the skull, instead of opting for an opening skull surgery.

2.3.4. Effect of sensory deprivation on the dynamics of dendritic spine remodeling

Due to their highly dynamic nature, dendritic spines have been long thought to play important roles in learning and memory. Since one of the fundamental properties of the cerebral cortex is its ability to accommodate and adjust to its surrounding cellular environment, the topic of whether sensory activity induces dendritic spine remodeling is of great interest to developmental neuroscientists. Recently conducted studies have demonstrated that sensory deprivation, regardless of being chronic or acute, profoundly impacts the activity of dendritic spines. For instance, it was found that long-term sensory deprivation via whisker trimming from P0 to P30 dramatically reduced spine elimination, but not spine formation (Zuo et al., 2005). This effect is most likely mediated through the decreased activity of NMDA-receptors, as chronically blocking NMDAR via MK801 injection yielded similar outcomes. In adult mice, the extent of sensory deprivation is not as dramatic as seen in juvenile mice, as suggested by a decreased rate of dendritic spine turnover. Other studies, using a more complex paradigm of sensory deprivation (i.e. checkerboard trimming), reached similar findings that the rate of spine turnover is accelerated (Trachtenberg, 2002; Holtmaat, 2006) following prolonged sensory deprivation compared with control adult animals.

Similar to the findings following long-term sensory deprivation, studies have shown that acute (i.e., 2 days) sensory deprivation also influences dendritic spine activities. It has been demonstrated in V1 that monocular deprivation increases spine motility and decreases spine density (Oray et al., 2004; Mataga et al., 2004). It is postulated that this enhanced spine motility is due to the loosening of cell adhesion molecule bonding because of tPA cleaving, as detailed above (see section 2.3.2). Moreover, the effect of acute sensory deprivation on spine motility and density is lamina-specific, in which layer IV seemed to be more robustly resistant to changes in sensory activity than the infragranular layers. Interestingly, this finding matches with the discrepancy of tPA expression levels (Oray et al., 2004). Currently, no studies have been conducted on the effect of chronic sensory deprivation and the role of tPA expression on developing dendritic spines in primary sensory areas, and therefore may be particularly rewarding if the knowledge of these relationships and pathways are elucidated.

2.3.5. Molecular control of dendritic spine plasticity and clinical implications of the abnormal features of dendritic spines

Several key molecular mechanisms have been identified that influence dendritic spine development. For example, the role of the glutamatergic receptor family and molecular structures associated with its pathways has been intensely studied over the past several years. It was found that blocking the NMDAR increases dendritic spine density *in vivo* and *in vitro* (Rocha and Sur, 1995, Datwani et al., 2002; Zuo et al., 2005). This pathway is most likely affecting the intracellular small signaling molecules such as

calcium ions and ras proteins, which have been demonstrated to play important roles in programming and executing dendritic spine remodeling *in vitro* (Araya et al., 2006; Harvey et al., 2008). Furthermore, it has been suggested that two key proteins, *spinophilin* and *drebrin*, also play crucial roles in the remodeling of dendritic spine morphology by influencing the activity of F-actin, an important cytoskeletal protein (see Sala et al., 2008). The current view is that spinophilin plays an essential role in the formation of spine heads, while drebrin regulates the length of spine necks (Takahashi et al., 2003). Other neurochemical substrates such as gonadal and stress hormones can also greatly impact the density and morphology of dendritic spines (Woolley et al., 1990; Hao et al., 2006; Radley et al., 2008). Interestingly, although the phenomenon of hormonal regulations of dendritic spines is observed in the dorsolateral prefrontal cortex, the hormones do not seem to have a significant effect on spine activity in the primary sensory cortices (Tang et al., 2006), suggesting that the molecular trigger of spine plasticity in the prefrontal lobe is quite different from the primary sensory areas. Regardless of the difference in triggering mechanisms, loss of dendritic spines (due to stress/age) in the prefrontal lobe is associated with decline of cognition, which further validates the importance of normal dendritic spine functioning.

Since normal dendritic spine development is a prerequisite for the proper maturation of the nervous system, abnormal dendritic features are inevitability associated with the neuropathological signs of poor cognitive functioning. Indeed, as first described by Dominic Purpura (1974), the postmortem brain samples of patients with low cognitive profiles (i.e., extremely low intelligence quotients; mental retardation) displayed highly abnormal morphology of dendritic spines. These patient's cortical neurons exhibited

dendritic spines with unusually thin necks with noticeably lower frequencies of spine heads. A key to understanding the pathoetiology of mental retardation was the identification of *Fmr1*, in which mice lacking this particular protein showed very little learning, as well as abnormal dendritic spine morphological features similar to those of human patients diagnosed with Fragile X mental retardation (see Bear et al., 2004). Specifically, the cortical neurons of mice lacking *Fmr1* displayed significantly more numerous yet immature dendritic spines (Comery et al., 1997; Irwin, 2002), which are presumably non-functional. It is now known that the specimens in the Purpura (1974) study were likely from patients afflicted with Fragile X (at the time of the discovery the disorder was not classified) and had spine abnormalities extremely similar to the *Fmr1* knockout mice (Irwin et al., 2000). It has been proposed that *Fmr1* plays the important role of pruning and/or shortening the length of dendritic spines, which mediates the maturation process of spine development (Huber et al., 2002, also see Bear et al., 2004). These data highlight the paramount importance of normal dendritic spine functioning as a promoter of normal cognitive abilities, and the close association between abnormal spine morphology/density and loss of cognition.

Chapter Two: Research Plan & Methods:

Aim 1: Characterize somatic and dendritic geometry of layer VI cortical neurons in the mouse barrel cortex. *Prediction:* Employing a combination of unbiased statistical methods consisting of principal component analysis (PCA) and Ward's method, layer VI cortical neurons can be taxonomized into distinct functional classes based on their morphometric properties.

Adult CD1 mice of either sex were sacrificed and their brain tissues treated according to our Golgi-staining protocol, which labels the cortical neurons in their entirety. Neurons were digitally reconstructed in 3D, with their morphological parameters recorded, and followed by principal component analysis that extracts the variables that accounted for the most variability within the data matrix. Using the extracted principal components as the main splitting factor, we aim to use the Ward's Method in combination with Euclidean Distance to taxonomize the cortical neurons into distinct morphological classes. In order to provide additional support for our clustering algorithm, several post-clustering confirmatory methods were conducted, including laminar location of the reconstructed cortical neurons, Sholl analyses, and dendritic fanning polarity. Characterizing neuronal elements using unbiased quantitative techniques provides a framework for better understanding structure-function relationships within neocortical circuits in general.

Aim 2: Characterize the morphological profile of layer VI neurons by investigating the geometric properties of cellular somata and dendrites, and elucidate the effect of

sensory deprivation on somatic and dendritic morphometric development.

Hypothesis: **Chronic sensory deprivation from birth significantly influences the morphological development of layer VI cortical neurons, thereby causing a considerable morphological reorganization of dendritic features.**

Juvenile CD1 mice (P30) of either sex were separated into two groups: control (normal sensory experience with untrimmed whiskers) and sensory-deprived (bilaterally trimming the whiskers every other day from P1 to P30). The brain tissues from both groups were treated with our Golgi-staining protocol and their barrel cortical neurons in layer VI are digitally reconstructed in 3D using Neurolucida (MicroBrightField, Inc). We investigated the somatic and dendritic properties in a variety of geometric parameters. This is in an attempt to elucidate the effect that chronic sensory deprivation immediately following birth has on the morphological development of layer VI barrel cortical neurons.

Aim 3: Investigate the maturation profile of dendritic protrusions (density and morphology) in barrel cortex neurons, and elucidate the effect of chronic sensory deprivation on spine development in the thalamocortical recipient zones (layers IV and VI). ***Hypothesis:*** **The density and morphology of dendritic protrusions vary as a function of developmental age (as a sign of cortical maturation), and chronically reducing the activity of cortical neurons following birth during the critical period significantly disrupts the normal developmental profile of dendritic spine features.**

CD1 mice of either sex were divided into three groups: control (untrimmed), sensory-deprived, and injected (mice that were treated with MK801, a drug that blocks NMDA glutamate receptors). By analyzing five developmental time points (P(post natal day)15, P30, P60, P100, P130) and their treated counterparts (trimmed or injected with MK801) using the Golgi impregnation method, we were able to visualize, reconstruct, and quantitatively record observable dendritic protrusions using the computer assisted anatomical reconstruction program Neurolucida. We characterized the dendritic spines and filopodia of approximately 15 pyramidal neurons at each developmental and sensory-deprived stage, and statistically compare their dendritic protrusion density and morphological characteristics. In order to clarify the cellular mechanisms responsible for the alterations in dendritic protrusion density/morphology, we also focused on the expression of tissue-type plasminogen activator (tPA), a key protein that plays a role in enabling the cellular environment for morphological remodeling. We aim to understand the role that sensory input plays in determining synaptic connectivity, which underlies the abilities of an animal to perform neurocognitive computations.

Chapter Three: Introduction:

Taxonomizing Layer VI Neurons in Mouse Barrel Cortex Based on Morphological Characteristics Using a Quantitative Approach

The neocortex is composed of six distinct layers, with each layer containing different morphological phenotypes that presumably subserve different processing roles (Mountcastle, 1997). For example, the excitatory spiny stellate cells and small pyramidal neurons in layer IV receive strong thalamocortical input (see White, 1989; Davis & Sterling, 1979). By contrast, the excitatory neurons of the infragranular layers (V and VI) are composed predominantly of larger pyramidal cells (Jones, 1984; White, 1989; Rocco & Brumberg, 2007). While layer IV is the principal input layer, layers V and VI originate most of the cortical output (Jones 1984, White 1989). Within the infragranular layers, layer VI is of particular interest, primarily due to the diverse population of neurons and its complicated microcircuitry. Layer VI receives thalamic and cortical inputs, and gives rise to corticothalamic feedback projections as well as cortico-cortical, cortico-claustral, and commissural fibers (Tombol, 1984; Katz, 1987; Brumberg et al., 2003; Chakrabarti & Alloway, 2006). Therefore, this layer is at the pivotal point to impact thalamocortical/corticothalamic loops, which may gate the information that ultimately ascends to the cerebral cortex.

As a first step toward understanding the structural and functional relationships within layer VI, studies have linked some characteristic neuronal morphologies with specific functional classes (Katz, 1987; van Brederode & Snyder, 1992; Yang et al, 1996). However, due to the morphological diversity of the neuronal population in layer VI, the full spectrum

of phenotypic classes remains unclear. Understanding the cytoarchitecture of layer VI neurons provides a basis upon which models of cortical circuits can be built. Prior studies have used qualitative descriptions to identify the cell types (Lorente de No, 1949; Simons & Woolsey, 1984; Prieto & Winer, 1999). One approach to remove possible selective bias is to perform multidimensional quantitative analyses of the morphological phenotypes (Cauli et al., 2000; Tamas et al., 2000; Tsiola et al., 2003), which utilizes statistical procedures to objectively categorize neuronal groups.

In the present study, we focused on layer VI of the mouse barrel field in the somatosensory cortex (S1). The barrel cortex has been shown to be a model system for the study of local cortical circuits and their relation to behavior (see Petersen, 2007). Furthermore, due to layer VI's pivotal role in the modulation of sensory activity (Sherman & Guillery, 2002) and in many different cortical circuits (see Mendizabal-Zabiaga et al., 2007), it is importance to clarify and identify the cytoarchitectural components of this morphologically and functionally diverse layer. In both the cat and mouse visual system, it was found that the apical dendrites of corticothalamic neurons do not extend superficially to layer IV, whereas the neighboring cortico-claustral neurons have different morphologies (Brumberg et al., 2003; Katz, 1987). These data highlight the correlations between morphology and the functional role that neurons play in cortical circuits. We extended these studies by morphologically characterizing the neurons of layer VI in mouse barrel cortex using unbiased and quantitative methods as a means of determining the basic building blocks of local cortical circuits.

Chapter Four: Material and Methods:

Taxonomizing Layer VI Neurons in Mouse Barrel Cortex Based on Morphological Characteristics Using a Quantitative Approach

1. Experimental Animals

The selection and treatment of experimental animals is in accordance with the Queens College, CUNY Institutional Animal Care and Use Committee and NIH guidelines.

2. Golgi Staining Protocol

The FD Rapid GolgiStain Kit, a simplified and a reliable version of Golgi impregnation, was used to label neurons (FD Neurotechnologies, Inc.). This kit provides patented solutions A, B, C, D and E. It is based on the staining principles previously described by Ramón-Moliner (1970) and Glaser & Van der Loos (1981), which have demonstrated complete labeling of neuronal somata and dendrites. The procedure stains approximately 10% of the total neurons in the neocortex, thereby minimizes background noise to allow accurate neuronal reconstruction (Figure 1).

3. Preparation of Animals and Tissue Processing

Seven CD1 mice of either sex (female N=3, male N=4) of 80-90 postnatal days (PND) were randomly selected and anesthetized with an interperitoneal injection of

Euthasol (Virbac AH, Inc). The brains were immediately removed and rinsed in 0.1M phosphate buffer (PB) for three minutes. Following the PB rinse, retrieved brains were immersed in solution comprised of equal volumes of solution A and B. This mixture of solutions was replaced once after 12 hours of initial immersion, and stored at room temperature in darkness for two to three weeks.

After the immersion period, the embedded brains were transferred to solution C, and were stored at 4^{o}C for at least one week in the dark before cutting. The brain slices were sectioned in coronal plane at approximately 200-250µm thickness on a freezing cryostat (approximately -25 ^{o}C). In order to prevent ice crystal damage, tissues were rapidly frozen with dry ice and quickly embedded in optimal cutting temperature (OCT) medium. Sliced tissues were transferred onto triple-dipped gelatin slides, and were coated with solution C. Cut sections were air-dried at room temperature in the dark for at least three weeks before further processing.

Following the drying period, brain tissues were rinsed in distilled water twice (two minutes each) and were placed in a mixture of solution D, E, and distilled H_2O for ten minutes. Next, the stained brain sections were rinsed twice with distilled H_2O and dehydrated with 50%, 75%, 95% and 100% ethanol for four minutes each, respectively. Finally, the sections were defatted in xylene-substitute and coverslipped using SHUR/Mount (Triangle Biomedical Sciences, Inc.).

4. Identification of Barrel Field and Cortical Layer VI

Barrel cortex location was identified by observing the characteristic clusters of cells that are typically found in granular and supragranular layers, and by matching with a previously published atlas of Golgi stained mice brain (Valverde, 1998). In the rostral-caudal axis, the barrel cortex was defined by the initial appearance of the anterior commissure. Golgi-impregnated neurons were located with respect to the layer VI boundaries. Subdivision of layer VI can also be observed, where VI_a borders the large pyramidal neurons of layer V while VI_b is immediately lateral and superior to the white matter. Layer VI neurons were obtained at all depths, providing an unbiased sampling of morphologies. Images were acquired from prepared slides using a 10x (NA=0.25) air objective lens on a Nikon E4 microscope. These images were used to keep track of which neurons had been reconstructed.

5. Neuronal Selection and Reconstruction

Neurons were viewed with Neurolucida 7.5 software (MBF Bioscience, Inc.) using an Olympus Bx51 microscope equipped with a high resolution digital camera (Optronics, Microfire), a mechanical stage (Ludl, Thornwood, NY), and an x-y-z axis encoder connected to a Windows Pentium 4 PC. Each neuron was scanned under high (20x, oil immersion, NA=0.8) magnification by varying the depth of the Z plane, in order to ensure that all parts of the cell (especially dendrites) were intact. Dendrites that tapered to a point were assumed complete and uncut. Typically, the reconstructed neuronal somata were located at ~100μm deep in resolution to the section surface, although a few

exceptions exist. Only the neurons that exhibited complete Golgi impregnation with limited amount of staining artifacts were traced.

150 neurons were selected from layer VI of the neocortex. 3D neuronal reconstruction took place under a 60x objective (oil immersion, 1.4 NA) of an Olympus Bx51 microscope. In addition, a systematic replication of the data using an independent set of data (N=72 reconstructed cortical neurons) were used to provide reliability and reproducibility of our initial cluster analyses data.

6. Statistical Methods of Classifying Neuronal Groups

The software program NeuroExplorer (MBF Bioscience, Inc.) was used to conduct various morphological measurements. Specific morphological characteristics including somatic shape and size, dendritic structure, and branching patterns were analyzed. For each reconstructed neuron, we measured the following 10 somatic and 25 dendritic components.

1) *Somatic Perimeter* and 2) *Somatic Area*: These and all somatic measurements refer to an XY projection since all somata were reconstructed as a 2D image at the plane of sharpest focus. The plane of the sharpest focus is typically calculated, for each neuron, at the midpoint of where the Z-plane first and last focuses for that particular neuron. 3) *Somatic Feret Maximum*, which refers to the longest diameter of the soma, while 4) *Somatic Feret Minimum* is the longest diameter perpendicular to the feret maximum. 5) *Aspect Ratio* = (Feret Max)/(Feret Min). As aspect ratio approaches one, it is indicative that the soma is closer to a symmetric shape (e.g. circle or square). 6) *Somatic*

Compactness = [$\sqrt{(4/\pi)}\times$Area]/(Feret Max). Numerical values of somatic compactness closer to one represent a more compact soma. 7) *Convexity* = (Convex Contour) / (Perimeter). This parameter is indicative of the somatic morphological profile; higher somatic convexity yields to more indentations, which translates to higher estimated surface area to cellular volume ratio. 8) *Somatic Form Factor* = $(4\pi\times\text{Area})/(\text{Perimeter}^2)$. This value directly reflects the complexity of somatic perimeter; higher numerical value represents a more complex somatic perimeter. 9) *Somatic roundness* = $(4\times\text{Area})/(\pi\times\text{Feret Max}^2)$, i.e. similar to compactness but makes it easier to differentiate objects with small compactness values. 10) *Somatic solidity* refers to the ratio of somata area as a whole over convex area, while values closer to one represent more solid (i.e. smooth, uniform) somata. 11) *Quantity of apical dendrites*. 12) *Quantity of apical dendritic nodes* (including bifurcating as well as trifurcating nodes). 13) *Quantity of apical dendritic endings*. 14) *Total length of apical dendrite* in micrometers. 15) *Mean length of apical dendrites* in micrometers. This number is derived from taking total length of apical dendrites and divided by the number of apical dendrites. 16) *Total surface area of apical dendrites*. 17) *Mean surface area of apical dendrites*. 18) *Total volume* and 19) *Mean volume of apical dendrites*. 20) *Quantity of basilar dendrites*. 21) *Quantity of basilar dendritic nodes*. 22) *Quantity of basilar dendritic ends.* 23) *Total length of basilar dendrites.* 24) *Mean length of basilar dendrites.* 25) *Total surface area of basilar dendrites.* 26) *Mean surface area of basilar dendrites.* 27) *Total volume of basilar dendrites.* 28) *Mean volume of basilar dendrites.* 29) *Quantity of total dendrites.* This includes the summed number of apical dendrite and the basilar dendrites in a particular neuron. 30) *Quantity of total dendritic nodes*. 31) *Quantity of total dendritic ends*. 32) *Total dendritic length*, i.e. regardless of basilar or apical, the summation of the

total dendritic length. 33) *Mean dendritic length*, i.e. regardless of basilar or apical, the mean of the overall dendritic length. 34) *Total dendritic surface area* and, 35) *Mean of total dendritic surface area*.

Following the compilation of descriptive variables, a principal component analysis (PCA) was conducted to determine which morphological variables accounted for the greatest degree of variance within the traced cell sample. One concern is that the PCA is influenced more by variables with larger absolute numbers (e.g. the total dendritic length in micrometers) than smaller numbers (e.g. number of dendritic nodes). To address this concern, we normalized each variable across the reconstructed neuronal sample using Z-scores transformation. Another concern is the high correlations between two variables, hence we would eliminate one of the two variables to avoid double-weighing on the cluster analysis. Following the selection of significant principal components (with absolute loading values ≥ 0.7), we conducted a cluster analysis using Ward's method (Ward, 1963) and Euclidean distance which, based on several Monte Carlo tests, is a highly reliable and valid method for population clustering (for a review, see Scheibler & Schneider, 1985). The neuronal groups and subgroups were identified by Statistica (StatSoft, Inc.) based on the factor loadings of specific measurements of somata and dendrites.

7. Post-Clustering Validation

A number of methods were performed "post-hoc" in order to support the validity of the clustering. Each methodology provides added validity from several different aspects such as location of soma with respect to cortex, dendritic fanning pattern as a

function of distance away from the soma, and dendritic branching polarity across the clustered neuronal groups.

Systematic Replication. In addition to our original N=150 population of neurons, we reconstructed another separate population (N=72) of neurons from an independent group of animals comprising four mice. The statistical methods and the morphological variables that were employed for this separate population of neurons were identical to what was described above. This systematic replication was conducted to support the reliability, validity, and consistency of our initial morphological classification scheme.

Laminar Location of Somata. Location of neuronal somata in relation to the cortical thickness supports the notion that the reconstructed neurons are indeed within layer VI. For each reconstructed neuron, laminar data are exemplified by the following measurements: the shortest distance from pia mater to soma (PIA-SOMA), the shortest distance from pia mater to the most distal dendritic process (PIA-DISTAL), and the shortest distance from the white matter to pia (WM-PIA) which bisects the soma of that particular neuron. From the obtained measurements, we calculated two metrics: the ratio of somatic location over cortical thickness (PIA-SOMA/WM-PIA), and the ratio of distal process over cortical thickness (PIA-DISTAL/WM-PIA).

Sholl Analyses. Based on Sholl's method (1956), concentric spheres were placed around the center of each cell's soma. These concentric spheres increased in pre-selected radii of 10μm. Such analyses provide useful information regarding the number of dendritic intersections, nodes, endings, spines, and length of dendrites passing through

the shells within each incrementing sphere. An Analysis of Variance (ANOVA) was performed for the number of dendritic intersections, spines, and nodes. These variables were withheld from the original PCA list and did not participate as the loading factors which determined the neuronal clustering.

Dendritic Fanning Polarity. From the center of each cell's soma as the pivot point, 12 pie-shaped regions were created, with each region occupying a 30° angle. Arbitrarily setting pia mater as 0° and white matter 180°, we analyzed the total dendritic length that falls under the particular jurisdictions of the wedged regions. Furthermore, we corrected the cerebral hemispheric (*left vs. right*) orientation by flipping the left hemispheric images 180°. We arbitrarily set the lateral/inferior direction as 90° and the proximal/superior direction as 270° (in terms of gross anatomy of the brain). We flattened the Z-axis and investigated only the XY plane. This was accomplished by selecting the "3D wedge analysis" function that is included in the Neurolucida 7.5 software package (NeuroExplorer, version 4.0). Doing so, the elucidation of polarity of dendritic patterning was provided in the coronal plane.

8. Statistics

We did not perform between-groups Analysis of Variance across the 11 dimensions that were responsible for splitting the sampled neurons into morphological groups. This is due to the fact that Ward's Method using Euclidean distance is already an ANOVA-type approach in itself (also see Results). However, since the post-clustering

data were withheld from the original PCA matrix, it was therefore appropriate to conduct between-groups Analysis of Variance on these "post-hoc" data. Similarly, it would also be statistically appropriate to conduct ANOVA-type comparisons for the other branch structure parameters that were not selected by the PCA (and therefore were not responsible for splitting the neuronal sample into groups.) All of the post-clustering pairwise tests are two-tailed independent t-tests unless otherwise indicated. Furthermore, all of the multiple post-hoc tests following a statistically significant ANOVA (or Kruskal-Wallis) were corrected for inflated alpha rate with Bonferroni-correct (unless otherwise noted). Statistical significance wad set with p-values less than 0.05, with apriori alpha levels set at 0.05.

Chapter Five: Results:

Taxonomizing Layer VI Neurons in Mouse Barrel Cortex Based on Morphological Characteristics Using a Quantitative Approach

1. Determination of Principal Components

Our Golgi material produced excellent resolution of dendritic arborization, dendritic spines, and somatic labeling, with minimal background staining artifacts (Figure 1A-F). The somatic and dendritic data were derived from 150 reconstructed neurons from layer VI of the adult mouse barrel cortex. A total of 10 somatic and 25 dendritic variables (Table 1) were chosen as candidates for a PCA matrix that determined the parameter(s) which accounted for the greatest degree of variance within the reconstructed cell sample. Out of these 35 parameters, *total apical dendritic length* and *mean apical dendritic length* significantly overlapped one another ($r>0.9$). Other significant overlapping pairs included *total apical dendritic surface area* and *mean apical dendritic surface area* ($r>0.9$), and *total apical dendritic volume* and *mean apical dendritic volume* ($r>0.9$). *Mean apical dendritic length*, *mean apical dendritic surface area,* and *mean apical dendritic volume*, therefore, were removed from the variable list that participated in the PCA. 11 out of the 32 variables (labeled bold in Table 1) had absolute loading values greater than or equal to 0.7, and thus were used to separate neurons into specific morphological groups with a subsequent cluster analysis.

2. Cluster Analysis of Morphological Neuronal Classifications.

The selected 11 principal components were loaded into a cluster analysis matrix that maximizes between-cluster differences and minimizes within-cluster differences (Ward's method, Euclidean Distance). Figure 2 represents the results of a dendrogram, and shows that six distinct groups were categorized based on our objective criteria. While each point on the X-axis is arbitrarily preselected and signifies a neuron, the Y-axis depicts the linkage distance across the 11 dimensions selected, i.e. neurons clustered within the same group share more similarity than neurons in other groups. Two of the strongest splitting factors, *total dendritic length* and *quantity of apical dendrites*, were primarily responsible for dividing the reconstructed neurons into six groups. Due to the sum of squares (SS) calculations that were utilized in the cluster analysis, it is inappropriate to use between-groups ANOVA or pairwise testing to contrast the groups for the 11 selected morphological factors (which were responsible for splitting the neurons into groups). As the cluster analysis itself is already a reversed ANOVA-type approach, performing an ANOVA and/or pairwise testing would be statistically circular.

2.1. Group 1: Pyramidal neurons with elaborate dendrites.

Common Features of Group 1 (n=16 in this group***, 10.6%*** of the total reconstructed population***).*** Group 1 (Figure 3) are composed of pyramidal neurons with elaborate dendrites. The most distinctive characteristics are the extremely long apical dendrites (679.5µm ± 56.9, all data are reported as mean ± SEM), the numerous apical dendritic bi/trifurcations (14.7 ± 2.6), and the extensive overall dendritic length (1347.9µm ± 81.9). Other common features of Group 1 include extremely large *total and apical dendritic surface area* (5000.9µm² ± 305.4, 2827.2µm² ± 231.8, respectively).

Their apical dendrites tend to have a large number of branching points as well as secondary oblique dendrites that originate from the apical trunk. These neurons also exhibited the longest overall basilar dendritic processes out of all pyramidal neuronal groups (*group 1* = 668.4µm ± 60.4, *group 3* = 431.8µm ± 22.9, *group 4* = 232.6 ± 18.3). Group 1 could be further divided into two subgroups based on our objective morphological splitting criteria.

Subgroups of Group 1. Subgroups of Group 1 include 1A (n=4, representative neurons shown in Figure 3A) and 1B (n=12, Figure 3B-D). Although morphological differences are minimal, cells in subgroup 1A possess relatively more apical dendritic nodes (26.3 ± 7.2 vs. 10.8 ± 1.4), basilar dendritic nodes (30.25 ± 7.2 vs. 8.3 ± 1.2), and total dendritic nodes (56.5 ± 6.1 vs. 19.2 ± 1.9) than cells in subgroup 1B. In addition, neurons in subgroup 1A also exhibit a higher number of apical (25.5 ± 6.9 vs. 11.9 ± 1.4), basilar (36.3 ± 6.8 vs. 15.3 ± 1.1), and total dendritic endings (61.8 ± 7.2 vs. 27.2 ± 2) than subgroup 1B.

Subgroup 1B can be further subdivided into $1B_1$ (n=3, Figure 3B) and $1B_2$ (n=8, Figure 3D). In terms of somatic components, subgroup $1B_1$ displays significantly less *convexities* and *form factors* than subgroup $1B_2$ (*convexity* 0.85 ± 0.03 vs. 0.96 ± 0.01, $p<0.05$; *form factor* 0.53 ± 0.08 vs. 0.73 ± 0.05, $p<0.05$), thus indicating that cells in $1B_2$ have smoother somatic edges yet more complex perimeters compared to cells in $1B_1$. With regard to dendritic components, neurons in subgroup $1B_2$ demonstrate notably higher numbers in *total dendritic length*, *total dendritic mean length*, and *total dendritic mean surface area* (1367.3µm ± 70.3 vs. 1036.8µm ± 87.1; 201.7µm ±17.7 vs. 111.7µm

± 18.1; and 5155μm² ± 345.1 vs. 4278.5μm² ± 300.6, respectively). Out of the 16 pyramidal neurons clustered in Group 1, two neurons in $1B_1$ were observed to have an atypically oriented dendritic pattern (example in Figure 3C).

2.2. Group 2: Non-pyramidal neurons with elaborate dendrites.

Common Features of Group 2 (n=8, 5.3%). Figure 4 represents examples of neurons clustered in Group 2. These neurons tend to have large circular/oval cell bodies (*somatic area* = 275.9μm² ± 48.5). Their most noticeable features are the high numbers of *dendritic nodes* and *dendritic ends* compared to the other five groups (*dendritic nodes* = 27.6 ± 4.2; *dendritic ends* = 33.3 ± 7.6). Out of the six distinct neuronal groups, Group 2 neurons exhibited the highest *dendritic surface area* (4357.2μm² ± 520.2) and *dendritic volume* (1631.9μm³ ± 309.7), suggesting the important roles these neurons play in integrating signals within deep cortical layers. Our data indicated that this particular group of neurons displays highly complicated dendritic fanning patterns (see below).

Subgroups of Group 2. Two subgroups can be further divided within this group: subgroup 2A (n=3, Figure 4A) and 2B (n=5, Figure 4B). Neurons in subgroup 2A are exemplified by their relatively circular/spherical dendritic fanning pattern, whereas neurons in subgroup 2B have more bitufted dendritic patterns throughout. It is therefore postulated that neurons in subgroup 2B may play crucial roles in integrating information between layer VI_a and VI_b. Comparing subgroup 2A and 2B, while there are negligible differences in somatic parameters ($p>0.15$ for all), considerable disparities are observed in dendritic parameters. Neurons in subgroup 2A possess significantly higher *dendritic*

surface area as well as *dendritic volume* comparatively to the neurons in subgroup 2B (*dendritic surface area* 6007.3μm² ± 171.7 vs. 3367.1μm² ± 308.8; *dendritic volume* 2564.3μm² ± 368 vs. 1072.5μm² ± 139.2).

2.3. Group 3: Pyramidal neurons with moderate apical & basilar dendritic pattern.

Common Features of Group 3 (n=46, 30.6%). Neurons in Group 3 (Figure 5) are characterized by relatively small somata (*somatic perimeter* = 48.83μm ± 1.14, *somatic area* = 164μm² ± 7.7, *feret max* = 17.76μm ± 0.52, *feret min* = 12.48μm ± 0.27). Despite their small cell bodies, it was observed that several somatic parameters such as *compactness* (0.812 ± 0.01), *convexity* (0.98 ± 0.002), *form factor* (0.85 ± 0.01), and *solidity* (0.97 ± 0.003) are particularly high for neurons clustered in this group. The commonly shared dendritic features include similar range of apical dendritic parameters (*apical dendritic nodes* = 6.86 ± 0.4; *apical dendritic length* = 461.8μm ± 19.5; *apical dendritic surface area* = 1835.2μm² ± 93.3; *apical dendritic volume* = 750.9μm³ ± 54.2). Similarity in ranges of basilar dendritic parameters was also demonstrated (*basilar dendritic nodes* = 7.77 ± 0.86; *basilar dendritic total length* = 431.8μm ± 22.9; *basilar dendritic surface area* = 1119.8μm² ± 61.3; *basilar dendritic volume* = 305.3 μm³ ± 22.8). Compared to Group 1, neurons in Group 3 possess considerably shorter and noticeably less complicated basilar dendrites. It was also observed that the apical dendritic complexities of Group 3 cells are not as elaborative as neurons in Group 1. However, the neurons in Group 3 are still distinctly more elaborate than neurons clustered in Group 4, which also possess apical dendrites. Furthermore, the overall morphological structures of Group 3 neurons suggest that a subset of corticothalamic neurons may belong in this

particular neuronal cluster, when compared to previously conducted studies (Brumberg et al., 2003).

Subgroups of Group 3. Two main subgroups of neurons were observed: Subgroup 3A (n=24, Figure 5A-5C) and 3B (n=22, Figure 5D-5F). Overall, neurons clustered in subgroup 3A have significantly larger somata than 3B, as indicated by several somatic variables (*somatic perimeter* = 58.7µm ± 5.44 vs. 48.83µm ± 3.13, $p<0.05$; *somatic area* = 200.31µm² ± 24.57 vs. 164.04 µm² ± 21.13, $p<0.05$, *feret max* = 20.30µm ± 1.78 vs. 17.76µm ± 1.43, $p<0.05$; *feret min* = 14.00µm ± 1.10 vs. 12.48µm ± 0.74, $p<0.05$, *two-tailed independent t-tests* for all). In various indicators of somatic shape/contour, neurons in subgroup 3B displayed significantly larger *convexity* (0.98 ± 0.01 vs. 0.94 ± 0.02, $p<0.05$), *form factor* (0.84 ± 0.01 vs. 0.75 ± 0.06, $p<0.05$), and *solidity* (0.97 ± 0.01 vs. 0.94 ± 0.02, $p<0.05$) than neurons in subgroup 3A. This type of pattern in somatic variants reflects that there are considerable somatic disparities in both size and shape between subgroup 3A and 3B. In dendritic parameters, our data suggested that cells in subgroup 3A possess significantly larger *basilar dendritic surface area* as well as larger *basilar dendritic volume* than subgroup 3B (*basilar dendritic surface area 1812.61µm² ± 144.88* vs. 1119.80*µm² ± 168.36*; *basilar dendritic volume* 612.22*µm³* ± 71.03 vs. 305.30*µm³* ± 62.49). It is therefore postulated that neurons in subgroup 3A may process more intralaminar information than 3B. However, neurons clustered in subgroup 3B exhibited more extensively patterned and longer apical dendrites than subgroup 3A (*apical dendritic nodes* = 6.86 ± 1.08 vs. 3.58 ± 0.87*; apical dendritic ends* = 7.82 ± 1.14 vs. 4.58 ± 0.83; *apical dendritic length* = 461.80µm ± 53.48 vs. 264.95µm ± 39.83, all significant at $p<0.05$). Therefore, the results strongly indicated that the neurons in

subgroup 3B may be important for interlaminar communication, while neurons in subgroup 3A are possibly important for intralaminar communication in the barrel cortex.

Subgroup 3A can be further subdivided into $3A_1$ (n=15, Figure 5A & 5B) and $3A_2$ (n=9, Figure 5C). Neurons in subgroup $3A_1$ have considerably more elongated cell bodies compared to those in $3A_2$, as indicated by elevated values in somatic components such as *perimeter* (63.89µm ± 3.48 vs. 50.05µm ± 3.34, $p<0.05$), *feret max* (22.10 ± 1.12 vs. 17.28 ± 1.03, $p<0.05$), and *aspect ratio* (1.59 ± 0.07 vs. 1.26 ± 0.05, $p<0.05$). This elongation of somata in subgroup $3A_1$ is further validated by significantly decreased values in *compactness* (0.74 ± 0.01 vs. 0.86 ± 0.02), *somatic roundness* (0.55 ± 0.02 vs. 0.75 ± 0.04), and *solidity* (0.92 ± 0.01 vs. 0.98 µm ± 0.01) when compared side-by-side with subgroup $3A_2$. Consequently, neurons in subgroup $3A_2$ possess relatively more spherical somata than $3A_1$. In general, subgroup $3A_1$ demonstrated significantly increased apical dendritic components than $3A_2$ when it comes to overall length and area (*apical dendritic length* = 314.96µm ± 22.23 vs. 181.59µm ± 21.58, *apical dendritic surface area* = 1779.93µm² ± 103.54 vs. 1058.05µm² ± 128.07, *& apical dendritic volume = 947.51*µm³ ± 86.49 vs. 597.61µm³ ± 93.50). With regard to basilar dendritic components, subgroup $3A_2$ exhibited far more dendritic nodes and longer processes than subgroup $3A_1$ extending into other cortical laminae (*basilar dendritic node* = 8.44 ± 1.75 vs. 4.53 ± 0.71, $p<0.05$; *basilar dendritic mean length* = 111.3µm ± 10.76 vs. 76.29µm ± 8.39), hinting that the neurons in $3A_2$ may be more involved than $3A_1$ in roles such as intralaminar communication. Within subgroup $3A_1$ two subdivisions can be defined: $3A_{1\text{-}\alpha}$ (Figure 5A) and $3A_{1\text{-}\beta}$ (Figure 5B). Comparing $3A_{1\text{-}\alpha}$ and $3A_{1\text{-}\beta}$ in somatic parameters, $3A_{1\text{-}\beta}$ exhibited higher values than $3A_{1\text{-}\alpha}$ in *convexity* (0.95 ± 0.02 vs. 0.88 ±

0.03, $p<0.05$) and *form factor* (0.75 ± 0.04 vs. 0.59 ± 0.04, $p<0.05$). Upon visual inspection, there seemed to be a dramatic difference in apical dendritic parameters between $3A_{1\text{-}\alpha}$ and $3A_{1\text{-}\beta}$. Numerical calculations and analyses, however, revealed that there were no significant disparities in terms of apical dendritic parameters ($p>0.05$ for all apical dendritic parameters). Various basilar dendritic variables of $3A_{1\text{-}\beta}$ were significantly larger than $3A_{1\text{-}\alpha}$, specifically *basilar dendritic quantity* (9.67 ± 0.99 vs. 5.00 ± 0.50, $p<0.05$), *basilar dendritic ends* (13.67 ± 1.43 vs. 10.13 ± 0.72, $p<0.05$), *basilar dendritic length* (591.82μm ± 40.92 vs. 401.18μm ± 27.47, $p<0.05$), and *basilar dendritic surface area* (2045.69μm² ± 99.32 vs. 1556.20μm² ± 111.26).

Subgroup 3B gives rise to three smaller sub-clusters of neurons: $3B_0$ (n=2, not shown), $3B_1$ (n=13, Figure 5D), and $3B_2$ (n=7, Figure 5E & 3F). Subgroup $3B_0$, comprised of only two neurons, shared limited morphological characteristics with the rest of subgroup 3B. Therefore, this independent subgroup was separated from the rest of 3B, according to our objective clustering criteria. Comparing the somatic parameters, $3B_1$ displayed several significantly larger variables over $3B_2$, including *somatic area* (178.30μm² ± 15.56 vs. 130.89μm² ± 16.21, $p<0.05$), *feret maximum* (19.18μm ± 1.15 vs. 15.16μm ± 1.01, $p<0.05$), *convexity* (0.99 ± 0.002 vs. 0.96 ± 0.008, $p<0.05$), and *solidity* (0.98 ± 0.003 vs. 0.95 ± 0.01, $p<0.05$). It is therefore inferred that $3B_1$'s somata are generally larger and more elongated, with more complicatedly shaped somatic perimeter. In terms of apical dendritic variables, despite the fact that $3B_1$ exhibited significantly less branching than $3B_2$ (*apical dendritic nodes* = 5.83 ± 0.58 vs. 8.86 ± 1.37, $p<0.05$), neurons in $3B_1$ still displayed significantly larger dendritic surface area and dendritic volume over $3B_2$ (*apical dendritic surface area* 1911.35μm² ± 133.08 vs. 1307.56μm² ±

167.02, $p<0.05$; *apical dendritic volume* 839.50μm³ ± 94.77 vs. 392.92μm³ ± 50.33, $p<0.05$). This suggests the possibility that neurons in $3B_1$ process significantly more interlaminar information than $3B_2$. Although there were no significant disparities between $3B_1$ and $3B_2$ in the *quantity of basilar dendrites* ($p>0.05$), neurons of $3B_1$ showed several significant decreases in the *number of basilar dendritic branching* (4.91 ± 1.00 vs. 14.57 ± 2.14, $p<0.05$), *basilar dendritic endings* (9.91 ± 1.19 vs. 19.71 ± 2.42, $p<0.05$), *total basilar dendritic length* (372.42μm ± 43.75 vs. 554.50μm ± 51.40, $p<0.05$), and *average basilar dendritic length* (72.75μm ± 5.25 vs. 120.04μm ± 14.24, $p<0.05$). This suggests that neurons in $3B_2$ may play a significant role in integration of intralaminar information within neocortical layer VI.

2.4. Group 4: Pyramidal neurons with short overall dendrites.

Common Features of Group 4 (n=40, 26.6%). Similar to Group 3, neurons clustered in Group 4 (Figure 6) also exhibited small somata (*somatic perimeter* = 51.56μm ± 2.45, *somatic area* = 166.51 μm² ± 12.90, *feret max* = 18.01μm ± 0.83, *feret min* = 12.87μm ± 0.65. Every neuron clustered in Group 4 has an apical dendrite. A subset of neurons in Group 4 has anatomical features that highly resemble the morphology of star-pyramidal neurons in layer IV. Despite the similarities in somatic variables, there are distinct differences of dendritic parameters between Group 4 neurons and neurons in other groups. Out of the neuronal groups that possess apical dendrites (Group 1, 3, & 4), Group 4 neurons have the shortest and least complicated apical as well as basilar dendritic processes. This morphological uniqueness is exemplified by low values obtained in *apical dendritic bi/trifurcations* (3.33 ± 0.30), *apical dendritic endings*

(4.40 ± 0.31), *apical dendritic length* (225.51μm ± 12.79), *apical dendritic surface area* (903.61μm² ± 63.69), and *apical dendritic volume* (399.58μm³ ± 45.38). Consequently, it is rare that the apical dendrites of Group 4 neurons extend beyond layer VI; the few exceptions are described below. Neurons of Group 4 also displayed a limited fanning pattern of basilar dendrites, as reflected by low numbers in *basilar dendritic nodes* (3.21 ± 0.33), *basilar dendritic endings* (8.19 ± 0.57), *total basilar dendritic length* (232.58μm ± 18.25), *mean basilar dendritic length* (50.18μm ± 4.48), *total basilar dendritic surface area* (652.56μm² ± 68.26), *mean basilar dendritic surface area* (131.39μm² ± 11.73), *total basilar dendritic volume* (193.90μm³ ± 27.64), and *mean basilar dendritic volume* (37.52μm³ ± 4.45). Due to the restricted branching pattern of dendritic processes, we postulate that Group 4 pyramidal neurons manage information in a more spatially localized fashion compared to neurons in Group 1 and/or Group 3, and perhaps are the layer VI homolog of the layer IV spiny stellate cell.

Subgroups of Group 4. Two main subgroups were identified within Group 4: Subgroup 4A (n=17, Figure 6A-B) and Subgroup 4B (n=23, Figure 6C-6E). Within somatic parameters, cells in Subgroup 4A demonstrated considerably longer *perimeter* than cells in Subgroup 4B (59.74μm ± 3.18 vs. 45.42μm ± 1.98, $p<0.05$), with no significant disparity in *somatic area* (193.26μm² ± 21.24 vs. 146.44 μm² ± 14.63, $p>0.05$). Subgroup 4A neurons exhibited significantly longer *feret maximum* than Subgroup 4B (20.67μm ± 1.06 vs. 16.02μm ± 0.66, $p<0.05$). This discrepancy between the two subgroups was, however, not observed in *feret minimum* (14.06μm ± 0.99 vs. 11.98μm ± 0.64, $p>0.07$). This type of data pattern suggests that the neurons in Subgroup 4A have more elongated cell bodies than the neurons in Subgroup 4B. A statistical significance

between Subgroup 4A and 4B in their *aspect ratios* (1.54 ± 0.07 vs. 1.36 ± 0.04, $p<0.05$) further suggests that notable differences exist in their overall somatic shape, in terms of how elongated their cell bodies are. Various indicators revealed that the neurons in Subgroup 4B have significantly more intricate cell bodies than Subgroup 4A (*compactness* 0.833 ± 0.012 vs. 0.738 ± 0.019, $p<0.05$; *convexity* 0.978 ± 0.005 vs. 0.924 ± 0.013, $p<0.05$; *form factor* 0.854 ± 0.015 vs. 0.650 vs. 0.024, $p<0.05$; *solidity* 0.971 ± 0.005 vs. 0.902 ± 0.009, $p<0.05$). Comparing Subgroup 4A and 4B with respect to apical dendritic parameters, no significant differences were found with the exception of *apical dendritic length*, in which neurons clustered in 4B revealed considerably longer apical dendrites than neurons in 4A (249.75μm ± 13.31 vs. 193.20μm ± 18.92). Although there was no significant difference between 4A and 4B in their *basilar dendritic length* (240.76μm ± 29.36 vs. 226.45μm ± 23.10, $p=0.65$), there was a significant difference between 4A and 4B in their *basilar dendritic quantity* (6.61 ± 0.59 vs. 3.79 ± 0.30, $p<0.05$). Consequently, neurons in Subgroup 4B possess considerably longer *mean basilar dendritic length* than Subgroup 4A (59.73μm ± 6.27 vs. 37.44μm ± 4.74, $p<0.05$). Although there is no significant difference in *mean basilar dendritic surface area* or *mean basilar dendritic volume* ($p=0.84$ & 0.38, respectively), Subgroup 4A exhibited dramatically larger basilar dendritic surface area (868.35μm^2 ± 129.64 vs. 490.71μm^2 ± 53.54) and total basilar dendritic volume (291.57 μm^3 ± 53.70 vs. 120.64μm^3 ± 17.90) than subgroup 4B. It is inferred that neurons in Subgroup 4B play crucial roles in interlaminar communications, and neurons in Subgroup 4A are important for intralaminar information processing within layer VI.

Subgroup 4A is composed of two smaller clusters of neurons: $4A_1$ (Figure 6A) and $4A_2$ (Figure 6B). Surprisingly when comparing the somata between $4A_1$ and $4A_2$, no significant differences were found across all ten somatic variables nor for any apical dendritic variables. The only exception was *apical dendritic volume*, which neurons in $4A_1$ have significantly larger volume than $4A_2$ ($590.37\mu m^3 \pm 89.35$ vs. $316.88\mu m^3 \pm 65.12$). Therefore, it is inferred that the neurons in $4A_1$ possess thicker apical dendrites than neurons in $4A_2$. Despite the similarities between $4A_1$ and $4A_2$ in both somatic and apical dendritic variables, basilar dendritic variables between $4A_1$ and $4A_2$ were distinctively different. With the exception of *basilar dendritic quantity*, which yielded no significant difference ($p>0.05$), cortical neurons in $4A_1$ exhibited greater values in all basilar dendritic parameters comparative to $4A_2$ ($p<0.05$ for all). The data suggest that although basilar dendritic quantity may be similar, Subgroup $4A_1$ has significantly broader spatial processing capacity than $4A_2$ when it comes to intralaminar cortical communication.

Subgroup 4B gives rise to three smaller clusters: $4B_1$ (Figure 6C), $4B_2$ (Figure 6D), and $4B_3$ (Figure 6E). Subgroup 4B is primarily populated with neurons in Subgroup $4B_1$ and $4B_2$. Comparing Subgroup $4B_1$ and $4B_2$, there were no distinct differences in somatic morphology ($p>0.05$ for all) except for *somatic solidity* (indicator of unitary, smooth somata), in which Subgroup $4B_2$ displayed significantly smaller average values than $4B_1$ (0.960 ± 0.007 vs. 0.981 ± 0.002, $p<0.01$). Although there were no significant morphological differences in *apical dendritic quantity*, *apical dendritic nodes*, *apical dendritic endings*, and *apical dendritic length* ($p<0.05$ for all), there were considerable morphological differences in *apical dendritic surface area* ($727.67\mu m^2 \pm 68.87$ vs.

1120.38μm² ± 154.44, $p<0.05$) and *apical dendritic volume* (252.67μm³ ± 36.88 vs. 532.81μm³ ± 141.68, $p<0.05$), in which $4B_1$ displayed lower numbers than $4B_2$ for both variables. This pattern of data reflects that Subgroup $4B_2$ possess significantly thicker apical dendrites than neurons in $4B_1$. Within the basilar dendritic parameters, the data suggests that neurons in Subgroup $4B_2$ have significantly broader spatial processing capacity than Subgroup $4B_1$, exemplified by significantly higher numbers in variables such as *total basilar dendritic surface area* (642.55μm² ± 81.82 vs. 362.55μm² ± 48.77, $p<0.05$), *mean basilar dendritic surface area* (156.58μm² ± 18.51 vs. 90.87μm² ± 13.16, $p<0.05$), *total basilar dendritic volume* (175.93μm³ ± 22.90 vs. 66.82μm³ ± 12.01, $p<0.05$), and *mean basilar dendritic volume* (42.63μm³ ± 4.95 vs. 17.02μm³ ± 3.35, $p<0.05$). Since Subgroup $4B_3$ has only two neurons, quantitative analyses were not performed in comparison to $4B_1$ and/or $4B_2$.

Atypically Oriented Neurons in Group 4. Compared to Group 1 and Group 3 neurons, a high proportion of Group 4 neocortical neurons demonstrated an atypical orientation (Figure 6F), in which the apical dendrites are pointing horizontally or towards the white matter. Out of the 40 observed neurons in Group 4, 25% (n=10) exhibited atypical orientation, while only 12.5 % of Group 1 (2 out of 16) and 2.2% of Group 3 (1 out of 46) neurons exhibited atypical orientation.

2.5. Group 5: Large non-pyramidal neurons.

Common Features of Group 5 (n=28, 18.6%). Figure 7 depicts representative cells from group 5. Out of the 6 neuronal groups defined by the present cluster analysis, these neurons have the largest cell bodies, indicated by the highest value obtained in

somatic variables such as *somatic perimeter* (76.43μm ± 2.94), *somatic area* (317.48μm² ± 19.56), *feret maximum* (28.27μm ± 1.35), and *feret minimum* (16.35μm ± 0.54). These neurons do not possess apical dendrites, and have limited *dendritic node to quantity ratio* (0.76), which indicates that the amount of bifurcations are rather restricted. However, despite the paucity of dendritic nodes, Group 5 neurons still exhibited the second highest *dendritic surface area* (2661.01μm² ± 155.30) as well as *dendritic volume* (1031.63 μm³ ± 70.90), trailing only Group 2. This type of data suggests that the dendrites of Group 5 neurons are quite thick in diameter.

Subgroups of Group 5. Group 5 are further divided into two Subgroups: Subgroup 5A (n=17, Figure 7A & 7B) and 5B (n=11, Figure 7C). Based on visual inspection, the morphology of Subgroup 5A resembles neurons that have been previously described as stellate neurons, while Subgroup 5B resembles strongly of horizontal (bipolar) neurons (Furtak, 2007). Therefore it was no surprise that somatic comparison revealed many significant differences, where subgroup 5A exhibited significantly smaller and less elongated somata than subgroup 5B (*somatic perimeter* = 67.86μm ± 2.42 vs. 89.45μm ± 4.45, $p<0.05$; feret max = 33.75μm ± 2.38 vs. 24.64μm ± 0.96 vs. 33.75μm ± 2.38). Somatic data further suggested that these two sub-clusters of Group 5 exhibit differences in somatic shape and somatic surface complexity, reflected by significant differences in *compactness* (0.800 ± 0.019 vs. 0.614 ± 0.023), *convexity* (0.969 ± 0.009 vs. 0.900 ± 0.025), *form factor* (0.810 ± 0.029 vs. 0.521 ± 0.039), *roundness* (0.629 ± 0.029 vs. 0.382 ± 0.029), and *solidity* (0.960 ± 0.013 vs. 0.865 ± 0.030). In terms of dendrites, data indicated that although bipolar neurons on average possess significantly more numerous dendrites than stellate neurons (*dendritic quantity* 9.18 ± 0.736 vs. 6.44 ±

0.483, $p<0.05$), stellate neurons have significantly longer as well as thicker dendrites (*dendritic mean length* 100.99μm ± 5.19 vs. 73.75μm ± 9.79; $p<0.05$; *dendritic mean surface area* 425.88μm² ± 24.64 vs. 318.11μm² ± 35.40, $p<0.05$).

Subgroup 5A gives rise to two smaller sub-clusters: Subgroup $5A_1$ (Figure 7A) and Subgroup $5A_2$ (Figure 7B). As previously mentioned, upon visual examination it is suggestive that both of these two sub-clusters are stellate neurons compared to the results of prior studies. Quantitative comparison further supported that there are no significant somatic differences between Subgroup $5A_1$ and $5A_2$ ($p>0.25$ for all somatic variables). Dendritic comparisons, however, revealed that there are some subtle differences between these sub-clusters. Specifically, neurons in Subgroup $5A_1$ displayed a higher number of dendrites (7.75 ± 0.49 vs. 5.13 ± 0.52, $p<0.05$), longer dendrites (832.88μm ± 35.62 vs. 461.15μm ± 47.06, $p<0.05$), as well as more *dendritic surface area* (3334.03 μm² ± 185.86 vs. 1989.72μm² ± 142.34) and *dendritic volume* (1204.45 μm³ ± 144.86 vs. 814.53 μm³ ± 68.80) $5A_2$. Since neurons in $5A_1$ have more dendritic processes as well as longer dendrites than $5A_2$, this suggests that neurons in $5A_1$ have larger spatial processing capacity in cortical layer VI than $5A_2$.

2.6. Group 6: Simple neurons without apical dendrites.

Common Characteristics of Group 6 (n=12, 8%). Representative cells from group 6 are presented in Figure 8. This particular group contained neurons with relatively simple dendritic organization. Collectively, neurons clustered in this group have somata that are medium-sized (*perimeter* = 63.73μm ± 3.61, *somatic area* =

247.19μm² ± 25.45), symmetrical (aspect ratio = 1.50 ± 0.074), and well-uniformed somata (0.938 ± 0.017). Although *overall dendritic quantity* is comparable to other neuronal groups (6.08 ± 0.81), neurons in Group 6 possess surprisingly few *dendritic nodes* (2.58 ± 0.379) as well as the shortest dendrites on average (*mean dendritic length* = 42.08μm ± 4.70). Despite exhibiting the least complex dendritic fanning pattern and the shortest dendrites, Group 6 neurons still showed relatively high *mean dendritic surface area* (183.72μm² ± 16.93) as well as *mean dendritic volume* (76.56μm³ ± 8.52), suggesting that the dendritic diameter of these neurons are quite thick on average.

Subgroups of Group 6. Several Subgroups are observed: 6A (n=3, Figure 8A), 6B (n=6, Figure 8B), and 6C (n=3, Figure 8C). Quantitatively, the three subgroups exhibited very little significant differences in somatic variables except for *somatic complexity* [*Between-groups ANOVA*: $F(2,9)=4.66$, $p<0.05$]. A post-hoc test using Fisher LSD criterion revealed that the average somatic complexity was significantly lower in Subgroup 6B than the Subgroup 6C ($p<0.05$). Statistical significance was also found for *form factor* [$F(2,9)=15.32$, $p<0.05$], in which Fisher LSD post-hoc suggested that Subgroup 6B exhibited lower values than both Subgroup 6A and Subgroup 6C ($p<0.05$ for both pairs). Subgroup 6A and 6C, however, did not significantly differ from one another in *form factor*. In addition, Subgroup 6B exhibited lower *solidity* than both Subgroup 6A and Subgroup 6C [$F(2,9)=6.70$, $p<0.05$; Fisher LSD post-hoc, $p<0.05$]. As regards to dendritic components, there were no statistical significances across all three subgroups.

To summarize, we defined six neuronal groups using quantitative and objective data in barrel cortex layer VI.

3. Results of Post-Clustering Analyses

In attempt to provide additional support for our results, we held back a number of variables from the PCA/cluster analyses. We then performed conventional analyses of variance on these variables using the groups determined by the cluster analysis as the categorical predictor. Our intent was to use these analyses as "post-hoc" confirmations of our classification scheme since it is not possible to assign significance to the results of a cluster analysis.

3.1. Systematic replication

To determine the reliability and repeatability of our methodology we reconstructed an additional 72 neurons and quantified their morphologies exactly as described above. The clustering results that we obtained from our systematic replication were strikingly similar to that of our original clustering. This is especially evident in the similarities in the classification dendrogram (compare Figure 9A to Figure 2). Our clustering algorithm once again was able to discriminate six morphological classes and when we analyzed the distribution of the neurons within these six groups, there was no significant difference from our original dataset [Chi-Square: Test of Independence, $\chi^2(5, N=222)=0.805$, $p=0.977$]. In addition, the morphological characteristics of this replicated

population were also strikingly similar, if not almost identical, to that of our original clustering (compare Figure 9B-G to Figures 3-8, also see Table 2). Taken together, the similarities of results between our original and replicated neuronal populations strongly suggest that our clustering scheme is a reliable and valid way of objectively categorizing neurons based on morphological quantifications.

3.2. Laminar location

It has been previously demonstrated that neurons in layer VI_a differ from those in the VI_b (Ferrer et al. 1986), which suggested the possibility of different roles in cortical processing. Furthermore, converging data have demonstrated that layer VI_a and VI_b are developed at different embryological timeline, in which VI_b is developed approximately the same time as the subplate and is earlier than VI_a (Valverde et al, 1989; Del Río et al., 2000; Arimatsu et al., 2003). This diversity between VI_a and VI_b has been further supported by recent studies showing that neocortex VI_a and VI_b express different mRNA (Heuer et al., 2003; Watakabe et al., 2007). By measuring the ratio of somatic location over the cortical width, we intend to demonstrate that the overall morphological characteristics of cortical neurons are strongly associated with their roles in information processing.

To determine whether traced neurons are located in layer VI, the width of the cortex was measured at the midpoint of the reconstructed soma from the pia to the white matter (Figure 10A). For each data set, the distance is expressed as a percentage, in which the total distance (from pia to white matter) for that particular data set is 100%.

Therefore, we calculated the *relative location* of the reconstructed neuron. This was done in order to account for the shrinkage due to tissue processing. Neuronal group 6 as well as group 4 displayed the closest relative distance to white matter, followed by group 5 and 2, respectively. Groups 1 and 3, composed predominantly of excitatory pyramidal neurons, had the closest relative distance to the pia mater. Figure 10B shows that the different neuronal groups, although overlapping, indeed have their somata located at different cortical depths [Kruskal-Wallis, $H(5, N=150) = 14.09$, $p<0.05$]. Additionally, the most proximal dendritic process in relation to the pia mater was also measured. These data sets are also expressed in percentage form where *relative location* of the most distal dendritic process was obtained and analyzed. Figure 10C depicts the trends of the relative distance from distal dendritic process to pia. The present data indicate that Group 3 has the closest distal processes to pia while groups 5 and 6 have the farthest. Statistical analyses revealed that each neuronal group indeed demonstrated significant differences in terms of distal dendritic location [Kruskal-Wallis: $H(5, N=150) = 38.18$, $p<0.001$] relative to cortical width. In summary, these analyses provided additional support for our classification methodology, since these relative distance data were withheld from the initial PCA/cluster analysis, and statistical significance was still found when post-clustering analyses were performed between the neuronal groups.

3.3. Sholl analyses

Sholl analyses were utilized to determine the complexity of the traced dendrites. The number of intersections, dendritic spines, and dendritic nodes in 10μm increments

away from the soma were calculated as described in methods. Figure 11A illustrates a schematic of how the measurements were made.

Intersections: Figure 11B depicts the number of intersections with the Sholl annuli for each group of their basilar dendrites. Since not all groups have definable apical dendrites, we confined our between group analyses to non-apical dendrites. The peak number of intersections for all groups is approximately at 30-50μm away from the soma. In general, Group 2 neurons contained significantly more intersections at every distance point, followed by groups 1, 3, 5, 4 and 6. Statistical results (Kruskal-Wallis) indicated that the number of dendritic intersections significantly varied across neuronal groups ($p<0.001$), and there is also a significant effect of the distance from the soma (one-way repeated ANOVA, $p<0.001$). These differences across neuronal groups were no longer significant at distance points greater than 180μm from the soma, most likely due to the small numbers of basilar dendrites that exceeded this length.

***Spines*:** Dendritic spines are the principal sites of excitatory inputs onto cortical pyramidal cells (White, 1989). During the reconstruction of the neurons, the location of the spines was noted and Figure 11C shows the number of *total dendritic (i.e. apical + basilar) spines* for each group. Overall, the number of observable dendritic spines peaked at approximately 30-50μm away from the soma, with Group 2 neurons exhibiting the highest number of spines at every distance compared to other groups. Statistical results (Kruskal-Wallis) indicated that the number of dendritic spines significantly varied across neuronal groups ($p<0.001$), and a main effect of distance away from the soma was also found (one-way repeated ANOVA, $p<0.001$). These differences between groups are no

longer significant past the 250μm mark from the soma, mainly due to the small number of dendrites present. In addition, there is a significant difference in the overall, averaged dendritic spine density across the clustered six neuronal groups [*Kruskal Wallis:* H(5, N=120) = 26.13, $p<0.01$]. We corrected the density of spines by taking the accumulative dendritic length into account. Figure 11C (*inset*) showed that neuronal Group 2 exhibited the highest average density of dendritic spines, followed by Groups 1, 3, and 4. Group 5, and particularly Group 6 displayed very few spines overall.

Dendritic Nodes: Dendritic nodes (origin of bi/trifurcation) are indicators of the complexity of neuronal morphologies (Uyling et al. 1986; Libersat & Duch, 2004). To investigate the variability of dendritic morphology across neuronal groups, we examined the number of nodes as a function of distance from the center of somata (Figure 11D). A significant statistical finding suggested that distinct variability of dendritic nodes indeed exists across groups (Kruskal-Wallis, $p<0.01$). Although there is a significant effect of distance on the number of dendritic nodes displayed (one-way repeated ANOVA, $p>0.01$), very much like dendritic intersections and spines, the differences between groups are no longer significant past the 170μm mark from the soma.

In summary, our Sholl analyses sampled neurons in parameters of dendritic intersections, spines, and nodes. The obtained data were consistent, in that Group 2 neurons exhibited the highest values in all surveyed dimensions, followed by Groups 1 and 3. The vast number of statistical significances found across multiple zones of concentric spheres as a function of distance away from the somata have further supported

that our clustering methodology is an effective method to objectively determine neuronal classes.

3.4. Dendritic fanning polarity

Using the center of soma as the pivot point, twelve 30° pie-shaped regions were created for each neuron. We arbitrarily selected the direction of pia to be 0°, and the direction of inferior/lateral to be 90°. The direction towards the white matter and the superior/medial path would be 180° and 270°, respectively (for a schematics showing the dendritic orientation with respect to the gross anatomy of neocortex, see Figure 12A). Results of polarity analyses revealed that each neuronal group has a unique dendritic fanning pattern (Figure 12B-G). For this part of the analysis, atypically oriented pyramidal neurons were excluded in order to preserve the internal consistency and the reliability of the data, especially in regards to the projecting orientation of the apical dendrites.

Group 1 (Figure 12B): It is clear that this particular group of neurons exhibited extremely long apical dendrites (shown by dotted line). Excluding the atypically oriented pyramidal neurons (n=2), results of repeated-measure ANOVA followed by Tukey's post-hoc criterion revealed that the apical dendrites of this neuronal group have a strong tendency to point towards the pia (0°) [$F(11,143) = 39.50$, $p<0.001$; post-hocs: $p<0.01$]. Surprisingly, results of the basilar dendritic analysis (shown by solid line) also reached statistical significance [$F(11,143) = 2.10$, $p<0.05$]. The findings of Tukey's post-hoc criterion suggested that these basilar dendrites tend to avoid the 30° and 330° wedges,

which are the regions immediately adjacent to 0°, and have a strong tendency to spread in the 180° direction [p values < 0.05].

Group 2 (Figure 12C): This group of neurons displayed relatively spherical dendritic fanning pattern, as suggested by non-significant result of ANOVA [$F(11,77)=1.19$, $p=0.31$]. However, due to the small sample of neurons clustered in this particular group (n=8), a more powerful pairwise test was utilized to compensate for the lack of power. Indeed, results of the pairwise Hayter-Fisher LSD suggested that the dendrites of this neuronal group tends to point towards the white matter (180°), and avoid horizontal projection (evident by small values obtained in 60° & 300°).

Group 3 (Figure 12D): Morphologically, this group of cells exhibited morphometric characteristics that are consistent with classical pyramidal neurons. Excluding the atypically oriented pyramidal neuron (n=1), statistical analyses revealed that there is a tendency for the apical dendrites to project towards the pia (0°), as well as a slight predilection for the 30° lateral/inferior direction [$F(11,473)=133.49$, $p<0.001$; Tukey post criteria: $p<0.05$]. The differences of basilar dendritic fanning as a function of geographic polarity is also significant [$F(11,473=8.65$, $p<0.01$]. Results of post-hoc analyses using Tukey criterion showed that Group 3 neurons exhibit high basilar dendritic fanning in 60° to 240° from pia mater, and tend to avoid the 0°, 30°, and 270° degree regions where the apical dendrites usually occupy.

Group 4 (Figure 12E): As previously mentioned, this group exhibited a high percentage (25%) of atypically oriented neurons. Excluding the atypically oriented

pyramidal neurons (n=10), it is clear that the apical dendrites of this group have a strong predilection for the pia mater (0°) [$F(11,275)=104.73$, $p<0.01$; Tukey post-hocs: $p<0.05$], with no fanning preference for other polar-wedged regions. Their basilar dendrites are inclined to spread 210° and 240° from pia mater, and shun from the direction of the pia [$F(11,27)5=4.93$, $p<0.01$; Tukey post-hocs: $p<0.05$]. In converse, statistical analyses of the atypically oriented pyramidal neurons revealed that the apical dendrites of these neurons have a strong predilection to project toward the 270° direction (medial and superior) with no preference of any other direction [repeated-measure ANOVA, $F(11,99)=2.96$, $p<0.01$; post-hoc criterion: Fisher LSD, $p<0.01$]. However, there was no clear indication of the preferred projecting direction for these atypically oriented neurons when it comes to the basilar dendritic fanning pattern [$F(11,99) = 0.88$, $p>0.55$].

Group 5 (Figure 12F): For this group, there is a significant correlation between dendritic fanning pattern and polarity region [$F(11,286)=2.87$, $p<0.01$]. Post hoc criterion using Fisher-LSD criterion indicated that overall, dendrites in this group tend to project in the direction towards 0°, 150°, 330° (p values <0.05), and avoid directions towards 30°, 90°, 120°, 180°, 210°, 240°, and 270° degrees (p values <0.05).

Group 6 (Figure 12G): Neurons clustered in this particular group exhibited a weak predilection for dendritic projection towards the pia at 0° [$F(11,121)=3.64$, $p<0.01$; Fisher LSD post-hocs: $p<0.05$]. Furthermore, there are no predilections for other polarity regions displayed by Group 6 neurons.

The results of this post-clustering analysis suggested that each distinct neuronal group displayed its own unique dendritic fanning polarity, indicating that perhaps each neuronal group is sampling different inputs. Moreover, it reflected the difference in spatial capacity across classified neurons group. For example, it can be inferred that Group 1 neurons have much better interlaminar processing capacity than Group 4 neurons, due to the dramatically higher dendritic length in the 0° direction. The results also support the validity of our initial morphological classification.

Chapter Six: Discussion:

Taxonomizing Layer VI Neurons in Mouse Barrel Cortex Based on Morphological Characteristics using a Quantitative Approach

The goal of this portion of the dissertation is to understand the cellular components of layer VI of the mouse barrel field. We reconstructed 150 Golgi-impregnated neurons and analyzed 35 morphological variables that included somatic and dendritic factors. Using a PCA followed by a cluster analysis (Ward's Method, Euclidean Distance), we were able to use strict and objective morphological criteria to effectively cluster the neurons into six distinct groups.

The reconstructed neurons in the present study fall in two major categories: neurons with and without apical dendrites. Specifically, the neurons clustered in Groups 1, 3, and 4 exhibited apical dendritic features while Groups 2, 5, and 6 did not. Group 1 neurons are pyramidal neurons with elaborate dendrites, characterized by extensively long overall dendritic length. Group 2 includes complex multipolar and bipolar neurons which are presumed to be interneurons. These neurons possessed intricate dendritic fanning pattern and thick dendrites. Group 3 consists of pyramidal neurons with apical dendrites that typically terminate in lower layer IV or upper layer V. Group 4 is composed of simple, small pyramidal neurons that have both limited apical and basilar dendritic processes. In addition, a high proportion of Group 4 neurons displayed atypical fanning orientation. Group 5 non-pyramidal neurons based on their somatic properties and lack of apical dendrites included stellate, bipolar, and horizontal cells. Group 6 contained small interneurons with limited dendritic processes. A subgroup of Group 6, despite possessing triangular somata, did not present with apical dendritic features. Collectively, the results

indicated that a variety of neuronal morphological classes can be quantitatively defined within this heterogeneous layer of the mouse barrel field.

The post-clustering analyses strongly supported the validity of our initial choice of statistical methods (a PCA followed by a cluster analysis), and therefore suggest that neuronal populations can be quantitatively analyzed and classified using this methodology. Non-parametric statistical procedures (e.g. Kruskal-Wallis) were the tests of choice due to the highly unequal number of cells clustered across neuronal groups. Homogeneity of the relative somata locations indicated that most likely all of the reconstructed neurons were within layer VI. Moreover, laminar location analyses revealed that the distal dendritic processes of each neuronal group varied significantly, which further supported the validity of our clustering method. The data derived from our Sholl analyses reflected that the neuronal groups differed considerably in all surveyed parameters of dendritic *intersections*, *spines*, and *nodes*. These Sholl results further supported the trends of significance across the categorized neuronal groups, suggesting that each neuronal group exhibits its own unique dendritic pattern as the distance from the somata varies. Additionally, analyses of the dendritic polarity also revealed remarkable differences in dendritic fanning pattern across neuronal groups. In summary, these post-clustering data have provided support that our initial classifying methodology was valid. Previous studies exploring the neuronal morphologies have also used similar classification techniques (Sultan and Bower, 1998; Tsiola et al., 2003). The finding that each group had distinctly different dendritic architectures and spine densities suggests that they might have different roles in local cortical circuits.

1. Functional Implications

Neocortical layer VI provides important feedback to the thalamus and layer IV, and therefore plays a crucial role in gating / modulating sensory information. This in turn influences sensational and perceptual experiences in general. It is highly probable that the differences in cellular morphology are correlated with different cortical roles, as well as different microcircuits. For instance, the larger dendritic fields of group 2 suggest that they may integrate information from a greater part of its associated cortical column than neurons from group 4 and 6 that have more confined dendritic trees. Our spine density analyses can be used as possible correlates of the number of synaptic inputs that a specific neuronal class generally receives. Based on our spine density analysis, group 2 neurons receive the greatest density of neuronal inputs. By applying the size principal (Fromm & Evarts, 1981), it may be inferred that the larger pyramidal neurons (e.g. Group 1) are more difficult to be recruited to fire than pyramidal neurons with smaller somata (e.g. Group 4). It is also possible that the diversity in layer VI is reflective of the neurons participating in the many different networks of afferent and efferent projections, such as corticothalamic, ipsilateral and contralateral cortico-cortical, and cortico-striatal pathways. In sum, characterizing the neuronal elements within layer VI is an important first step towards understanding the building blocks of cortical circuits and their role(s) in cortical computations.

Following this approach, we can start to elucidate this extremely diverse cortical layer by understanding the physiology of each type of neurons. It is also essential to investigate the functional anatomical properties of the categorized neurons based on afferent/efferent inputs. By implementing recently developed genetic labeling

techniques, future studies may aim to investigate the nature of monosynaptic restriction of transynaptic tracing in the barrel field (Wickersham et al., 2007). In summary, layer VI is a poorly understood layer in terms of the microcircuitry of the neocortex, mainly because of its complexity. Furthermore, it is also due to this complexity, along with the role of this layer as a gateway for feedback to subcortical structures such as the thalamus (Tombol, 1984; White, 1989), that this layer is of great interest. Therefore, it becomes important to analyze layer VI quantitatively, since this analytical approach provides a more accurate and unbiased way of studying neuronal cytoarchitectures. Identifying specific types of neurons within layer VI is the first step of understanding the role of this complicated cortical layer plays in sensation and perception.

2. Methodological Considerations

It has been previously shown that the intensity of impregnation increases as the age of animal increases (Furtak, 2007), in which by PND15, silver chromate impregnation appears to be complete. Since we chose to use adult mice with ages of ~PND 90, the Golgi impregnation method should completely fill all, or at least nearly all of the neurons that were reconstructed. Moreover, although rare during our neuronal reconstruction phase, if we were to encounter a neuron that was suspected of being incompletely filled, we discarded that particular neuron from the reconstruction. Therefore, it likely that our reconstructed neurons are an extremely accurate reflection of the cellular components in layer VI.

In order to avoid tracing error, during the reconstruction phase we avoided neurons that clumped together with a high proportion of staining artifacts. It is possible that these neurons exhibited yet another morphological type than the neurons that are presented in the current study. However, technical problems arise from tracing neurons with adjoined cell bodies, as their dendrites are located very closely together, therefore making it difficult to distinguish which dendrite belongs to which neuron. In terms of validity of the sampling, prior studies have suggested that the Golgi staining method has a slight predilection for labeling neurons with larger somata (Pasternak & Woolsey, 1975). We reconstructed every neuron that exhibited complete staining, with the exception of neurons with cut dendrites and neurons that were clumped together. It is important to note that we observed a wide range of somata diameters (small to large), and since we did not attempt to predict the relative frequency of the different groups, the Golgi method is well suited for our study. Therefore, our "combing" method of neuronal sampling is most likely an extremely effective and accurate presentation of all Golgi labeled neurons in mouse barrel field layer VI. In conclusion, our accurate tracing of the completely filled neurons as well as our relatively unbiased sample are very likely a correct reflection of the morphologically diverse layer VI.

Many prior studies interested in neuronal classification have relied on qualitative and subjective criteria for categorizing neuronal groups (Furtak et al., 2007, Prieto & Winer, 1999; Ferrer et al, 1986; Lorente de No, 1922). By contrast, our study uses quantitative measurements as the criteria to categorize neurons based on their morphologies. Other prior studies, although limited in number, have also used PCA and cluster analyses to classify neurons quantitatively (Tsiola et al, 2003; Sultan & Bower, 1999). We followed

the progression of these studies' objective and unbiased methodology of characterizing neuronal groups and at the same time performed additional confirmatory and post-clustering analyses in order to support the validity of our neuronal categorization results. It is important to note that our quantitative method still allowed the neurons with similar phenotype to be clustered in the same group or subgroup, as if they were qualitatively grouped together. This further supports the validity of our methodology since the human element of bias is removed, and yet we were still able to classify the neurons based on their morphology efficiently. Additionally, our data indicated that the density of spines significantly differed across the classified neuronal groups. Since the spine data were withheld from the initial PCA and cluster analysis, our significant finding in the post-clustering analysis strongly supports the validity of our methodological choice. The layer VI of the mouse cortical system may be different from that of other mammals such as felines (Prieto & Winer, 1999) and primates (Brigs and Callaway, 2001). The overall results of the current study indeed had some discrepancies with these prior studies. For instance, Brigs and Callaway (2001) found several distinct subgroups of neurons with apical dendrites extending well beyond layer IV in the primary visual cortex. Prieto & Winer (1999) observed horizontal cells with very elaborate dendritic patterning in the primary auditory cortex, whereas we observed similar neurons with less elaborate dendritic arborizations. It is likely that the mouse barrel system required different adaptations than these other mammals. It is also possible that the observed discrepancies are correlated with the differences in perceptual modality between studies.

Chapter Seven: Introduction:

Investigating the Effect of Chronic Sensory Deprivation on the Morphological Development of Cortical Neurons in Layer VI of Mouse Barrel Cortex.

One of the fundamental features of the cerebral cortex is its remarkable ability to adapt to the sensory environment. These adaptations can be observed in behavioral, physiological, neuroanatomical, genetic, and/or biochemical changes (for reviews see Buonomano and Merzenich, 1998; Sur and Rubenstein, 2005; Feldman and Brecht, 2005; Fox and Wong, 2005). Neuroanatomically, these adaptations are correlated with changes observed in cortical areal patterning, cytoarchitecture, dendritic spinogenesis / synaptic pruning, all resulting from significant disruptions in sensory experience during post-natal development (Van Der Loos and Woolsey, 1973; Simons and Land, 1987; Carvell and Simons, 1996; Maravall et al., 2004; Zuo et al., 2005; McRae et al., 2007; Bruno et al., 2009; Hardingham et al., 2008; Takasaki et al., 2008; Briner et al., 2010; Popescu and Ebner; 2010). Of particular interest is the reorganization of dendritic arborizations following alterations in sensory experience and cellular activity. For example, it has been demonstrated in the visual system that following monocular deprivation, the dendritic fanning of layer IV spiny stellate cells showed directional preference towards the innervated ocular dominance column while simultaneously avoiding the deprived cortical column (Kossel et al. 1995). Similarly in the whisker-to-barrel system, blocking cellular activity by knocking out a subunit of the cortical glutamate receptor resulted in dendritic fanning with significant areal overlap and crossings into the neighboring layer IV barrels (Datwani et al., 2002), a phenomenon not observed in wild-type animals. In addition, this change in dendritic cytoarchitecture is not limited to layer IV, the main recipient

zone of thalamocortical afferents, but is also observed in the overlying layer III pyramidal cells whose basilar dendrites reach into layer IV (Maravall et al., 2004). In the adult cerebral cortex, it has been suggested that neuronal morphology is more stable and therefore requires considerably more dramatic measures such as peripheral lesions to induce dendritic reorganizations (Trachtenberg et al., 2002; Hickmott and Steen; 2005, Taibey et al., 2005).

Despite the focus on the effects of sensory experience on neuronal architecture in the principal thalamic recipient zone (layer IV), surprisingly little data are available on its influence on pattern formation of dendrites originating from layer VI neurons which also receive direct thalamic input. Developmentally, layer VI is the earliest cortical layer to differentiate from the ventricular zone, with the glutamatergic pyramidal cells being the first neurons to move into position in the cortical plate (for reviews see Rakic, 2009; Thomson, 2010). Anatomically, layer VI also provides an abundance of projections to diverse regions such as the thalamus, multiple cortical areas, basal ganglia, claustrum, and the spinal cord (for review see Thomson, 2010). This strategic anatomical positioning and wealth of connectivity suggests that this deepest cortical layer plays roles in multiple cortical functionings such as memory, object recognition, perceptual adjustment / gain control, sensori-motor integration, hemispheric balancing, and perhaps ultimately, consciousness (Katz, 1987; Sherman and Guillery, 2002; Crick and Koch, 2005; Andolina et al., 2007; Rocco et al., 2007; Ramos et al., 2008; Denton et al., 2009; Lopez-Aranda et al., 2009; also see Thomson, 2010). Therefore, it is of great interest to understand how disruptions of sensory experience during development may potentially impact the structure, and in turn functioning, of layer VI.

This section aims to investigate the alterations of layer VI neuronal structures that resulted from chronic sensory deprivation in developing animals. Sensory deprivation was induced via whisker trimming as has been done previously (Simons and Land, 1987; McRae et al., 2007) and in combination with our recently developed morphometric analyses (Chen et al., 2009), we digitally reconstructed Golgi-impregnated neurons and quantify morphological changes of somata, apical and basilar dendrites of pyramidal and non-pyramidal cells.

Chapter Eight: Material and Methods:

Investigating the Effect of Chronic Sensory Deprivation on the Morphological Development of Cortical Neurons in Layer VI of Mouse Barrel Cortex

1. Experimental Animals and Chronic Sensory Deprivation

The selection and treatment of experimental animals were followed exactly as previous described (McRae et al., 2007) and in accordance with the Queens College, CUNY Institutional Animal Care and Use Committee and NIH guidelines. Briefly, each animal from a litter of CD-1 mice was arbitrarily assigned at birth to be either in the control (n=4) or sensory deprived (n=4, whisker trim) condition. For the sensory deprived animals, the whiskers were manually clipped by precision microscissors as close to the base of the follicle as possible every other day for the animals' first 30 postnatal days. Brief administration (~1 minute) of anesthesia (5% isoflurane, Aerrane) was used from postnatal day 14 to prevent the animals from moving during the trimming procedure. The within-litter control method was followed: all animals were exposed to the same conditions such as bedding texture, food and water source, maternal influence, anesthesia, handling, etc. The control animals were handled, anesthesized, and returned to the cage on the same trimming session as the sensory-deprived animals.

2. Golgi Staining Procedure and Tissue Processing

Brains were processed with our Golgi protocol as previously described in Chapter Four (section 2) portion of this thesis.

3. Cell Selection, Reconstruction, Morphometric Quantification, and Statistical Analyses.

S1 barrel cortex was located by identifying the characteristic clusters of cells that are typically found in granular, supragranular, and infragranular layers (Figure 1A-B) and by comparing with an atlas of a Golgi-stained mice brain (Valverde, 1998). Neuronal somata and dendritic arborizations were examined and carefully reconstructed using an Olympus BX51 microscope with a 60x (oil immersion, NA 1.4) objective. The microscope was equipped with a digital camera (Microfire, Optronics, Inc.), a mechanical stage (Ludl, Thornwood, NY), and an x-y-z axis encoder connected to a Windows Pentium-4 PC. Neurolucida software (version 8.0 by MBF Bioscience, Inc.) was used to visualize and manually reconstruct the cell bodies and dendrites as closely as possible (see Figure 1C-D). Only the neurons that exhibited complete Golgi impregnation without significant staining artifacts were selected for reconstruction. Since the role of atypically oriented (e.g., inverted) pyramidal neuron is still unclear and might be rather heterogeneous (Mendizabai-Zubiaga et al., 2007; Chen, 2009), the pyramidal cells that exhibited atypical orientation were excluded from our reconstructions. NeuroExplorer (MBF Bioscience, Inc.) was used to quantify numerous morphological measurements (see Tables 1, 2, and Results), as previously described (Chen et al., 2009). The explored morphological characteristics included somatic shape and size, dendritic structure, branching patterns, and Sholl analysis (Sholl, 1956). We quantified approximately ~35 morphological variables per reconstructed neuron (see Tables 1, 3, 4 and Results), and treated each neuron as an individual case (see Chen et al., 2009). We then performed

parametric pair-wise comparisons (two-tailed independent group t-test) between the control and sensory-deprived groups due to the relatively comparable number of neurons across groups.

Chapter Nine: Results:

Investigating the Effect of Chronic Sensory Deprivation on the Morphological Development of Cortical Neurons in Layer VI of Mouse Barrel Cortex

We previously reported that layer VI neurons (as defined by somata located between the white matter and layer V, using the large pyramidal neurons to mark the superficial layer V to VI border, see Chen et al., 2009) in S1 barrel field can be morphologically classified into two distinct categories: those with and without apical dendrites (e.g., pyramidal and non-pyramidal cell types; Chen et al., 2009). In this present study we therefore divided layer VI neurons into these two categories as well (for the visual representation of digitally reconstructed neurons, see Figure 13), and performed corresponding morphometric analyses in the sensory deprived vs. control conditions in these two groups of neurons. Since the conditions were held constant (handling of animals, anesthesia, tissue processing methodologies, tissue sectioning thickness, etc.), we propose that the observed differences in morphological variables are most likely due to the effect of peripheral sensory deprivation from birth.

1. Effect of Chronic Sensory Deprivation on Dendritic Arborizations of Non-pyramidal Neurons

The results of our morphometric quantification of non-pyramidal neurons (*sensory deprived n=21 neurons, control n=35 neurons,* all data are expressed as per neuron unless otherwise noted) suggested that the shape of somata were not significantly

affected by chronic sensory deprivation (statistically non-significant for all 10 investigated somatic variables). By contrast, we observed several significant changes in the dendritic components of these non-pyramidal neurons as a result of chronic sensory deprivation (see Table 3 and Figure 14). Overall, with exception of the primary *dendritic quantity* (defined as the number of dendritic trunks sprouting from somata), which did not vary significantly between conditions, all other dendritic components were significantly elevated in the animals that experienced chronic sensory deprivation compared to control animals (p's <0.05). These dendritic components included the number of *dendritic nodes* (bi- or tri-furcations per neuron), *dendritic ends*, *dendritic length*, *mean dendritic length* (per dendrite per neuron), total *dendritic surface area*, *mean surface area* (per dendrite per neuron), *dendritic volume*, and *dendritic mean volume* (per dendrite per neuron). The non-pyramidal neurons of animals that experienced chronic sensory deprivation showed increased total length of dendritic trees as well as increased number of higher order (non-primary) dendritic branches. Results from our Sholl analyses (between-groups ANOVA; posthoc: Tukey HSD, significant at $p<0.05$; Figure 15) showed that the changes are in dendritic segments between 30-90 µm from the soma, with significant increases seen in the number of intersections and increases in dendritic length in this region of the dendritic arbor. The unchanged segments are the immediately proximal (<30µm from the soma) and the very distal segments of the dendritic tree (>100µm for dendritic intersections and >120 µm for dendritic length, see Figure 15A and 15B). This pattern of data suggests that sensory deprivation does not significantly influence the proximal cellular architecture components of layer VI non-pyramidal neurons. These results are consistent with our findings that there were no changes in any of the somatic parameters, nor in the number of primary dendritic trees, nor the number of immediate proximal dendritic segments.

However, the effect of chronic sensory deprivation on the intermediate neuronal regions is evident, as indicated by the increased number of bi/trifurcations and dendritic ends, which are indicators that there was more dendritic branching in this region of the cell's dendritic tree (see Table 3). The results of our Sholl analyses further supported the finding that the intermediate dendritic areas are largely affected as well (Figure 15A and 15B).

2. Effect of Chronic Sensory Deprivation on Pyramidal Neurons

The somata of pyramidal neurons, unlike the non-pyramidal neurons, were affected by chronic sensory deprivation from birth. This might be the due to the fact their apical dendrites, unlike the dendrites of non-pyramidal neurons which only extend within layer VI, are sampling across layers VI, V, and in some cases, layer IV (see Chen et al., 2009). It was observed that soma *perimeter, area, feret maximum* (longest axis of the soma) *and minimum* (longest axis perpendicular to *feret maximum*) were considerably increased in the sensory deprived condition compared to the control animals (*sensory deprived n=39 neurons, control n=35 neurons*). Other somatic factors that indicated the intrinsic shape of somata (*aspect ratio, compactness, convexity, form factor, roundness, solidity*, for descriptions see Specific Methods Part I, also Table 3) were not affected significantly (Table 4). This suggests that while there is a proportional increase of somata size following sensory deprivation, the fundamental geometric shapes of the pyramidal somatic morphology was unchanged (i.e., sensory deprivation did not alter the triangular somata of pyramidal neurons into spherical ones or vice versa).

Apical and basilar dendrites of layer VI pyramidal neurons responded to chronic sensory deprivation in opposite ways. The apical dendrites in the sensory-deprived mice showed significant decrease in a variety of related parameters, including *apical dendritic nodes*, *apical dendritic ends*, *apical dendritic length*, *apical dendritic surface area*, and *apical dendritic volume* (Figure 16, also see Table 4). Detailed investigation using Sholl analyses (between-groups ANOVA; posthoc: Fisher LSD, statistical significance at $p<0.05$) on *apical dendritic intersection, apical dendritic length* indicated that these differences were predominantly distal to the somata (see Figures 17), suggesting that this significant decrease of apical dendritic features was most likely occurring outside of layer VI. In sum, these findings are consistent with an overall retraction of the apical dendrite.

In contrast to the overall decrease of apical dendritic components, the basilar dendritic components showed significant increases in their dendritic span (Figure 18, also see Table 4), exemplified by elevated *basilar dendritic nodes*, *basilar dendritic ends*, and *basilar dendritic length* (between-groups ANOVA; posthoc: Fisher LSD, statistical significance at $p<0.05$). Interestingly, this increase of basilar dendritic parameters was also observed in the dendrites of non-pyramidal neurons. One of the commonalities they shared was that most of these dendrites were limited to layer VI. Even though the increase might not be as robust as the nonpyramidal neurons, the overall trend still suggested that the basilar dendritic features of pyramidal neurons experience significant expansion. Further examination with the Sholl analyses revealed that similar to the nonpyramidal neurons, this increase in basilar dendritic arborization is mostly observed in the intermediate-to-proximal region (Figure 19), indicating that its effect is generally confined to layer VI. Lastly, the total dendritic (apical + basilar) components showed no

significant change, including *total dendritic quantity*, *nodes*, *ends*, *length*, *surface area*, and *volume* (Table 4), indicating that there might be homeostatic mechanisms of dendritic morphology similarly to previously proposed in the hippocampal system (Samsonovich and Ascoli, 2006). Taken together, our data suggest that apical and basilar dendritic components responded to chronic sensory deprivation in opposite fashions; however these changes counterbalance each other resulting in no significant change in the total dendritic components.

Chapter Ten: Discussion:

Investigating the Effect of Chronic Sensory Deprivation on the Morphological Development of Cortical Neurons in Layer VI of Mouse Barrel Cortex

The goal of the current research was to describe the effect of chronic sensory deprivation on the development of neuronal morphologies, specifically in somatic, apical dendritic and basilar dendritic components in neocortical layer VI. The rodent whisker-to-barrel cortex is an ideal system to study the impact of sensory experience on neuronal morphology due the ease of inducing sensory deprivation and correlating it with known anatomical structures (see Fox and Wong, 2005; Feldman and Brecht, 2005; Petersen, 2007). Our data suggest that neurons in layer VI of barrel cortex respond to chronic sensory deprivation by altering their somata (in case of pyramidal neurons) and dendritic architectures during development. While the somata of non-pyramidal neurons do not respond to chronic sensory deprivation, their dendrites are dramatically affected and showed a significant increase in almost every dendritic variable investigated. In pyramidal neurons, key somatic structures such as *perimeter, area, feret maximum and feret minimum* showed significant elevation following chronic sensory deprivation, and the apical and basilar dendrites of layer VI pyramidal neurons responded differentially. Apical dendrites showed an overall trend to decrease following chronic sensory deprivation while basilar dendrites showed an overall trend to increase.

It has been previously demonstrated in the primate striate cortex that chronic dark rearing from birth induced the expansion of dendritic fields (Neal et al., 1985). Also, a recent study in the whisker-to-barrel system showed that brief sensory deprivation at birth

(for three days) led to increased dendritic span in layer IV spiny stellate cells (Lee et al., 2009). Here, our data provide evidence that similar phenomenon is also observed in developing layer VI of the rodent somatosensory cortex, in which significant changes in dendritic arborizations results from chronic sensory deprivation. In addition, we show that this effect exists in both pyramidal and nonpyramidal neurons, with its effect more pronounced in nonpyramidal cells. Within the developmental period, it is known that the dendrites of layer VI neurons dramatically increase in both number and length during the first several weeks after birth, followed by massive dendritic pruning (Lübke and Albus, 1989). This study also showed that the size of somata, as indicated by the length of diameter, also steadily increased during the first month of postnatal development. One possible explanation of our results is that chronic sensory deprivation has stunted the dendritic pruning process, leading to comparatively elevated dendritic parameters such as increased dendritic length, ends, surface area, and volume that are reported here. This idea has been previously proposed (Bestman et al., 2008) and is consistent with the finding that dark rearing delays the dendritic pruning process (Tian and Copenhagen, 2003). Likewise in present study, chronic sensory deprivation resulted in increased somata size and basilar dendritic field in pyramidal neurons, as well as an overall increase of dendritic field in nonpyramidal neurons, suggesting that sensory deprivation delays experience-dependent changes in both dendritic and soma maturation.

Physiological studies have shown that there is a shift in the balance of excitatory / inhibitory cortical networks following chronic sensory deprivation (Lee et al., 2007; Marik et al., 2010; Sun, 2009). This shift in balance is exemplified by the excitatory regular spiking units (RSUs) and the inhibitory fast spiking units (FSUs) responding in different ways following chronic sensory deprivation (Lee et al., 2007; Sun, 2009). The

increased expression of parvalbumin in GABAergic neurons and associated decrease of perineuronal net expression has been proposed to be responsible for this sensory deprivation induced network shift (Jiao 2006; McRae et al., 2007). The net result is increased noise activity in response to whisker stimulation (after whisker regrow) within layer IV and decreases in signal to noise ratio (Simons and Land, 1987) which may underlie the finding that deprived animals have poorer discriminatory abilities (Carvell and Simons 1996).

Our findings add to the growing body of knowledge that the cerebral cortex adapts to environmental manipulations in a layer-specific fashion (Oray et al., 2004, Lee et al. 2007), and based on the present data in a cell specific manner as well. The differences in reorganization of the apical and basilar dendrites of pyramidal neurons are reminiscent to what is seen in response to chronic stress (by placing the experimental animals in plastic restrainers, hence increasing plasma corticosterone) (Cook and Wellman, 2004; Garrett and Wellman, 2009). This type of cellular homeostasis in which that apical and basilar dendrites responds in opposite fashion following stress has been proposed and demonstrated previously in the hippocampal pyramidal neurons (Samsonovich and Ascoli, 2006). Our finding suggests that dendrites do not function as an independent unit within a cell, but rather are coordinated: when the source of sensory input is limited, other dendrites may look for active inputs in order to compensate for the optimal activity that the neurons need, perhaps in order to survive. This is further highlighted by our data that total (apical + basilar) dendritic components of layer VI pyramidal neurons did not show a significant difference following trimming, even though apical or basilar components, did show a significant difference in opposite directions.

Golgi impregnation is a staining procedure which removes human selectivity elements, thereby reducing possible bias in labeling the neurons (Paterernak & Woolsey, 1975). The limitation of this particular staining technique is that, one cannot assign a specific functional class of the neuronal type labeled, other than pyramidal vs. nonpyramidal neurons based on the presence or lack of apical dendritic features (Chen et al., 2009). Since the observation of the morphological change in somata and dendrites was made post-manipulation (control vs. sensory-deprived), we cannot rule out the possibility that there was a phenotypic change in the morphology of specific functional classes of neurons. Rather, we can only observe a general morphological alteration of all the labeled pyramidal neurons by Golgi impregnation method. It may be particularly rewarding for future studies to discern the effect of chronic sensory deprivation on specific functional neurons in this understudied layer of the cerebral cortex (e.g., the effect of chronic sensory deprivation on the morphological development of VPm, callosal, S1-M1, projecting neuron, etc.).

Our findings have provided further structural evidence that cortical neurons indeed respond to changes in sensory activation by reorganizing cellular resources in the form of morphological remodeling, perhaps to keep the homeostatic balance within the affected neuronal network.

Chapter Eleven: Introduction:

Investigating the Effect of Chronic Sensory Deprivation on the Development of Dendritic Protrusions in the TCA Recipient Layers (Layers VI and IV) in Mouse Barrel Cortex

Previous studies have investigated and described the circuitry behind the whisker-to-barrel pathway and recent studies are focusing on the molecular and cellular mechanisms that govern cortical activity-dependent synaptic plasticity as result of sensory experience. Plasticity in the barrel cortex was first described by Woolsey and Van der Loos (1973), and it was demonstrated that if vibrissae follicles were ablated shortly after birth, before postnatal day 4, the formation of the barrel cortex was dramatically disrupted. This is often referred as the critical period of barrel cortex formation because the phenomenon was only found to occur during the animal's first few days of life (Weller and Johnson 1975, Woolsey and Wann 1976). Moreover, depriving sensory experience after birth, in addition to altering whisker-related behavior (Carvall and Simon, 1996), also impacts the functional properties of neurons (Simons and Land 1987, Kossut, 1992, Popescu and Ebner, 2010) resulting in alteration of the size of their receptive field of neurons and the strength of their responses to whisker stimulation. Of particular interest is the impact of tactile sensory deprivation on the cellular and molecular components of the barrel cortex during early postnatal development..

In identifying and understanding the substrates that are involved in activity-dependent neocortical development, depriving the animal of sensory experience during the critical period by whisker-trimming has been considered as the gold-standard (Chen et al. 2011, McRae et. al 2007, Zuo et al. 2005, also see Feldman and Brecht, 2005). It

has been previously shown that chronic sensory deprivation from birth resulted in a decrease in the expression of aggrecan; a proteoglycan substrate involved in the formation of the perineuronal net components of the extracellular matrix (McRae et. al 2007). Such a decrease might be linked to the changes in the expression of related cellular constituents such as tissue-plasminogen activator (tPA) which has been proposed as a degrader of extracellular matrix proteins (Mataga et al. 2004, Oray et al. 2004, Chen et al. 2003). These studies have suggested that the cellular expression of proteins can be directly altered by chronically influencing the sensory experience during an animal's development. The current trend of research interest in this field has been on even more subtle aspects, such as the impact of sensory experience on morphological development of dendritic arborizations and spines which are the points of excitatory synaptic contact with axons (Briner et al. 2010, Zuo et al. 2005, Chen et al 2011). Dendritic spines are highly motile structures (Lendvai et. al. 2000, Oray et al. 2004) and it has been shown that depriving animals of sensory experience during the critical period influences spine motility in areas such as the primary somatosensory area and primary visual area. Although these studies have found that sensory experience induces dendritic and spine plasticity in supragranular layers of the cortex, its effect on the principal thalamocortical recipient layers (layers IV and VI) remains unclear.

In this section, we aim to investigate the development of dendritic protrusions in pyramidal neurons located in thalamocortical recipient layers of the rodent primary somatosensory cortex. We first describe the normal maturation profile of dendritic spine and filopodia morphology and density in the barrel cortex, followed by the description of the disrupted pattern of these dendritic parameters due to the peripheral manipulations of sensory experience. In addition, we restored the sensory experience (i.e., allowing the

whiskers to grow back to full-length) as a means to provide recovery of tactile sensation after early postnatal development. We report that chronic sensory deprivation impact dendritic protrusions in a profound way, and restoring sensory experience provides partial recovery of dendritic spine density, depending on the cortical layer. Next, we attempt to correlate the findings of spine density and morphology with the activity of NMDA-R by means of chronically blocking this particular glutamatergic receptor that is known to play a significant role in long-term potentiation (LTP) and long-term depression (LTD). Last, we provide immunohistochemical evidence that a key protein, tissue-plasminogen activator, exhibited correlative alterations following both chronic sensory deprivation and sensory restoration.

Chapter Twelve: Material and Methods:

Investigating the Effect of Chronic Sensory Deprivation on the Development of Dendritic Protrusions in the TCA Recipient Layers (Layers IV and VI) in Mouse Barrel Cortex

1. Animals and experimental groups

CD-1 male and female mice obtained from pregnant mothers were kept in standard laboratory housing with unlimited access to food and water. For the developmental profile portion of the study, we investigated the untreated control animals in these age groups: Postnatal (P) 15, 30, 60, 100, and 130, making this a cross-sectional study investigating the dendritic protrusions (also see Table 6 for n of animals and neurons per condition). In the disrupted development portion of the study, mice were randomly assigned to control, sensory deprivation (see Material and Methods 2) or NMDA receptor blockage group, a subsequent sensory restoration and NMDA antagonist withdrawal group. For the (chronic) sensory deprivation group, whiskers were unilaterally or bilaterally trimmed from post-natal day (P) 0 to 30. For the NMDA receptor blockage group, mice were administered the NMDA antagonist MK801 twice daily from P0 to P30 in the dosage that is previously established (Zuo et al., 2005; in the dosage of 0.25µg per 1*g* of animal body weight, twice per day, intraperitoneally injected). For the sensory restoration group, sensory deprived mice were allowed 1 month for their whiskers to re-grow before their brains were analyzed. For the NMDA antagonist withdrawal group, mice administered MK801 were allowed 1 month without the drug before sacrifice.

2. Sensory Deprivation and Restoration

The sensory deprivation paradigm is identical to that described above in Material and Methods section (2). For the animals that were selected in the sensory restoration condition, we simply stopped trimming and allowed the whiskers to grow back for one month after postnatal day (PND)30. We also performed an ear punch at PND31 for the purpose of identifying which animals belong to the re-grow condition so we can discern these experimental animals from their control littermates at PND60. For the adult sensory deprivation portion of the study, trimming commenced from when the animals were P100 postnatal days of age, and were trimmed every other day and sacrificed at P130.

3. MK801 Injection and Withdraw

Previous findings have implicated the importance of glutamatergic activities in influencing the dendritic arborization as well as protrusions (Zuo et al. 2005, McAllister 1996). To explore the possible mechanisms that are responsible for the effect of sensory deprivation on the development of dendritic spine entities, we intraperitoneally injected MK801, a non-competitive NMDA-R blocker (0.25μg g^{-1} body weight) twice per day, starting from the P0 of the treatment animals. Due to the fact that MK801 is a hypothermic inducer, the cages were periodically kept artificially above room temperature one hour after administering MK801 for the purpose of reducing the mortality rate of experimental animals. Typical mortality of MK801-injected animals in

the first postnatal week is approximately 80-85% without placing the pups in above-room temperature conditions. Placing them one hour in above-room temperature (~28 - 30˚C) decreased the mortality rate to approximately 50% during the first postnatal week. For the animals that were selected in the drug withdrawal condition, we simply stopped administering MK801 after postnatal day (PND) 30. We also performed an ear punch at PND31 for the purpose of identifying which animals belong to the drug-withdrawal condition so we can discern these experimental animals from their control littermates at PND60.

4. Golgi Impregnation

Brains were processed with our Golgi protocol as previously described earlier in Material and Methods (see Chapter Four, section 2) portion.

5. Identification of Barrel Field

In order to accurately identify the barrel cortex, the characteristic cluster of cells found in granular and supragranular layers were observed (See Figure 1) and then matched with an atlas of a Golgi-stained mouse brain (Valverde, 1998), same as mentioned in previous chapters. The anterior limit of the barrel cortex was identified by the appearance of the anterior commissure and Golgi-stained pyramidal neurons in layer IV and VI were identified on opposite borders of the large pyramidal neurons characteristic of layer V. The posterior limit of the barrel cortex was identified by the separation of the corpus callosum at the midline.

6. Neuronal Selection/Reconstruction/Spine Classification

Imaging of neurons and their respective dendritic protrusions (basilar dendrites of pyramidal neurons those somata located in layers IV and VI, respectively) was accomplished with the Neurolucida system (MBF Bioscience, Inc) and an Olympus Bx51 microscope equipped with a high-resolution digital camera (Optronics Microfire), a mechanical stage (Ludl, Thornwood, NY), and an x-y-z axis encoder connected to a Windows XP Pentium 4 PC. Neurons were initially imaged under 10x (0.25 Numerical Aperture) magnification and in layer IV and VI, each candidate pyramidal cell for future reconstruction and dendritic spine analysis was labeled with a marker (small asterisk). At 60x oil magnification (1.4 NA), pyramidal cells were further examined for uncut basilar dendrites of length >100μm. Finally at 100x oil magnification (1.4 NA), the dendrite would be examined so as to ensure that its dendritic spines had been thoroughly labeled with the Golgi-Cox solution to reveal their distinct morphologies (See Figure 1). The experimenter would begin to reconstruct the soma and basilar dendrite and then move on to classify the dendritic spines into 5 major morphological categories (See Figure 20, adapted from classification scheme of William Greenough, see Comery et al. 1997, Irwin 2002) by labeling each type of dendritic protrusion with a different marker. Approximately 15-18 neurons per layer in each condition were used for reconstruction of dendrites and their representative dendritic spines. In general, only the basilar dendrites that are longer than 100μm are selected for the quantification of protrusions.

7. Statistical Methods of Analyzing Spine Density/Morphology

The NeuroExplorer software enabled detailed analyses of the lengths and overall dendritic spine densities. Spine density was computed as the total number of recorded spines in that particular dendrite divided by the total length of the dendrite (expressed in number of dendritic spines / 10μm dendritic length). The mean, standard deviation and standard error of the mean were computed for the density of dendritic protrusions in each condition for both layer IV and VI dendrites. Since we treated each neuron as a single independent case, independent sample t-tests and Analysis of Variance, where appropriate, were conducted between the protrusion densities of the control and the manipulated conditions for each respective layer. To estimate the net loss of dendritic protrusions, we obtained the numerical mean at the previous time point and subtracted the individual density of dendritic protrusions in the next sequential time point, and divided by the number of days elapsed between the two time points. For this part of the data, the highest and lowest data at each time epoch obtained from the difference were eliminated prior to the subtraction in order to prevent significant skewing of the data due to huge outliers. In terms of the morphological categories of dendritic protrusions (filopodia, stubby, mushroom, etc.), the data are expressed as the percentage distribution of the total observed spines. Specifically, the percentage of each spine type was determined for every neuron and then population means were constructed by averaging all these measurements. We opted to explore the percentage distribution rather than the total number of dendritic protrusions, primarily due to the fact that the length of each dendrite is different. Longer dendrites are more likely to yield overall higher quantities of dendritic protrusions and it is thereby more appropriate to investigate the percentage rather than the absolutely quantity of dendritic protrusions. Unless otherwise noted, the

Analysis of Variance (where appropriate with multiple groups comparisons) was utilized to distinguish the main effect(s), and if statistical significance was found ($p<0.05$), an appropriate posthoc test (Fisher LSD or Tukey HSD) was utilized to determine which pairs are significantly different from each other.

8. Immunostaining and Optical Density

Animals (control P30 n=8, bilateral trim P30 n=8, control P60 n=9, whisker regrow P60 n=9) for immunofluorescence histochemical analysis were anesthetized with an interperitoneal injection of euthanizing agent (0.1ml, Euthalsol, Virbac AH, Inc), and transcardially perfused with saline followed by 4% paraformaldehyde in 0.01M phosphate buffer (PB). The retrieved brain tissues were kept in fix for approximately 7 days followed by vibratome sectioning in room temperature (maximum amplitude, minimum speed, coronal plane, 50μm per slice). Slices were collected in 0.01M phosphate-buffered saline (PBS; pH 7.4). Free-floating sections were rinsed in 0.01M PBS three times, 10 minutes each, then non-specific binding were blocked using 5% normal rabbit serum (Sigma-Aldrich) containing 0.5% Triton X-100 (to increase permeability) dissolved in 0.01M PBS. The sections were incubated in sheep antimurine tPA antibody IgG fraction (catalogue number SASMTPA-GF, Molecular Innovation Inc., dilution ratio 1:300) for 72-hours at 4°C in 0.01M PBS. For the purpose of assuring the primary antibody was targeting the desired antigen [tissue plasminogen activator], we also performed a negative control slice study without primary antibody. We also performed another type of negative control slice study by pre-absorbing the primary antibody with active recombinant form of mouse tPA (catalogue number MTPA, Molecular Innovation Inc.). After rinsing in 0.01M PBS, the brain slices

were submerged in a secondary antibody, biotinylated rabbit anti-sheep (Jackson ImmunoResearch, dilution 1:200) dissolved in 0.01M PBS. Following the secondary antibody incubation, slices were rinsed in 0.01M PBS and incubated in fluorescein dichlorotriazine (DTAF)-conjugated streptavidin in the dark (excitation: 520nm, Jackson ImmunoResearch, dilution 1:50). Last, the brain tissues were counterstained with Hoechst (Sigma-Aldrich, dilution 1:10000, final solution 0.12 µg/ml) for 15 minutes, followed by extensive rinsing (6 times, 10 minutes each) in 0.01M PBS, briefly submerged in distilled water, mounted on fluorescence-free slides, air-dried, coverslipped with VectorShield (Vector Laboratory), and sealed with nail polish. For the double-immunohistochemical portion of the study, a separate group of animals (n=3, P30) were used to investigate the colocalization profile of tPA with parvalbumin immunopositive cells. The tPA immunofluorescent staining protocol was followed as previously described, with the exception of replacing the fluorophore of streptavidin with Alexa 647 (excitation: 650nm; Invitrogen). The parvalbumin immunostaining was conducted as is follows: Tissues were blocked in 5% normal donkey serum in 0.01M PBS, then incubated in anti-parvalumin (host mouse, Sigma-Aldrich, dilution 1:2000) for 24 hours at 4^0C in 0.01M PBS. After rinsing in 0.01M PBS, the tissues were submerged in a secondary antibody (Alexa 488-conjugated donkey anti-mouse, excitation: 519nm, dilution 1:200; Jackson Immuno Research) for 2.5h in room temperature, followed by the Hoechst staining, extensively rinsed (60mins minimum), air dried, dipped in distilled H_20, and covered-slipped as previously described in this section.

Immuno-positive tPA cells are visualized with a Leica TCS-SP5 (Leica Microsystems Wetzlar GmbH, Wetzlar, Germany) confocal microscope under 20x (NA 0.85) with excitation parameters for DTAP (excitation: 520nm) and Hoechst (excitation: 405nm). The

brain slice was first inspected under the blue laser channel to determine the location and the cortical laminae, followed by viewing in green channel. Image exposure, laser power (16%), field of view size, photomultiplier (PMT) frequency-sensitivity, and the digital magnification factor were all internally consistent (held constant) for the purpose of pre-standardizing the tissue background luminosity prior to densitometry analyses, in a manner similar to previously described studies (Gazzaley et al., 1996; Kozorovitskiy et al., 2005). The gain was manipulated to match the background fluorescence level to an arbitrary number of 30.00 (Leica TCS-SP5), with acceptable deviation of ± 0.5% (~29.85 – 30.15). To avoid significant photobleaching, the immunofluorescence photomicrographs were collected within 3 minutes after the initial exposure to laser. The absolute value of tissue background luminosity (area devoid of immunofluorescence staining) was further confirmed by directly measuring the pixel intensity using the Neurolucida software (under luminosity measurements). Photomicrograph snapshots were converted to grayscale images (using Photoshop 7.0), in which pixel values representing the intensity of staining were expressed in a grayscale (0–255). The overall luminosity and relative optical density (ROD) of barrel cortex (layers II – VI) were measured and assessed using the software Densita (MBF Bioscience, Inc.). Laminae were defined based on cell density and size determinations using the Hoechst labeled tissue. We derived the optical density index (ODI) of a specific cortical layer by taking the ROD of that cortical layer and divided by ROD of the corresponding white matter of the same slice (due to the finding that there are extremely few tPA-immunopositive cells residing in the white matter). The optical density of the white mater (WM) was obtained by taking the background fluorescence level of WM in the contour of region of interest (ROI) and divided by the aforementioned preselected arbitrary value of 30. We sampled four to five brain slices per animal, and calculated the averaged ROD of one

animal as an individual case and then averaged across animals to determine population means. Independent t-tests were performed comparing the P30 control vs. P30 sensory-deprived groups, as well as P60 control vs. P60 sensory-restored groups.

Chapter Thirteen: Results:

Investigating the Effect of Chronic Sensory Deprivation on the Development of Dendritic Protrusions in the TCA Recipient Layers (Layers IV and VI) in Mouse Barrel Cortex

Dendrites have spines and filopodia which we will refer collectively as dendritic protrusions. The Golgi impregnation technique allowed us to clearly visualize various types of dendritic protrusions (see Figure 20A) based on their morphology (see also Figure 20B for a schematic drawing based on morphological categorization of dendritic protrusions). We identified each protrusion length from its tip to its base on the parent dendrite. Each morphological class of dendritic protrusions yielded significant differences in terms of the length from the distal ending of the protrusion itself to the surface of the parent dendrite (Figure 20C, $p<0.05$ for all pairs except branched vs. filopodia; Unequal-N HSD test, n=623 protrusions quantified in 10 neurons from 4 animals). Our data suggested that branched and filopodia type of dendritic protrusions in general have the longest length, followed by mushroom spines and lollipop spines. The stubby (both small and fat) as expected, exhibited the shortest distance from the distal ending to the surface of the parent dendrite. We thereby demonstrated that our qualitative assessment method matches our quantitative analyses with regard to the length of the protrusion. It also provides a reliable basis for quantitatively assessing the influence of developmental maturation and the impact of peripheral manipulation (e.g., trimming, blocking NMDA-R) has on a morphological variety of dendritic protrusions.

1. Developmental Trajectory of Dendritic Protrusions

To explore the normal developmental trajectory of dendritic protrusions, we investigated the density of dendritic protrusions and the distribution of different morphological class at several developmental time stages: Postnatal day (P) 15, 30, 60, 100, and 130 in the basilar dendrites of both layer IV and VI of the barrel cortex (Figure 21A), for these two layers are the main recipient layers of lemniscal thalamocortical afferents. It was found that from P15, which exhibited the highest protrusion density, there is a significant and steady decline of dendritic protrusion density in both layer IV and VI [Layer IV: Between-groups ANOVA: $F(4,81)=34.392$, $p<0.001$; Layer VI: Between-groups ANOVA: $F(4, 74)=46.887$, $p<0.001$]. Posthoc comparisons (Fisher LSD) revealed that for both layers, this trend of decrease in dendritic protrusion density across development is statistically significant ($p<0.05$), with the exception of P100 vs. P130 where it yielded a non-significant result ($p=0.13$ for layer IV and $p=0.08$ for layer VI). Sholl analyses (Figure 21B and C) of dendritic protrusion density at these different developmental stages confirmed our initial overall density data, that P15 exhibited the highest density, followed by 30, 60, 100, and 130, respectively [mixed-model ANOVA (age × distance from soma); posthoc: Tukey HSD, significant at $p<0.05$]. Overall, it was observed that for both layers IV and VI, this age-dependent effect on protrusion densities are more pronounced in proximal sections and compared with distal segments of the basilar dendrites.

Consistent with previously published findings in other layers (Yang et al., 2009), we show here that there is a steady net loss of dendritic protrusions from P15 in both layers IV and VI as the animals mature. We therefore estimated the rate of net loss of the dendritic protrusions (see Chapter 12) across various developmental stages (Figure 22A

and B). The data suggested that the highest rate of dendritic protrusion loss happens in the time epoch between P15 and P30. Following this time period, the rate of net loss of protrusions significantly slows down, and the rate of net loss of protrusions differs depending on the cortical layer [Layer IV: Between-groups ANOVA: $F(3,63)=11.50$, $p<0.001$; Layer VI: Between-groups ANOVA: (3,59), $p<0.001$]. It appears that the rate of net loss of dendritic protrusion in layer IV is slowed down earlier compared to layer VI, as posthoc tests revealed the rate of dendritic protrusion loss is significantly decreased in the P31-60 epoch in layer IV (Tukey HSD, $p<0.05$), but not in layer VI ($p=0.32$). This suggests that, as the animals mature, the rate of net loss of dendritic protrusions is quite different, possibly implicating that layers IV and VI mature at two distinct rates.

We next investigated the shift in morphological makeup of dendritic protrusions as the animals mature in both layers IV and VI (Figure 23). It is evident that the distributions of different morphological classes of dendritic protrusion differ as the animals mature. A mixed-model ANOVA (protrusion type × developmental age) yielded a significant main effect for protrusion type [$F(5,450)=161.00$, $p<0.001$] and a significant interaction effect [$F(20,450)=27.00$, $p<0.001$] for layer IV. Similarly, for layer VI there was a significant main effect for protrusion type [$F(5, 380)=147.41$, $p<0.001$] and a significant interaction effect [$F(20,380)=17.14$, $p<0.001$], thus the types of dendritic protrusions differ over time as the animals mature into adulthood.

To further explore whether or not the morphology of dendritic protrusions changes over the animals' lifespan, we examined each class of dendritic protrusions as a function of the animal's age. Upon more detailed inspection (using Tukey HSD as a means of posthoc) in layer IV, the branched type did not vary significantly across developmental ages ($p>0.4$ for all comparisons). Layer IV filopodia showed an inverted-

U type of trend, in which there were significant elevation in P30 compared with P15 ($p<0.001$), followed by a brief plateau at P60, and dropping in the total percentage at P100 and P130 (P60 vs. P100 & P130, $p<0.001$; P100 vs. P130, $p>0.5$). Layer IV small stubby spines showed a dramatic decrease in its distribution as the animal matured ($p<0.001$ for all pairs except P100 vs. P130). Both layer IV thick stubby and lollipop spines, by contrast, showed absolutely no change in the distribution as the animals matured ($p>0.7$ for all pairs). The layer IV mushroom spines starts showing increased distribution from P60 all the way until P130 ($p<0.01$), but not before P60 (P15 vs. P30, $p>0.9$). Overall, the relative distribution of dendritic protrusions is not fixed, with mushrooms increasing, the lollipop and fat stubby remaining similar, and the small stubby spines and filopodia steadily decreasing throughout the animals' developmental lifespan.

The change of dendritic protrusion morphology in layer VI is quite similar to that of layer IV, with several small differences. As in layer IV branched type of protrusions showed no significant change in the distribution across developmental age ($p>0.4$ for all pairs; ANOVA) in layer VI. Filopodia in layer VI also showed an inverted-U type of trend similar to layer IV, but this elevation in distribution does not start until the second postnatal month (P60, $p<0.001$; Tukey HSD), followed by a quick drop in the percentage of distribution within total dendritic protrusions by P100 ($p<0.001$). The percentage of small stubby spines does not start to drop until P30-P60 (P15 vs. P30, $p>0.9$), but there is a dramatic drop from P30 to P60 ($p<0.001$) and this decrease in the percentage of small stubby spines continues through P130. The distribution of fat stubby spines remains comparable across age until between P100-P130, when there was a significant increase of the percentage of observed fat stubby spines between these two time points. The lollipop

spines, as was the case in layer IV, remain constant throughout the animals' developmental life ($p>0.4$ for all pairs; Tukey HSD). Last, the increase in the percentage of mushroom spines in layer VI is similar to that of layer IV, as the increased addition starts from P60 all the way until P130 ($p<0.01$ for all comparisons), but not before P60 (P15 vs. P30, $p>0.9$). Our data are in line with previous finding (Dumitriu et al., 2010) that as the animals' cortex mature, there is a significant redistribution of the morphology in the dendritic protrusions, and this shift is dominated by a significant increase of mushroom types as the animals become older. This supports the hypothesis that the role of mushroom-type spines are more likely to be the "memory" of neurons and therefore are more persistent and thus do not change dramatically throughout development (see Holtmaat & Svoboda, 2009; Yang et al., 2009).

2. Layer-Specific and Age-Dependent Effect of Whisker Trimming and Regrow on the Density and Morphology of Dendritic Protrusions.

Sensory experience plays a critical role in driving the maturation processes of the developing cerebral cortex (see Feldman and Brecht, 2005). We thus explored whether or not depriving somatic sensation via whisker trimming would have a significant impact on the dendritic protrusions of the pyramidal neurons in the thalamocortical afferent layers (IV and VI). We focused only on the basilar dendrites of the layer IV and VI pyramidal neurons due to the fact that apical dendrites traverse outside of their home layers, and it has been previously demonstrated that the impact of sensory deprivation on apical dendritic protrusions is dependent on which cortical lamina of the segment of the dendrite is located (Briner et al., 2009). We found that chronic sensory deprivation by

both methods of unilateral (investigating the contralateral barrel field from the trimmed mystacial pad) and bilateral trimming from P0-P30 yielded significantly higher density of dendritic protrusions in the basilar dendrites of layer IV pyramidal neurons (Figure 23A) [Between-groups ANOVA, $F(2,52)=4.46$, $p<0.02$, Cohen's $d=0.83$; control n=25 neurons from 5 animals, unilateral trim: n=14 from 5 animals, bilateral trim: n=16 from 5 animals]. Posthoc analysis (Tukey HSD for all of the posthoc pair-wise comparisons mentioned in this section) revealed that this elevated density in both whisker-trimmed conditions, while not significantly different from one another ($p>0.8$), are both significantly higher than their P30 control counterparts ($p<0.05$). This increase in spine density in our study might be correlated with the finding that following chronic trimming, layer IV regular spiking units (RSUs) exhibited higher excitability and faster averaged spiking kinetics (Lee et al., 2007). The impact of chronically depriving the sensations from birth to P30 on the morphological makeup of layer IV basilar dendritic protrusions is also evident (Figure 23C). While there were no significant shift in the distribution seen in filopodia, fat stubby, and mushrooms as a function of whisker trimming, the branched, small stubby and lollipop spines showed significant shifts as a result of chronic sensory deprivation ($p's<0.05$). The most apparent alterations are observed in the significant drop of small stubby spines and elevated lollipop spines in their distribution within total dendritic protrusions following whisker trimming, and depending on the method of trimming (unilateral vs. bilateral), the magnitude of the distribution shift varies (see Figure 24C). This elevated protrusion density is possibly a sign of stunted development resulting from diminished sensory input. It is highly likely that chronic sensory deprivation from P0-P30 delayed the spine pruning process, similar to what has been

previously shown in the apical dendrites of layer V pyramidal neurons (Zuo et al., 2005), in which the elimination of spines is greatly reduced following whisker trimming.

The effect of chronic sensory deprivation from birth to P30 on the density of dendritic protrusion in layer VI pyramidal neurons were opposite of what was observed in layer IV (Figure 24B), in which there was a significant reduction of density when compared bilaterally trimmed vs. P30 controls [$t(43)=3.76$, $p<0.001$, Cohen's $d=1.13$; control n=22 neurons from 5 animals, bilateral trim: n=23 from 5 animals]. Similar to layer IV, the distributional shift in layer VI dendritic protrusion morphology following bilateral trimming is evident as well (Figure 24D). Specifically, we observed a significant increase in the proportion of branched, filopodia, and lollipop spines ($p's<0.03$ for all), while the distribution of small stubby and mushroom spines were significantly reduced following bilateral trimming from birth to P30 ($p's<0.01$ for all). The fat stubby spines, similar to layer IV, following trimming did not show statistical significance when compared with the P30 control counterparts.

Next, we attempted to restore the sensory input of the vibrissa by allowing the whiskers to grow back to their full length for one month, and compared the dendritic protrusion parameters in the P60 control against the P60 whisker-regrow animals. The findings indicated that while the density of dendritic protrusions of layer IV neurons remained elevated [$t(30)=-2.56$, $p<0.03$, Cohen's $d=0.91$; control n=19 neurons from 4 animals, whisker-regrow: n=13 from 4 animals] (Figure 25A), the density of dendritic protrusions in layer VI returned to comparable levels to those of control P60 animals[$t(29)=0.35$, $p>0.7$; control n=17 neurons from 4 animals, whisker-regrow: n=14 from 4 animals] (Figure 25B). In exploring the distributional shift in dendritic protrusion morphology following sensory restoration (P60 control vs. P60 regrow), we observed that

in layer IV, the pattern stayed exactly identical to that of P30 control vs. P30 bilateral trimmed: branched and lollipop spines remained higher while the small stubby spines remained lower in the whisker-regrow condition when compared with the control P60s (p's<0.05 for all), with no statistical significance reached for filopodia, fat stubby, and mushroom spines, similar to P30 control vs. P30 bilateral trimmed in layer IV neurons. In layer VI, even though the density showed a return to comparable levels to that of P60 control animals, the impact of earlier sensory deprivation lingered for most morphological classes of dendritic protrusions, with the direction of the significance staying identical for all classes (p's<0.05 for all). The distribution of filopodia returned to comparable level to that of P60 following whisker-regrow, and the fat stubby spines remained unaffected, like previously observed in P30 control vs. trimmed condition (p's>0.05). It may seem that layer VI in terms of the density of dendritic protrusions, is more malleable and responsive to post-deprivation experiences compared to layer IV. The effect of deprivation from birth on the morphology of dendritic protrusions, however, lingered in both layers IV and VI even after the sensation was restored, thus suggesting the long-lasting impact of depriving sensation in early developmental period has on subsequent life period.

It has been previously demonstrated that chronic sensory deprivation in adult animals can lead to an elevated density of dendritic spines in layer V pyramidal neurons in the sensory cortices (Zuo et al., 2005; Hofer et al., 2009). However, the effect on the thalamocortical layers of adult sensory deprivation remains unknown, and thus we examined the repercussion of chronic sensory deprivation has on the density and morphology of dendritic protrusions. It was found in adult animals that were deprived of sensation (whisker trimmed bilaterally from P100-130), their layer IV dendritic

protrusion densities were significantly elevated compared with the P130 control group (Figure 26A) [$t(28)=2.23$, $p<0.05$, Cohen's $d=0.81$; control n=15 neurons from 7 animals, bilateral trim: n=15 from 6 animals]. In terms of the morphology of dendritic protrusions (Figure 26C), layer IV dendrites in the deprived condition showed a significantly higher percentage of lollipop spines but a lower percentage of small stubby and mushroom spines when compared with their P130 control counterparts (p's<0.05). Branched, filopodia, and fat stubby dendritic protrusions in layer IV were not dramatically influenced as a result of chronic sensory deprivation in adult animals (p's>0.05 for all). These results are very similar compared to P0-P30 trimmed animals, in which both P100-P130 and P0-P30 trimmed animals showed lower small stubby and higher lollipop spines distributions compared to their control counterparts. The only difference is that the adult trimmed animals exhibited a statistically significant reduction in the distribution of mushroom spines, which was trending similarly in the P0-P30 bilaterally trimmed animals but did not reach statistical significance.

In layer VI, chronic sensory deprivation in adult animals did not lead to a significant change in the overall density of dendritic protrusions (Figure 26B) [$t(27)=0.86$, $p>0.3$; control n=15 neurons from 7 animals, bilateral trim: n=14 from 6 animals]. Even though the density of dendritic protrusions did not differ significantly, there were still some subtle alterations in the morphological makeup of the dendritic protrusions, mainly in the significantly lower percentage of small stubby and mushroom spines, and the elevated percentage of lollipop spines in the P130 trimmed group when compared with their age-matched counterpart (p's<0.05 for all pairs). The branched, filopodia, and fat stubby types of dendritic protrusions did not show statistical indications of being different (p's>0.05). Taken together, the more dramatic effects in layer IV may be a reflection of

the relative importance of thalamic input in driving the activity in that layer compared to layer VI.

3. The Effect of Chronically Blocking NMDA-Receptor Transmission on Density and Morphology of Dendritic Protrusions.

It has been previously shown that interfering with the transmission of NMDA-R leads to alterations of spine dynamics in layer V pyramidal neurons (Zuo et al., 2005) and increased spine density in layer IV spiny stellate cells (Datwani et al., 2002), but the full spectrum of the role of NMDA-R has on layer IV and VI pyramidal neurons remains unexplored. We observed that following chronic intraperitoneal administration of the NMDA-R antagonist MK801 from birth to P30, both the basilar dendrites of layer IV and VI pyramidal exhibited significantly higher overall densities of dendritic protrusions (Figure 27A and B) [Layer IV: $t(40)=6.60$, $p<0.001$, Cohen's $d=2.03$; control n=25 neurons from 5 animals, MK801 n=17 from 3 animals. Layer VI: $t(38)=2.73$, $p<0.01$, Cohen's $d=0.85$; control n=22 neurons from 5 animals, MK801 n=18 from 3 animals]. There was also a significant impact of chronically blocking NMDA-R on the morphology of dendritic protrusions which is also evident (Figure 27 C and D), as both layer IV and VI branched and filopodia showed significant increases in their overall percentage of distribution, while the small stubby spines showed a significant decrease ($p's<0.05$). The fat stubbies remained unchanged for both layers ($p's>0.3$). While the lollipop and mushroom spines did not vary significantly in layer IV ($p's>0.5$), in layer VI there was a significantly higher percentage of the lollipop spines and lower percentage of mushroom spines ($p's<0.05$).

Comparing the P0-P30 MK801 inject group with the bilaterally trimmed group in terms of dendritic protrusion density, it was found that in both layers IV and VI, MK801 injected group showed dramatically higher density compared to the bilaterally trimmed group (p's<0.05). Thus, the NMDA-R activity may partially explain why following chronic sensory deprivation, there is an overall increase of dendritic protrusions in layer IV. It does not, however, explain the significant decrease of layer VI dendritic protrusions following trimming. Our data also suggests that blocking NMDA-R transmission is associated with the decrease of small stubby spines and increase of branched spines similarly seen in P0-P30 trimming. However, it does not readily explain the significant increase of lollipop spines observed in the deprived animals in both layers IV and VI, as chronically injecting MK801 failed to reproduce this type of data pattern.

Next, we withdrew the MK801 (no injections) for one month and compared these animals with their P60 control counterparts (Figure 28). We found that in both layers IV and VI the density of dendritic protrusions returned to comparable levels to the control group [Layer IV: $t(29)=0.82$, $p>0.42$; control n=19 neurons from 4 animals, Drug withdraw n=12 from 3 animals. Layer VI: $t(28)=1.4$, $p>0.15$, control n=17 neurons from 4 animals, Drug withdraw n=13 from 3 animals]. In terms of the morphological distribution of dendritic protrusions in layer IV pyramidal neurons, the branched, filopodia, fat stubby, and lollipop returns to comparable levels to that of controls (p's>0.05), while the small stubbies remain lower ($p<0.01$), and there was a significant increase in the distribution of mushroom spines that was observed ($p<0.001$). Within layer VI, the distribution of branched, filopodia, fat stubby, and mushroom spines returned to comparable levels (p's>0.05), while there was a significant increase of the small stubby and a decrease of the lollipop spines (p's<0.05). Overall, unblocking the

activity of previously perturbed NMDA-R activity returns to the protrusion densities to comparable levels to that of the control animals, although there are still subtle changes in the morphological makeup of the dendritic protrusions.

4. The Role of Tissue-Type Plasminogen Activator (tPA) in Sensory-Dependent Plasticity in Barrel Cortex.

Tissue-type plasminogen activator (tPA) has been shown to provide a permissive role for plasticity in the primary visual cortex (Mataga et al., 2004), and monocular deprivation spanning the developmental critical period is associated with a significant increase in tPA activity (Mataga et al., 2002). However, the role of this tPA-enabled deprivation-induced plasticity has been unexplored in the somatosensory system. Here we show that the expression of tPA is present in the barrel cortex (Figure 29A), and that the majority of the tPA immunopositive cells do not colocalize with somatostatin (Figure 29B), but do colocalize with parvalbumin immunopositive neurons (Figure 29C), suggesting the important role parvalbumin+ cells play in cortical plasticity, similar to what has been proposed in the visual cortex (see Hensch, 2005). Since it has been suggested in the visual system that the expression of tPA is transient in an age-dependent manner (Zheng et al., 2008), we thereby compared tPA expression using quantitative immunochemistry (see methods) in P30 against P60 untreated barrel cortex (P30 n=8 animals, P60 n=9 animals). With the exception of the supragranular layers (II and III) in which P60 untreated mice showed significantly higher tPA expression in their barrel cortex (Fisher LSD, $p<0.05$), there were no significant differences in other cortical laminae explored ($p's>0.3$ for all). Next, we explored the expression level of tPA as a

function of chronically depriving the sensations of the mystacial pad from birth to P30 (Figure 30A and B), and found that in every cortical lamina, the deprived barrel cortex exhibited heightened level of tPA expression (Mix-ANOVA (type of sensory experience × cortical lamina) followed by Fisher LSD, p's<0.05; P30 control n=8, P30 trimmed n=9). This heightened level of tPA expression lingers even after the whiskers were allowed to grow back for one month and is observed in every single cortical lamina (p's<0.05; P60 control n=9, regrow n=9; Figure 30C). Taken together, our data suggested that the expression of tPA in the somatosensory system is influenced by the sensory experience, and that alterations in the levels of sensory input can induce corresponding changes of tPA activity/expression. The elevated expression of tPA might be correlated with the decreased level of extracellular matrix following trimming (McRae et al., 2007), thereby making the system more permissive to morphological alterations.

Chapter Fourteen: Discussion:

Investigating the Effect of Chronic Sensory Deprivation on the Development of Dendritic Protrusions in the TCA Recipient Layers (Layers IV and VI) in Mouse Barrel Cortex

The goal of this portion of the dissertation is to investigate dendritic protrusion density and morphology as a function of developmental age within layer IV and VI pyramidal neurons of the mouse barrel cortex in normal and in response to peripheral manipulation (whisker trimming; injection of an NMDA antagonist). We provide histological evidence that the pyramidal neurons respond in a layer-specific manner to the same peripheral manipulation, and the same manipulation (i.e. chronic sensory deprivation) yields to different results depending on the age of the animals investigated. Exploring the effects of perturbing the sensory system in various developmental ages and subsequently analyzing dendritic protrusion density provide crucial first steps in describing sensory experience-dependent synaptic plasticity and the rearrangement of cortical circuitry in the cerebral cortex.

1. Dendritic Protrusion Density Decreases as a Function of Normal Development in Layer IV and VI

Our data from layers IV and VI is consistent with the previously published studies describing dendritic protrusions from layer V pyramidal neurons (Zuo et al., 2005; Yang et al., 2009). Specifically, as in layer V, pyramidal neurons in both layers IV and VI experience a net loss of protrusions as the animals mature into adulthood. Consistent

with these previously published studies, we showed that initially there was a sharp loss of protrusion densities from P15-30, and as the animals become more mature, the rate of net dendritic protrusion loss decelerates. This sharp net loss of dendritic protrusion density might be correlated with the onset of whisking in mice (see Prescott et al., 2011). In addition, we demonstrate that this rate of net protrusion loss is slightly different depending on the cortical layer. As described by previous findings (Zuo et al., 2005; Alvarez et al., 2007; Yang et al., 2009), this age-dependent net-loss of dendritic protrusions is an indication of synaptic refinement during the developmental critical period, a sign of cortical maturation. It is known that the metabolic interactions that govern the processes of spine elimination and formation are impacted by developmental age, predominantly with the rate of spine elimination surpassing the rate of spine formation (Zuo et al., 2005; Yang et al., 2009) following an early peak level of synaptogenesis. Our results are consistent with these findings as we saw a dramatic decrease in the protrusion density in both layers from P15 to P30, followed by considerably less rapid rate of protrusion loss thereafter. Similarly our finding that there is a shift in the morphology of the dendritic protrusions is consistent with previous reports (Dumitriu et al., 2010); the most noticeable is the significant decrease of the small stubby (sessile) spines and a significant increase of the mushroom spines as the animals reach developmental maturation.

Owing to histological limitations, we could not reliably investigate any developmental time points prior to postnatal day 15, as the labeling of the neurons was incomplete, preventing us from visualizing dendritic protrusions reliably and in acceptable quality prior to P15, a phenomenon observed similarly in previously published findings using the same technique (see Furtak, 2007). Work from primate cortices have

demonstrated that the density of dendritic protrusions follows an inverted-U shape, in which at the beginning of the postnatal development there is a rapid net increase of dendritic spines, presumably when the process of spinogenesis overshadows spine pruning (Elston and Oga., 2009; Elston et al., 2010). This peak spinogenesis is followed by a significant period of developmental spine pruning, in which decreased spine density is observed across a variety of species and in various cortical regions (Elson and Oga, 2009; Elston et al., 2010; Yang et al., 2009;), and seems to be a general rule across mammalian cortices.

2. Response of Dendritic Protrusions to Perturbation of Sensory Input is Age and Cortical Layer Specific

The significantly higher density of dendritic protrusions in sensory-deprived layer IV pyramidal neurons may indicate an increase in the number of excitatory synapses. Our results provide a possible structural basis as to why cells show increased excitability under a sensory deprived condition during the critical period, consistent with previously published data from *in vivo* recordings (Simons & Land, 1987; Shoykhet et al., 2005; Lee et al., 2007). Higher dendritic protrusion density is likely correlated with increased excitatory inputs onto these cells. Although our data does not directly provide a mechanism for this increased density of dendritic protrusions it may likely result from decreased spine elimination as suggested previously (Zuo et al., 2005) in layer 5 pyramidal neurons. Unexpectedly, there was a parallel decrease in spine density in layer VI pyramidal neuronal dendrites. Why these neurons respond to whisker trimming by decreasing their protrusion densities is unclear, for the current available literature on

sensory-deprived manipulations that investigate layer VI neurons are extremely limited. One possibility that shed light on this phenomenon might be related to the significantly increased length of basilar dendrites in layer VI pyramidal neurons (Chen et al., 2011; also see results [2]), thus making the dendritic protrusions more sparsely located from one another. Another possibility of this lowered level of protrusion densities might be due to the reduced axonal branches originating from L2/3 (Bruno et al., 2009) and the thalamus (Wimmer et al., 2010); thus likely to result in a decrease in the overall number of excitatory drive to layer VI. Taken together, these findings indicate that there are laminar differences in how sensory input is processed and thus lead to cortical layer-specific responses in response to changes in the sensory periphery during the developmental critical period.

It has been suggested in the cortex that morphological structure of postsynaptic dendritic protrusions might be correlated to the origin of their presynaptic inputs. Specifically, it was demonstrated that TCA axons are more likely to synapse onto "short stubby" spines and less likely to synapse onto spines with a distinctive spine-head (Richardson et al., 2009). In addition, findings from tract-tracing studies have suggested that following chronic sensory deprivation, there is significant decrease in the lemniscal TCA axons originating from VPm of thalamus (Bruno et al., 2009; Wimmer et al., 2010), resulting in a shift of thalamocortical / cortico-cortical connection ratios. Our data have provided additional evidence on the post-synaptic side in the cortical TCA recipient layers (IV and VI)., that this shift in thalamocortical / cortico-cortical connection following chronic sensory deprivation is observed in a structural shift of dendritic protrusions (see Figure 31). Following chronic sensory deprivation for a month, there is considerable reduction of the proportion of stubby spines and higher proportion of

lollipop spines in both layers IV and VI. It is hypothesized that the proportional reduction of thin stubby spines following chronic deprivation is due to reduction of TCA innervations, whereas the proportional increase of lollipop spines is most likely due to the relatively higher ratio of cortico-cortical connections. This might have occurred as a compensatory mechanism for the balance of postsynaptic input and intrinsic neuronal activity.

Our data suggested that one month of whisker regrow maintained the elevation of dendritic protrusion density in layer IV pyramidal basilar dendrites but resulted in a returning of the comparable level of density in layer VI. These discrepant results may lie within the fact that layer IV of the barrel cortex is tightly organized into discrete functional columns, as opposed to layer VI which is more continuous. This resulted in that layer IV receives much more homogeneous input (e.g., thalamus) compared to layer VI (e.g., M1, S2, thalamus, contralateral barrel cortex, and various intracortical layers), thereby suggesting that thalamocortical input only accounts for a small partition of the overall excitatory drive into layer VI and thus the remaining inputs can more easily overcome the loss of previous whisker-related sensations. Even though the trimming process was discontinued at P30, vibrissa take some time to grow back, hence the sensory restoration is gradually introduced, as opposed to in other modalities and paradigms of sensory deprivation and recovery (i.e., unsuturing of eyelid, etc.), which is rather rapid.

It has been previously demonstrated that the cellular environmental substrates such as the extracellular matrix protein aggrecan do not return to normal level in layer 4 following one month of sensory restoration after the initial deprivation during the critical period (McRae et al. 2007). Our current findings in layer IV is similar in that allowing the whiskers to regrow did not regain the control phenotype of dendritic protrusions in

layer IV. It may be instructive for future researches to focus on the effect of chronic sensory deprivation on the different layers of the cerebral cortex to fully unravel the molecular substrates involved in the plasticity in layer VI, even following the passing of the critical period.

3. Activity of NMDA Receptors in Barrel Cortex Greatly Influences Dendritic Protrusion Density and Morphology

Administration of the NMDA antagonist MK801 during the critical period resulted in an increase in dendritic spine density in both layer IV and layer VI dendrites. The NMDA receptor is a non-specific cation channel and is expressed on the surface of dendritic spines. (Ngo-Anh, 2005) at sites of excitatory synaptic input. Activity-dependent regulation of synapses requires activation of NMDA receptors (Malenka & Nicoll, 1993; Fox et al., 1996; Huang & Pallas, 2001) and changes in sensory experience results in the rearrangement of synapses in the somatosensory cortex (Trachtenberg et. al., 2002). It has been found that blockade of the NMDA receptor decreased the rate of spine elimination (Zuo et. al. 2005) similarly seen in chronically depriving the somatic senses, and therefore leads to significantly more numerous dendritic spines overall in the apical dendrites (at the pial surface) that originates from layer V pyramidal neurons. We showed that the same phenomenon exist in layers IV and VI, that the stunted rate of spine elimination may have resulted in the elevated spine density is observed in these two cortical layers. Due to the overall high mortality rate of MK801-administered animals (see Chapter 12), it is unclear whether or not the survived animals exhibited some unique

characteristics in which have allowed them to survive, and whether or not these unique characteristics would have impacted the development of their barrel cortex in any way.

Withdrawal of MK801 for one month and subsequent analysis of dendritic spines in layer IV showed a significant decrease in dendritic spine density. Again, activation of the NMDA receptor is involved in spine elimination and this significant decrease may be explained by an increase in spine turnover rate. Similarly, withdrawal of the MK801 drug also caused the dendritic spine density for layer VI to return to comparable levels to their control counterparts. Thus, we have shown that the activity of NMDA receptors is directly involved in the remodeling of dendritic spines, and this effect seems to be universal throughout the cerebral cortex, as seen in pial surface, layer IV, layer V, and layer VI. Other synaptic mechanisms such as metabotropic glutamate receptors, serotonin expression, brain-derived neurotrophic factors have been shown to play a role as facilitators of dendritic plasticity in the cerebral cortex (Wijetunge, 2009; Washbourne et al., 2004; Maya et al., 2008), but are beyond the scope of the present study. NMDA receptors are by far the most understood, and most studied synaptic mechanism responsible for this plasticity in the brain. Furthermore, our findings indicated that the elevation of dendritic spine density following sensory deprivation is strikingly similar to the elevation of dendritic density following chronic blockade of NMDA receptors. However, this is only true for layer IV but not in layer VI, suggesting that while the activity of NMDA receptors is predominantly responsible for the changes in spine plasticity. One possibility to explain the differential results seen in layers IV and VI may be due to the fact that the NMDA receptor is composed of multiple subunits and perhaps different subunits predominate in the different layers and respond differentially to changes in afferent activity (see Corson et al 2009).

4. Experience-Dependent Expression of Tissue-type Plasminogen Activator (tPA) in Barrel Cortex

Despite the abundant literature investigating the role of both normal development and sensory-dependent plasticity of tPA in the primary visual cortex (Mataga et al., 2002; 2004; Oray et al., 2004; Zheng et al., 2008), the role of tPA in the barrel cortex remains unclear. Here we show for the first time that tPA is present in all layers of the barrel cortex, and that tPA expression is upregulated following a period of chronic sensory deprivation during the critical period. Further, our current data have pinpointed the correlative significance of tPA and parvalbumin-positive cells, a finding that is consistent with the view that in the absence of tPA, the GABAergic-regulated plasticity in the cerebral cortex is abolished (Mataga et al., 2002). Other studies (Zhao et al., 2003; Zheng et al., 2008) have suggested that a subset of tPA-immunopositive cells in the cerebral cortex exhibit triangular somata shape with light labeling of the proximal segment of apical dendrites, consistent with the morphology of pyramidal neurons. In other brain areas (hippocampus), tPA is produced by both neurons and microglia (for a review, see Gravanis and Tsirka 2005). Further studies will be needed to clarify the heterogeneous cellular sources of tPA in the cortex.

The extracellular matrix (ECM) has been increasingly receiving attention as a major player in critical period plasticity, and our previous data have shown that the expression of a component of perineuronal net, aggrecan, is downregulated following chronic sensory deprivation (McRae et al., 2007), coinciding with our current tPA finding that it is increased after a period of chronic sensory deprivation. It has been proposed

previously that tPA might be the regulating key factor that allows the structural plasticity in the cerebral cortex during developmental critical period, and the proteolytic activity of tPA is responsible for inhibiting the condensation of extracellular matrix protein into perineuronal nets (Oray et al., 2004; Mataga et al., 2004; Mataga et al., 2002; Zheng et al., 2008), a major reason why it is more difficult to induce structural plasticity in mature cerebral cortices (Pizzorusso et al., 2002). It is known that tPA is the major serine protease in the postnatal mammalian brain (see Hensch, 2005; Gravanis, 2005), which plays the permissive role of GABA-regulated plasticity during the developmental critical period (Mataga et al., 2002), as well as dendritic spine structural remodeling (Mataga et al., 2004; Oray et al., 2004). The alteration in the tPA level may thereby be the link between the functional changes and structural modifications downstream of the excitatory-inhibitory balance that triggers the experience-dependent dendritic protrusion remodeling. It is the enabling role of tPA that may ultimately allow the structural alterations observed in dendritic protrusions to be possible.

Chapter Fifteen: General Discussions and Concluding Remarks

1. Limitations of the Golgi Impregnation Method

Recent studies have demonstrated that the intensity of Golgi impregnation varies as a function of the developmental age of the animals (Furtak et al., 2007). Specifically, the intensity of impregnation increases as the age of animal increases, in which by postnatal day 15, silver chromate impregnation appears to be complete. This limits the possibility to explore the development of neuronal morphology / dendritic protrusions prior to P15, which is when the synaptogenesis is at its highest. Therefore, the cortical developmental trajectory prior to P15 remains elusive to the Golgi method, and is perhaps more suited for other labeling methods such as DiOlistics or electroporation (Mataga et al., 2004; Cruz-Martin et al., 2010).

Another limitation of using the Golgi impregnation method to study the dendrites as well as dendritic protrusions, similarly to any other histological methods *in fix*, is that since dendrites and dendritic protrusions are dynamic entities that are constantly surveying, sampling, and updating to the ever-changing sensory environment, Golgi impregnation offers more of a snapshot that is frozen in a specific time-period, rather than capturing the observations of spinogenesis / spine pruning. Important dynamic information such as the dendritic structural remodeling (i.e., formation and elimination of filopodia and spines) seen *in vivo* imaging (Hubener et al., 2008; Zuo et al., 2005; Yang et al., 2009) cannot be observed using the Golgi impregnation technique. However, due to the nature of these genetically engineered mice (expressing yellow/green fluorescence), these aforementioned *in vivo* imaging studies exploring the dynamics of dendritic

protrusions only allow the visualization of the tufts of apical dendrites with somata located in layer V. This remains a current technical challenge in the field that is waiting to be resolved. Therefore, as of the writing of this dissertation, it is more technically practical to utilize *in fix* or *in vitro* approaches to investigate the dendritic protrusions in other (specifically, deeper) layers of the cerebral cortex.

In earlier part of this dissertation [see Chapter Ten], it was pointed out that other than nonpyramidal and pyramidal neurons based on the presence or absence of apical dendrites, the current Golgi labeling technique does not allow further specification such as segregating the neurons based on their local functional circuitry or histochemical properties [also see Chapter One: Section1.5]. Prior studies have demonstrated that even within the same layer (V), the two different morphological classes of pyramidal neurons respond in different manners to the same peripheral manipulation (Hubener et al., 2009), suggesting that the neurons respond with selective specificity to alterations in sensory experience. It will be particularly instructive for future studies, using other labeling techniques, to investigate the developmental trajectory and/or the effect of sensory experience has on specific classes of cortical neurons based on their functional connectivity as well as histochemical properties.

2. Studying the Structural Mechanisms of Cortical Plasticity

One of the most exciting aspects of studying the structural basis of neuroplasticity in the cerebral cortex is that, anatomical alterations can range from global scale to microscopic level in terms of structural remodeling (see Figure 32, panel A is most global and panel E is most microscopic). Therefore, when attempting to address a phenomenon,

it is crucial to contemplate the research technique and whether or not the considered technique is well suited for the interested phenomenon. Depending on the research question, plasticity might be observed in only one level of analysis, thus subtle nuances in structural alteration might be overlooked. For that reason, careful premeditation before the commencement of experimental investigations is required, as to making a decision regarding the appropriateness of anatomical level explored and the related research question in mind.

Studies investigating the gross level of structural alteration (disappearance, shift, expansion, or shrinkage of somatotopic map) are well suited for global level of anatomical analysis (Figure 32A). This global scale of anatomical changes provides useful information that allows the researchers to understand the effect of a specific manipulation has on the interested perceptual modality overall. For example, it was shown that the amount of secreted fibroblast growth factor-8 (FGF8) during embryonic development can influence the spatial location of barrel field within the cerebral cortex (Fukuchi-Shimogori and Grove, 2001), and ectopic application of FGF8 results in duplication of the barrel map. In a similar type of study, Bishop et al., (2000) demonstrated that *Emx2*$^{-/-}$ mice exhibited exaggerated and augmented primary somatosensory map, while *Pax6*$^{-/-}$ mice exhibited exaggerated and augmented primary visual map. These studies exemplify that this global level of analysis provides key information about how the cerebral cortex is patterned during development, and how the molecular control of cortical patterning can influence subsequent development of the entire sensory modality (or in some cases, a shift of balance in the entire brain, involving multiple modalities).

The next level of anatomical analysis (Figure 32B) provides key information regarding the regional relationships within the barrel cortex. Studies that investigate cellular population distribution, dendritic / axonal branching pattern, and local functional connectivity are well suited for this level of analysis. For example, Ballester-Rosado et al. (2010) demonstrated that in the absence of cortex-specific mGluR5 (Cx-mGluR5$^{-/-}$), the dendrites of spiny stellate cells in layer IV barrel cortex, which normally show directional fanning preference towards the center of barrels in wildtype animals, lose their directional preference. In the same study, leminiscal TCA axons are less exuberant in Cx-mGluR5$^{-/-}$ mice compared with wildtype animals. Furthermore, the neuronal somata in layer IV, which normally aggregate around the barrel walls, are now evenly distributed throughout the somatosensory cortex in Cx-mGluR5$^{-/-}$ mice. This indicates the key role that mGluR5 plays in regulating local circuitry within the barrel cortical region; without mGluR5 the cellular-spatial distribution, dendritic fanning pattern, and TCA axonal guidance are disrupted. Therefore, this level of anatomical analysis provides the researcher with more detailed information in cortical plasticity, mainly pertaining to the functional connectivity within one single sensory modality.

Studies investigating the neuronal morphology on a whole-cell level (Figure 32C) often explore the geometric relationship either with respective to the gross anatomy of the cerebral cortex and/or in somata-centered perspective (Chen et al., 2009; Mao et al., 2011). This is also the level in which the classification of neurons becomes important, as it was previously demonstrated that the morphology of neurons, regardless of cortical lamina, is heterogeneous in nature (Chen et al., 2009; Tsiola et al., 2003). The separation of apical dendritic features from basilar ones becomes critical here, as apical and basilar

dendrites respond in opposite manners to chronic sensory deprivation (Chen et al., 2011), and the same guidance molecule (Semaphorin-3A) can induce apical dendritogenesis but at the same time, having little effect on the growth of basilar dendrites (Polleux et al., 2000). These studies suggest that from the developmental and bio-molecular perspectives, apical dendrites should be considered as a separate level of compartmentalization to their basilar counterparts. Overall, this level of anatomical analysis provides the overall morphometric and computational capabilities of the entire neuron, with the dendrites serving as functional units to process sensory inputs in graded sub-threshold potentials (analog), and the soma serving as the integrating / executive CPU which makes sense of propagated electrical impulses and responding in all-or-none action potentials (digital).

Magnifying further to analyzing structural plasticity in a single-dendrite level (Figure 32D), studies investigating the relationship between one dendrite and the proximity to somata, the geometric angular relationship to the cortex (or somata), and quantifications / clustering of dendritic protrusions, are well suited in this level of analysis. The quantification of dendritic protrusions, as well as exploring the relationship of the spine/filopodia turnover is perhaps the most popularly used approach in the field recently. For instance, using two-photon *in vivo* imaging of dendritic protrusions, Yang et al. (2009) showed that persistent, stably spines are associated with life-long memories of experiences, which is not influenced by normal developmental spine pruning. In the same study, it was found that as the animals mature, the density of dendritic protrusions are steadily decreasing, thus suggesting the rate of spine elimination surpasses formation. At this level of analysis, the dendritic processing potential for computational capacity is scrutinized, as electrophysiological data have indicated that functional clustering of

synapses along dendrites are associated with spatial summation of synaptic inputs and can significantly influence the computing power of a neuron within a neural network (Fu et al., 2012).

At the individual dendritic protrusion level (Figure 32E), studies investigating anatomical evidence of learning and memory, as well as dendritic protrusion dynamics (motility, formation, elimination) are well suited for this level of analysis. With the revolutionizing advancement in optical imaging, particularly with the development of high-resolution two-photon microscopes, it has recently become possible to study very detailed structural alterations of dendritic spines. For example, Oray et al. (2004) have suggested that the motility rate of individual spines at P28 is approximately 0.2μm/minute in the visual cortex, and that brief monocular deprivation increases spine motility to 0.32μm/minute. However, the size of the spine neck, spine head, and spine length (for detailed illustration see Figure 32E) remain unchanged. In a similar type of study, Dumitriu et al. (2010) demonstrated that as the animals mature the overall size of dendritic spine head is augmented, indicated by increased spine head diameter and volume. Lastly, Araya et al. (2007) have suggested that the thickness of the spine neck is associated with the filtering of excitatory ionic current that ultimately enters the parent dendrite. These studies provide evidence that even at this subtle level, functional anatomical compartmentalization is still possible; these studies also highlight the promising potentials for future researches to explore structural plasticity at an extremely detailed level.

3. Using the Barrel System as a Model to Study the Sensory Cortex

Due to its distinctive cytoarchitecture, the barrel system has been used as a popular model to study the local functional microcircuitry, as well as an experimental paradigm to study cortical plasticity. The attractiveness of the whisker-to-barrel system lies within that it is composed of structurally organized and anatomically distinct units, particularly manifested in cortical layer IV, the principal leminiscal TCA recipient layer. These topographically organized discrete units in layer IV respond faithfully and reliably to stimuli on the mystacial pad, offering rodents with precise spatiotemporal coding representative to the constantly updating sensory environment (see Kleinfeld et al., 2006). The second major attractiveness in using the barrel system as a model to study the cortex is the ease of peripheral manipulation (e.g., electrocauterization, whisker-pairing, plucking or trimming the vibrissae, allowing the restoration of sensory input via whisker regrow, etc), without causing a great deal of discomfort to the experimental animals. Third, the barrel system is an extremely useful model in studying the molecular control of the TCA inputs and the development of sensory maps (for a detailed review, see Wu et al., 2011). Numerous studies have taken advantage of the topographic mapping properties of the barrel cortex, along with the genetic knockout / knockdown techniques to investigate the role of specific receptors (e.g., NR1 subunit of NMDA-R, mGluR5, adenyl-cyclase, protein kinase-A) play in the developmental mechanism of TCA. Since the pathfinding process of lemniscal TCA is a critical step in assuring proper sensory experience, the utilization of barrel system as a model has greatly contributed to our current knowledge of how (and which) the molecular mechanisms are responsible for cortical map formation.

4. Conclusion

Unraveling the complexity of the microcircuitry embedded in the cerebral cortex allows us to gain knowledge of how the brain functions. As the processing center of sensation and perception, the primary sensory areas collectively serve as an important window to elucidate the transformation from the physical stimuli of the outer world to the symphony of electrical impulses in our nervous system. It is only through the understanding of the organization and development in the cerebral cortex that we can start to appreciate the beauty and complexity of the designs that are all written within each organism. At the same time, it is through learning the neuronal mechanisms of cortical plasticity can we start to come up with possible pharmacological interventions to treat patients afflicted with neurodevelopmental or aging disorders associated with abnormal cerebral functioning. In conclusion, proper development and processing of the cerebral cortex is essential for cognition, and understanding the fundamentals of the neocortex would unlock the mystery of the conscious processing of perception.

Table 1. Morphological parameters of neurons that were analyzed with principal component analysis (PCA).

Morphological Variables Analyzed in PCA			
Somatic Variables	**Apical Dendrite**	**Dendrites**	**Total Dendrites**
Perimeter (µm)	**Quantity**	Quantity	Quantity
Area (µm²)	Nodes	Nodes	**Nodes**
Feret Max (µm)	Ends	Ends	**Ends**
Feret Min (µm)	**Length (µm)**	Length (µm)	**Length (µm)**
Aspect Ratio	**Surface Area (µm²)**	Mean Length (µm)	**Mean length (µm)**
Compactness	**Accumulative Volume (µm³)**	Surface Area (µm²)	**Surface Area (µm²)**
Convexity		Mean Surface Area (µm²)	**Mean Surface Area (µm²)**
Form Factor		Accumulative Volume (µm³)	
Roundness		Mean volume (µm³)	
Solidity			

Table 2. Statistical results (in p-values) of comparisons between the original (N=150) and systematically replicated (N=72) neuronal populations across 35 morphological variables. Please note that out of 210 possible pair-wise comparisons (Mann-Whitney U tests) between the two datasets only three comparisons reached statistical significance, indicating the consistency of our classification methodology.

Variable Name	Group 1	Group 2	Group 3	Group 4	Group 5	Group 6
Perimeter(µm)	ns	ns	ns	ns	ns	ns
Area(µm²)	ns	ns	ns	ns	ns	ns
Feret Max(µm)	ns	ns	ns	ns	ns	ns
Feret Min(µm)	ns	ns	ns	ns	ns	ns
Aspect Ratio	ns	ns	ns	ns	ns	ns
Compactness	ns	ns	ns	ns	ns	ns
Convexity	ns	ns	0.036*	ns	ns	ns
Form Factor	ns	ns	ns	ns	ns	ns
Roundness	ns	ns	ns	ns	ns	ns
Solidity	ns	ns	ns	ns	0.017*	ns
AP-Qty	ns	ns	ns	ns	ns	ns
AP-Nodes	ns	ns	ns	ns	ns	ns
AP-Ends	ns	ns	ns	ns	ns	ns
AP-Length(µm)	ns	ns	ns	ns	ns	ns
AP-mean len	ns	ns	ns	ns	ns	ns
AP-Surface(µm²)	ns	ns	ns	ns	ns	ns
AP-mean sur	ns	ns	ns	ns	ns	ns
AP-Volume(µm³)	ns	ns	ns	ns	ns	ns
AP-mean vol	ns	ns	ns	ns	ns	ns
D-Qty	ns	ns	ns	ns	ns	ns
D-Nodes	ns	ns	ns	ns	ns	ns
D-Ends	ns	ns	ns	ns	ns	ns
D-Length(µm)	ns	ns	ns	ns	ns	ns
D-mean len	ns	ns	ns	ns	ns	ns
D-Surface(µm²)	ns	ns	ns	ns	ns	ns
D-mean sur	ns	ns	0.048*	ns	ns	ns
D-Volume(µm³)	ns	ns	ns	ns	ns	ns
D-mean vol	ns	ns	ns	ns	ns	ns
TD-Qty	ns	ns	ns	ns	ns	ns
TD-Nodes	ns	ns	ns	ns	ns	ns
TD-Ends	ns	ns	ns	ns	ns	ns
TD-Length(µm)	ns	ns	ns	ns	ns	ns
TD-mean len	ns	ns	ns	ns	ns	ns
TD-surface area	ns	ns	ns	ns	ns	ns
TD-mean surface area	ns	ns	ns	ns	ns	ns

Table 3. Geometric analysis of the effect of sensory deprivation on somatic and dendritic parameters in nonpyramidal neurons.

Domain	Metric	Mean Sensory Deprived	Std. Dev. Sensory Deprived	Mean Control	Std. Dev. Control	t-value (Indep, Student)	p-value
		N=21		N=35			
Somatic	Perimeter(µm)	67.248	11.549	73.789	17.329	-1.56820	0.121844
Somatic	Area(µm²)	269.869	111.833	299.603	111.547	-1.00422	0.319112
Somatic	Feret Max(µm) (1)	24.614	6.008	26.609	7.102	-1.11026	0.271107
Somatic	Feret Min(µm) (2)	15.076	4.059	16.150	3.092	-1.18072	0.242152
Somatic	Aspect Ratio (3)	2.005	1.808	1.668	0.417	1.18366	0.240993
Somatic	Compactness (4)	0.733	0.127	0.741	0.108	-0.28795	0.774332
Somatic	Convexity (5)	0.942	0.114	0.940	0.073	0.10844	0.913995
Somatic	Form Factor (6)	0.731	0.179	0.708	0.177	0.48061	0.632460
Somatic	Roundness (7)	0.552	0.160	0.561	0.158	-0.21194	0.832834
Somatic	Solidity (8)	0.950	0.026	0.923	0.085	1.43483	0.156283
Dendritic	Quantity	7.000	2.627	7.023	2.715	-0.03189	0.974664
Dendritic	**Nodes***	10.619	6.144	5.523	4.577	3.74788	**0.000390**
Dendritic	**Ends***	17.857	7.016	12.545	5.797	3.22497	**0.001998**
Dendritic	**Length(µm)***	913.076	429.786	546.336	276.350	4.15466	**0.000100**
Dendritic	**Mean Length*** (9)	139.324	67.670	81.191	36.778	4.49564	**0.000030**
Dendritic	**Surface Area (µm²)**	3756.335	1862.085	2340.105	1188.486	3.71595	**0.000432**
Dendritic	**Mean Surface Area*** (9)	573.962	284.364	351.255	166.751	3.97381	**0.000185**
Dendritic	**Volume (µm³)***	1433.891	864.023	926.720	555.980	2.85697	**0.005788**
Dendritic	**Mean Volume*** (9)	219.502	125.816	141.495	82.652	2.98811	**0.003998**

(1) Feret Maximum: Longest diameter of the soma
(2) Feret Minimum: Longest diameter perpendicular to feret maximum
(3) Aspect Ratio: (feret max)/(feret min); as aspect ratio approaches 1, it is indicative that the soma is closer to a symmetric shape (e.g., circle or square)
(4) Compactness: [$\sqrt{}$(4/π) × area]/(feret max); numerical values of somatic compactness closer to 1 represent a more perfect spherical soma
(5) Convexity: (convex contour)/(perimeter); this parameter is indicative of the somatic surface areal profile; higher somatic convexity yields to more indentations, which translates to higher estimated surface area to cellular volume ratio.
(6) Form Factor: (4π × area)/(perimeter^2); this value directly reflects the complexity of somatic perimeter; a higher numerical value represents a more complex somatic perimeter.
(7) Roundness: (4 × area)/(π × feret max^2), similar to compactness but is another way to differentiate objects with small compactness values for the closeness to a perfect sphere.
(8) Solidity: the ratio of somata area as a whole over convex area, where values closer to 1 represent more solid (i.e. smooth, uniform) somata
(9) Dendritic mean length, mean surface area, and mean volume: are all derived from total dendritic length, total surface area, and total dendritic volume divided by the number of primary dendritic trunks, respectively.

Table 4. Geometric analysis of the effect of sensory deprivation on somatic, apical dendritic and basilar dendritic parameters in pyramidal neurons.

Domain	Metric	Mean Sensory Deprived	Std. Dev. Sensory Deprived	Mean Control	Std. Dev. Control	t-value (Indep, Student)	p-value
		N=39		N=35			
Somatic	**Perimeter(μm)***	66.24	12.04	58.28	1.60	3.136	**0.001**
Somatic	**Area(μm²)***	239.88	66.16	193.90	8.39	3.351	**0.001**
Somatic	**Feret Max(μm)** (1)	22.55	4.03	19.99	0.54	2.999	**0.002**
Somatic	**Feret Min(μm)** (2)	16.18	3.09	14.40	0.45	2.648	**0.005**
Somatic	Aspect Ratio (3)	1.4200	0.2699	1.4112	0.0383	.151	0.440
Somatic	Compactness (4)	0.7773	0.0751	0.7904	0.0135	-.728	0.234
Somatic	Convexity (5)	0.9379	0.0541	0.9551	0.0067	-1.554	0.062
Somatic	Form Factor (6)	0.6976	0.1254	0.7286	0.0195	-1.102	0.137
Somatic	Roundness (7)	0.6098	0.1170	0.6310	0.0212	-.753	0.227
Somatic	Solidity (8)	0.9030	0.0628	0.9191	0.0095	-1.154	0.126
Apical Den.	Quantity	1	0	1	0	n.a.	n.a.
Apical Den.	**Nodes**	3.36	2.47	6.09	0.75	-3.320	**0.001**
Apical Den.	**Ends***	4.26	2.54	7.54	0.77	-3.902	**0.000****
Apical Den.	**Length(μm)***	313.97	151.02	529.87	47.66	-4.165	**0.000****
Apical Den.	**Surface Area (μm²)***	1553.80	713.53	2492.17	193.88	-4.272	**0.000****
Apical Den.	**Volume(μm³)***	671.48	299.03	1103.80	87.67	-4.448	**0.000****
Basilar Den.	Qty	6.46	3.75	5.14	0.45	1.730	**0.044**
Basilar Den.	**Nodes***	7.79	9.13	3.11	0.34	2.968	**0.002**
Basilar Den.	**Ends***	14.33	11.96	8.11	0.53	2.983	**0.002**
Basilar Den.	**Length(μm)***	640.78	383.28	395.06	38.00	3.314	**0.001**
Basilar Den.	Mean len (9)	108.06	78.84	93.39	9.75	.905	0.184
Basilar Den.	**Surface(μm²)**	2350.31	1568.56	1505.21	156.63	2.781	**0.003**
Basilar Den.	Mean sur (9)	402.34	336.90	339.31	38.16	.934	0.177
Basilar Den.	**Volume(μm³)**	760.09	561.90	493.98	55.60	2.449	**0.008**
Basilar Den.	Mean vol (9)	131.43	120.80	110.75	13.61	.856	0.197
Total (Apical + Basilar)	**TD-Qty** (10)	7.46	3.75	6.14	0.45	1.73	**0.044**
Total (Apical + Basilar)	TD-Nodes (10)	11.15	10.28	9.20	0.96	.996	0.161
Total (Apical + Basilar)	TD-Ends (10)	18.59	13.05	15.66	1.09	1.203	0.117
Total (Apical + Basilar)	TD-Length(μm) (10)	954.75	482.02	924.93	74.23	.277	0.391
Total (Apical + Basilar)	TD-Surface Area (μm²) (10)	3904.12	2013.13	3997.37	306.34	-.208	0.418
Total (Apical + Basilar)	TD-Volume (10)	1431.56	744.21	1597.78	123.80	-.966	0.169

(10): Total Dendritic Variables (Qty, Nodes, Ends, Length, Surface Area, Volume): These are all derived from adding apical and basilar dendritic components together, e.g., total dendritic length = apical dendritic length + basilar dendritic length.

* Indicates Statistical Significance at α level preset = 0.05 ** Indicates p-value less than 0.0001

Table 5. Statistical results (in p-values, test: Unequal N HSD) of pair-wise comparisons between the different morphological categories of dendritic spines in their lengths of dendritic spines, defined as the distance from the most distal portion of the spine (spine head) to the base of the spine (surface of the dendritic shaft). (Also see Figure 20C)

	Branched	Filopodia	Mushroom	Stubby	Thin
Branched		0.641777	**0.023721**	**0.000017**	**0.000083**
Filopodia	0.641777		**0.014589**	**0.000017**	**0.000017**
Mushroom	**0.023721**	**0.014589**		**0.000017**	**0.004118**
Stubby	**0.000017**	**0.000017**	**0.000017**		**0.000031**
Thin	**0.000083**	**0.000017**	**0.004118**	**0.000031**	

Table 6. The number of animals and reconstructed neurons in various conditions (normal sensory vs. treatment groups).

Age and Condition of Animals	Cortical Layer	n of animals	n of reconstructed neurons
P15, normal sensory experience	IV	4	19
P15, normal sensory experience	VI	4	16
P30, normal sensory experience	IV	5	25
P30, normal sensory experience	VI	5	22
P30, unilaterally trimmed P0-30	IV	5	14
P30, bilaterally trimmed P0-30	IV	5	16
P30, bilaterally trimmed P0-30	VI	5	23
P30, MK801 inject P0-P30	IV	3	17
P30, MK801 inject P0-P30	VI	3	18
P60, normal sensory experience	IV	4	19
P60, normal sensory experience	VI	4	17
P60, bilateral regrow P31-60	IV	4	13
P60, bilateral regrow P31-60	VI	4	14
P60, MK801 withdraw P31-60	IV	3	12
P60, MK801 withdraw P31-60	VI	3	13
P100, normal sensory experience	IV	6	18
P100, normal sensory experience	VI	6	19
P130, normal sensory experience	IV	7	15
P130, normal sensory experience	VI	7	15
P130, bilaterally trimmed P100-130	IV	6	15
P130, bilaterally trimmed P100-130	VI	6	14

Figure 1. Golgi stained section of the barrel cortex. A: Low magnification image (4x) illustrating barrel cortex and its six distinct layers bounded by pia and the white matter. The white box highlights the region magnified in panel B; Scale bar: 250µm. B: Higher magnification (10x) highlighting the morphologies of layer VI neurons. Scale bar: 250µm. C: Higher magnification (20x) of a single pyramidal neuron located in layer VI. Scale bar: 50 µm. D: High magnification (100x) of the region in white in panel C. Please note the presence of dendritic spines, demonstrating entirety of the neuronal labeling. Scale bar: 50 µm. E: High magnification (100x) of the region in black in panel F. Please note the relative absence of dendritic spines. Scale bar: 25µm F: 20x magnification of a typical labeled nonpyramidal neuron located in layer VI. Scale bar: 25µm.

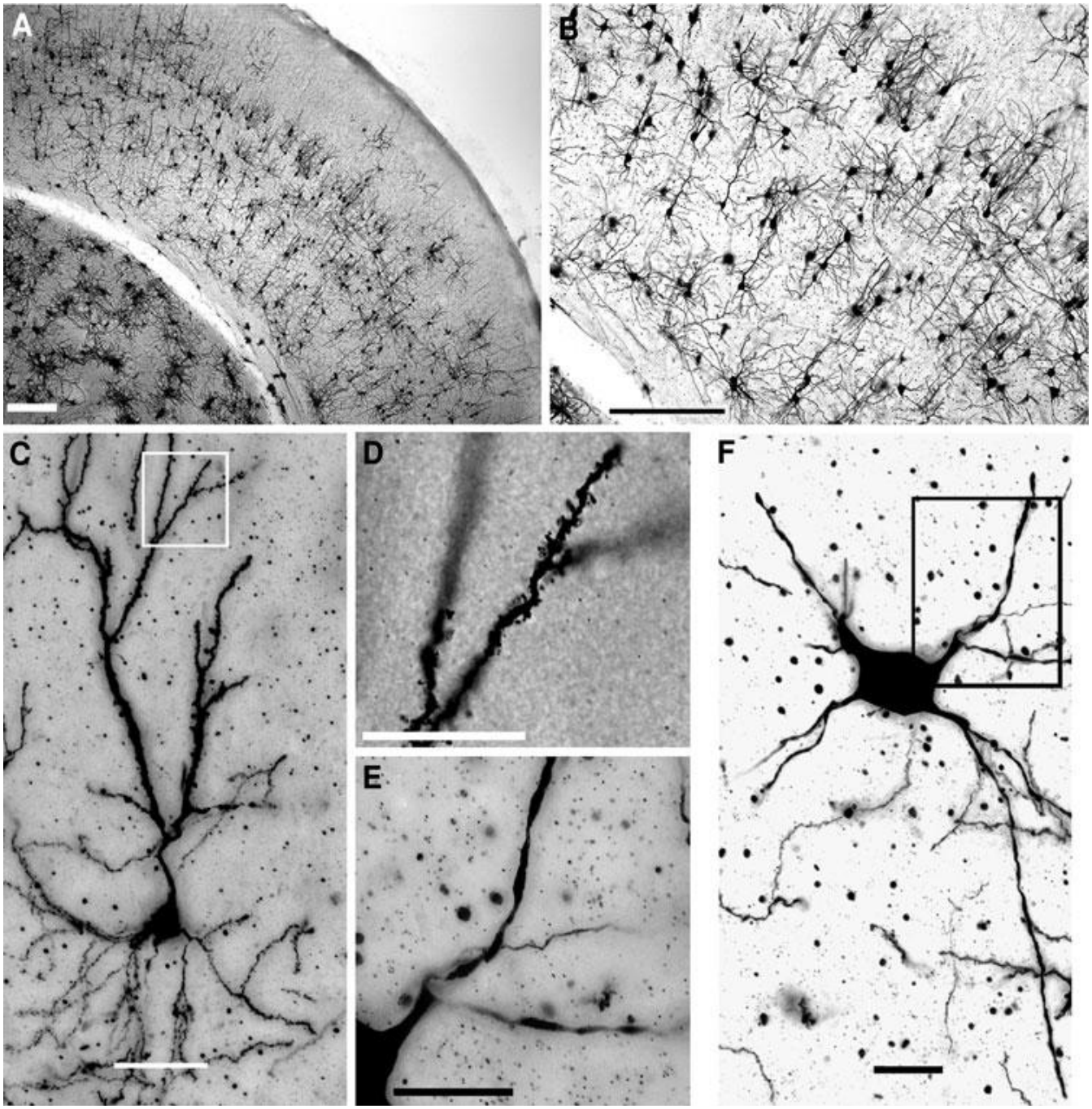

Figure 2. The results of cluster analysis (Ward's method, Euclidean distances) of 150 digitally reconstructed neurons. Each point on X-axis is arbitrary and represents one cell. The Y-axis depicts linkage distance; the degree of variance among neurons based on surveyed parameters. Neurons with short linkage distance represent high morphological resemblance to one another, whereas neurons with long linkage distance signify high morphological dissimilarity to each other. Six distinct groups and several subgroups are defined.

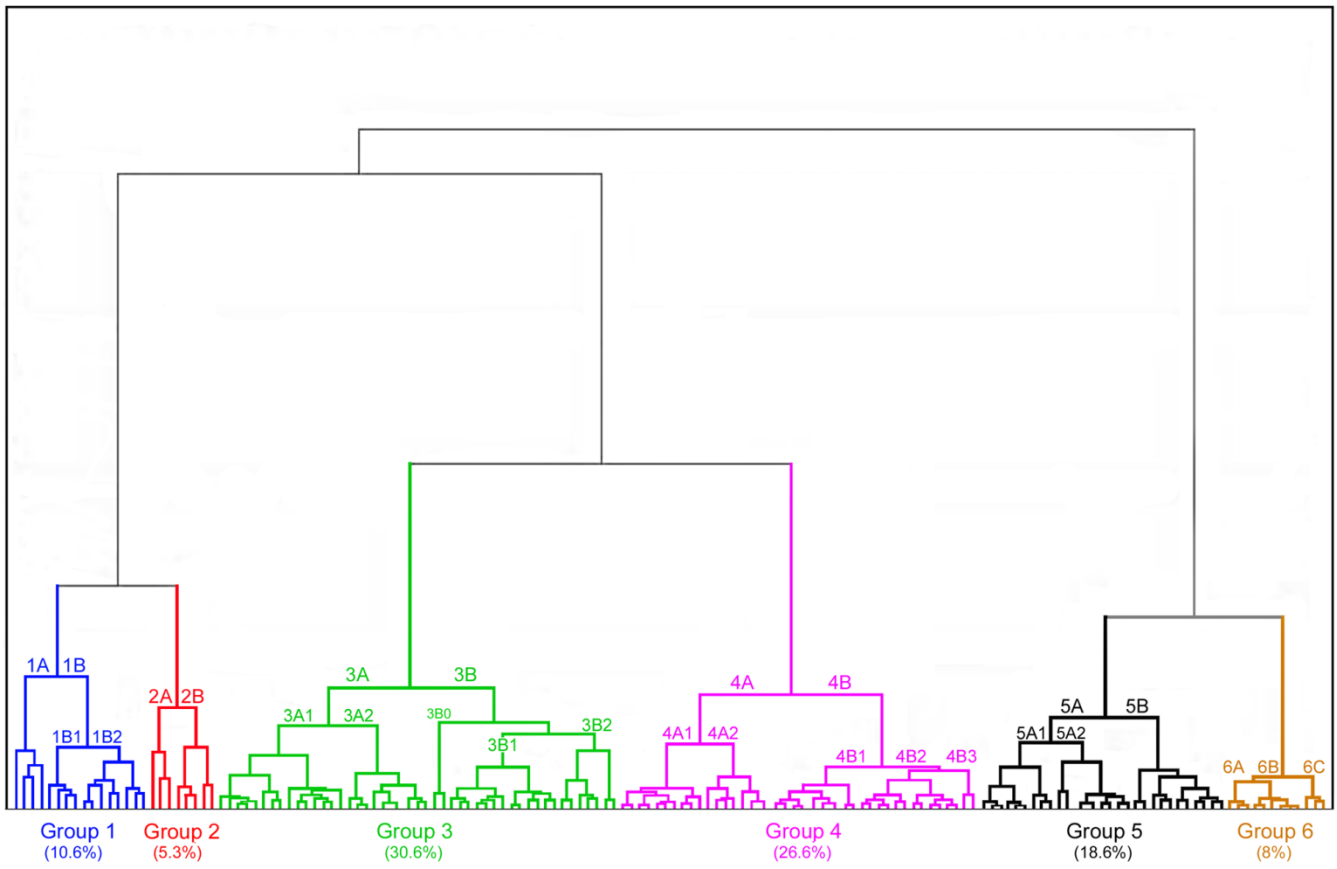

Figure 3. Group 1 representative cells. *Pyramidal neurons with elaborate dendrites.* **A:** Examples of cells in subgroup 1A, characterized by extensive and elaborate pattern of apical dendrites. **B:** Examples of cells in subgroup $1B_1$, characterized by slightly shorter but thicker apical tufts. **C:** Example of an atypically oriented pyramidal neuron. Note the apical tuft is pointing horizontally. **D:** Examples of subgroup $1B_2$, characterized by an elaborate basilar skirt and a long and relatively simple apical dendrite. Cells are oriented so that the pia mater is at the top, and medial is to the left. Scale bars represent 50μm.

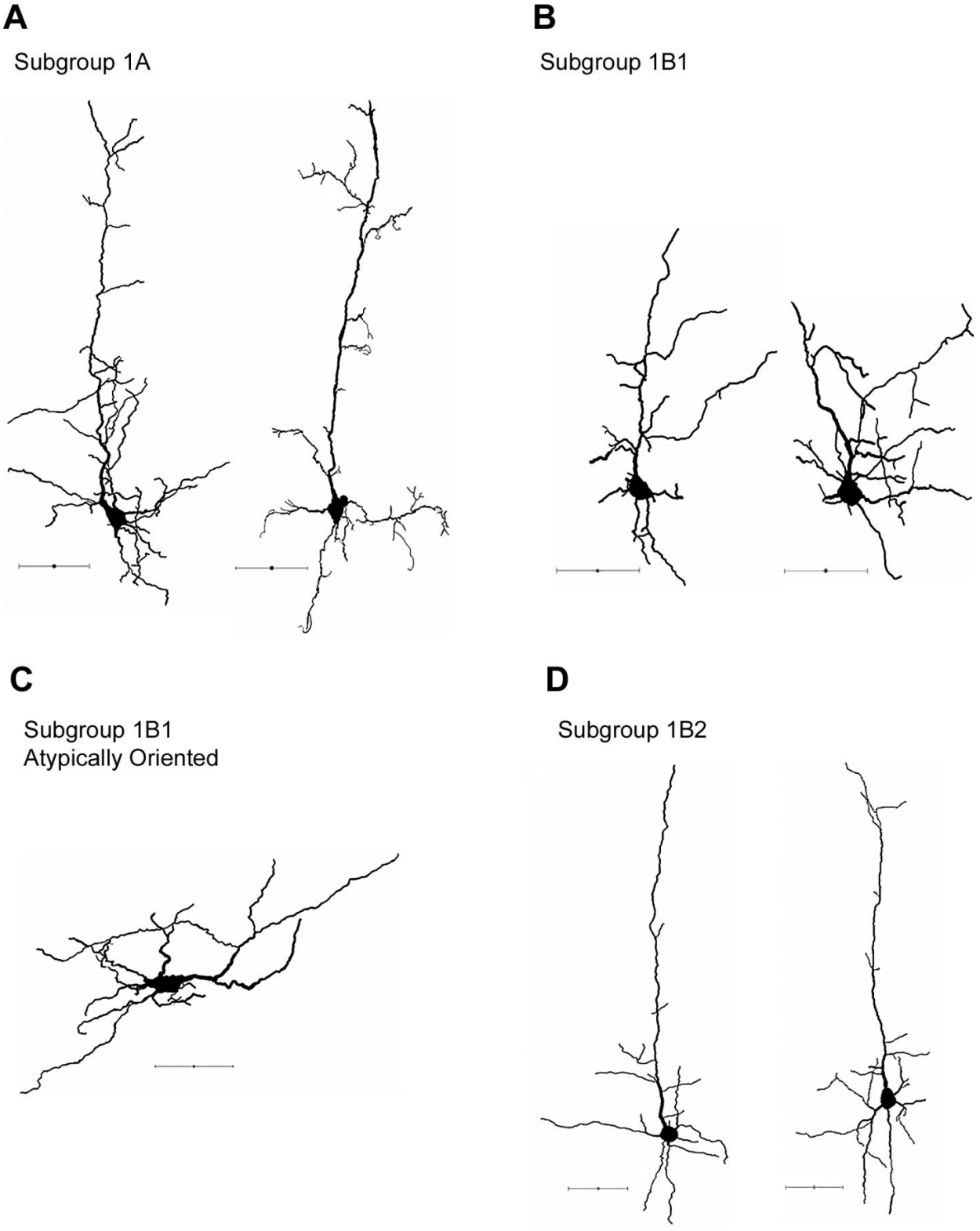

Figure 4. Group 2 representative cells. *Non-pyramidal neurons with elaborate dendrites.* **A:** Examples of cells in subgroup 2A, characterized by elaborate and relatively spherical dendritic fanning patterns. **B:** Examples of cells in subgroup 2B, characterized by bipolar fanning patterns particularly towards the pia mater and the white matter. Cells are oriented so that the pia mater is at the top, and medial is to the left. Scale bars represent 50μm.

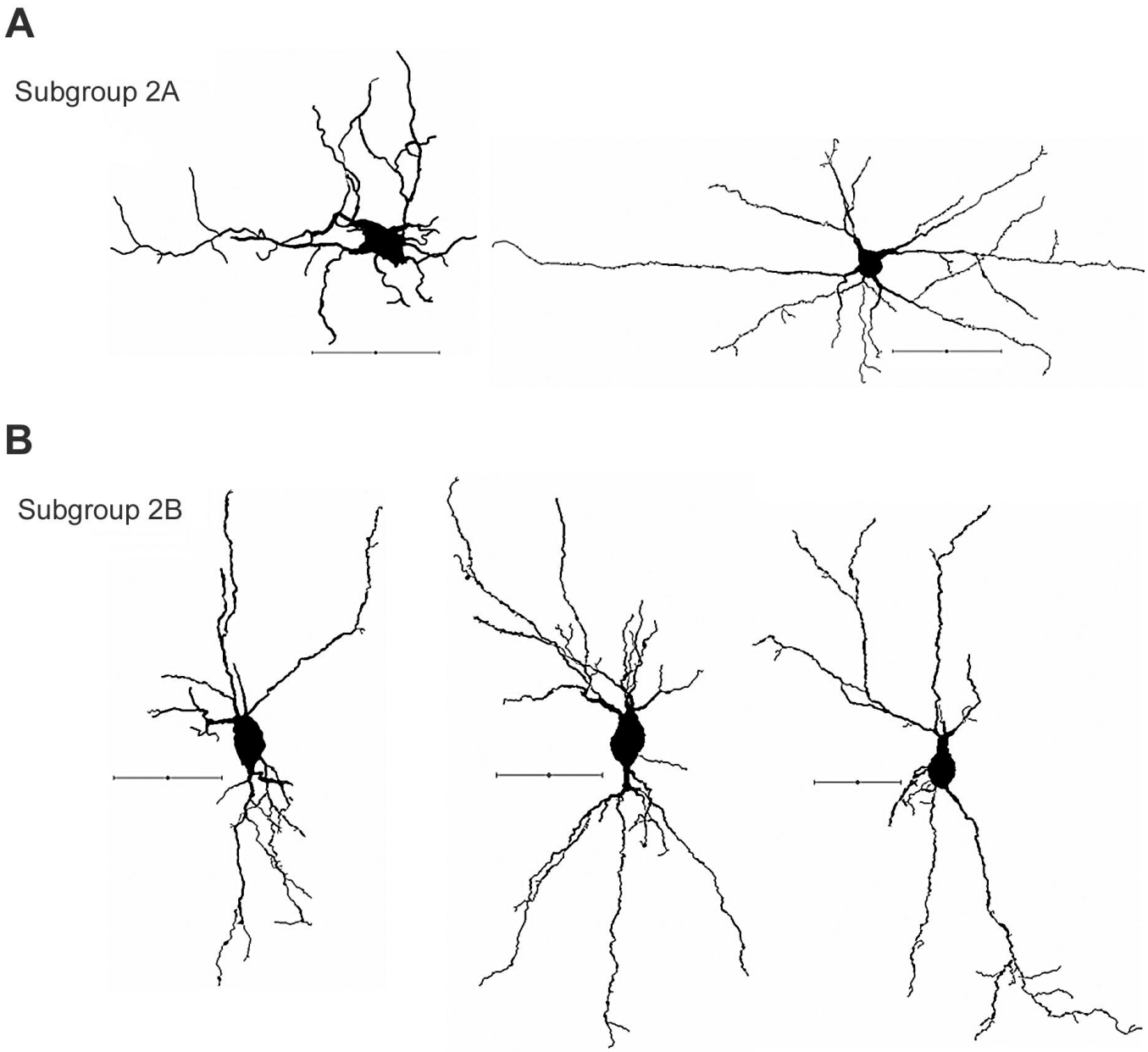

Figure 5. Group 3 representative cells. *Neurons with moderate apical & basilar dendritic pattern.* **A:** Examples of cells in subgroup $3A_{1\text{-}\alpha}$, characterized by long apical dendrites that typically terminate in upper layer V. **B:** Examples of cells in subgroup $3A_{1\text{-}\beta}$, characterized by medium length apical dendrites that typically terminate in lower layer V. **C:** Examples of cells in subgroup $3A_2$, note the spherical soma compared to those of $3A_1$. **D, E, F**: Examples of cells in Subgroup 3B, all with long apical dendrites that typically terminate in upper layer V (D) or lower layer IV (E&F). Cells are oriented so that the pia mater is at the top, and medial is to the left. Scale bars represent 50μm.

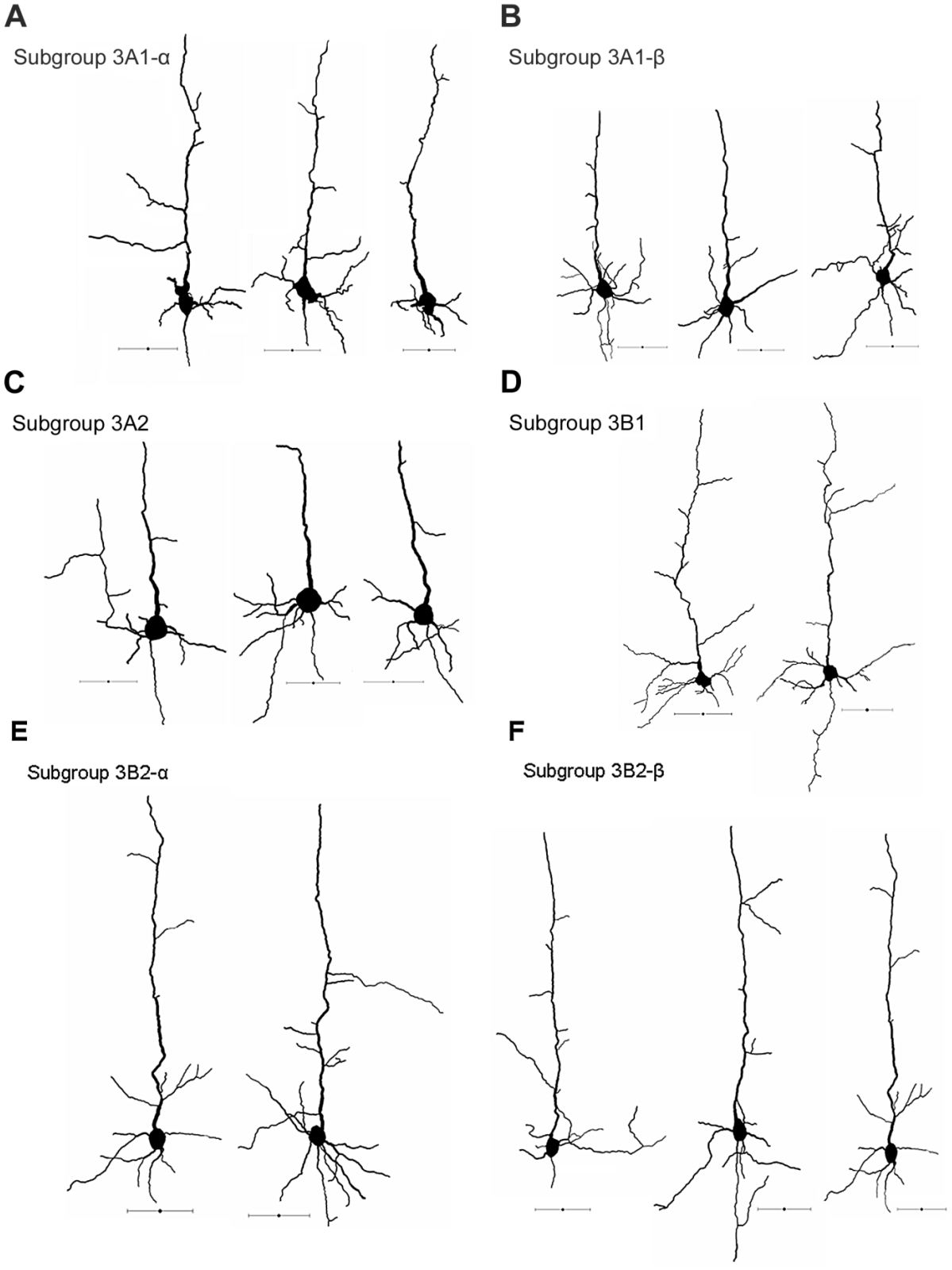

Figure 6. Group 4 representative cells. *Pyramidal neurons with short overall dendrites.* **A, B:** Examples of cells in Subgroup 4A, typically with apical dendrites terminating within Layer VI. Note that Subgroup $4A_1$ (A) exhibits more elaborative fanning pattern than $4A_2$ (B). **C, D, E:** Examples of cells in Subgroup 4B, characterized by circular/oval somata and short total length of dendrites. Note that although (E) has longer apical dendrites, the averaged total lengths of dendrites are comparable to C & D. **F:** Observed cells with atypical orientation. Cells are oriented so that the pia mater is at the top, and medial is to the left. Scale bars represent 50μm.

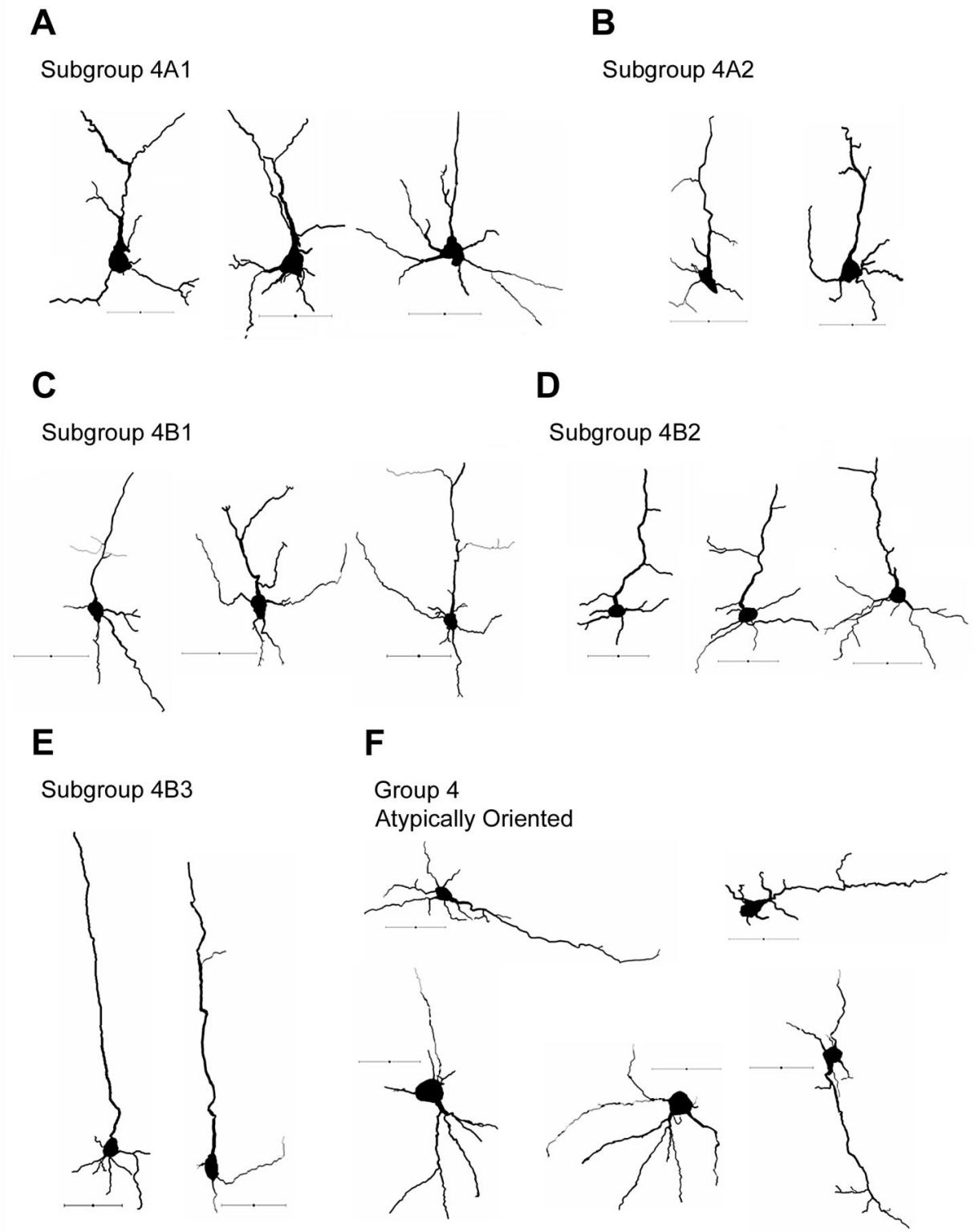

Figure 7. Group 5 representative cells. *Large Nonpyramidal Neurons.* **A:** Examples of cells in Subgroup $5A_1$, characterized by circular/oval somata and moderate dendritic fanning pattern. **B:** Representative cells in Subgroup $5A_2$. Note the dendritic pattern is simpler compared to (A). **C:** Examples of cells in Subgroup 5B, characterized by a dendritic fanning pattern typically oriented along the contours of white matter. Cells are oriented so that the pia mater is at the top, and medial is to the left. Scale bars represent 50μm.

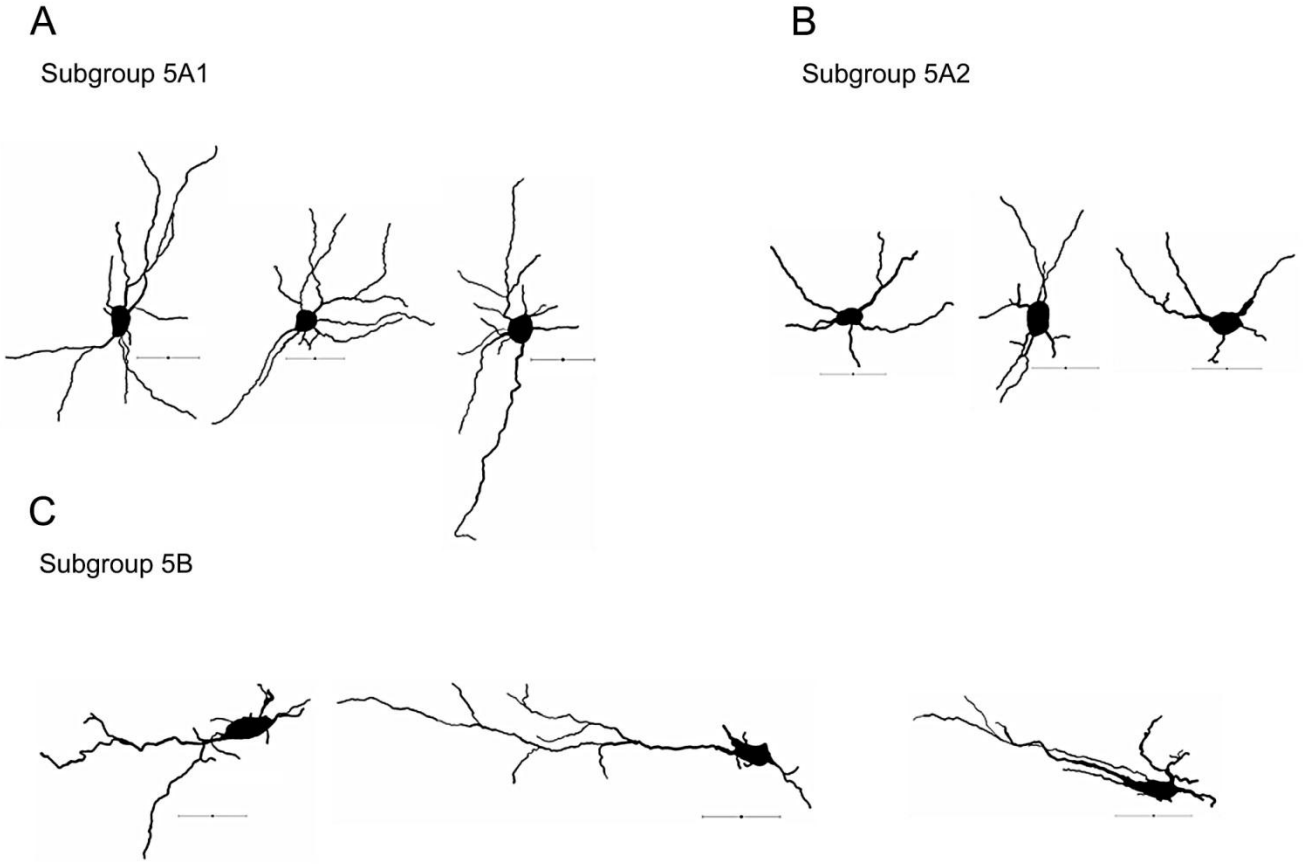

Figure 8. Group 6 representative cells. *Small neurons without apical dendrites*. Cells in this group are characterized by small somata and absence of an apical dendrite. **A, B:** Examples of cells in Subgroup 6A and Subgroup 6B. Note that cells in (A) have more circular somata compared to cells in (B). **C:** Cells in subgroup 6C are suspected to be incompletely stained and/or incompletely reconstructed neurons. Only a small (3 out of 150) portion of neurons belong in this category. Cells are oriented so that the pia mater is at the top, and medial is to the left. Scale bars represent 50μm.

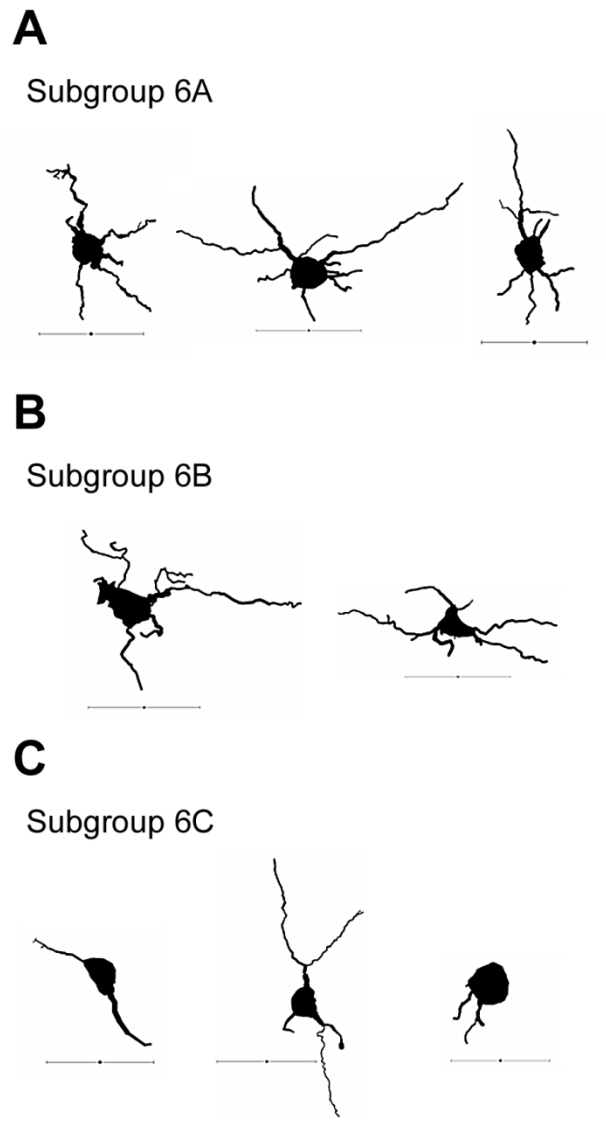

Figure 9. A: The replicated results of cluster analysis of 72 digitally reconstructed neurons from a separate, independent group of animals. Similar to Figure 2, six distinct groups are defined. **B:** Representative cortical neurons of Group 1 from the replicated population. Note the morphological similarity to Group 1 (See Figure 3) in the original clustering. **C:** Representative cortical neurons of Group 2 from the replicated population. Note the morphological similarity to Group 2 (See Figure 4) in the original clustering. **D:** Representative cortical neurons of Group 3 from the replicated population. Note the morphological similarity to Group 3 (See Figure 5) in the original clustering. **E:** Representative cortical neurons of Group 4 from the replicated population. Note the morphological similarity to Group 4 (See Figure 6) in the original clustering. **F:** Representative cortical neurons of Group 5 from the replicated population. Note the morphological similarity to Group 5 (See Figure 7) in the original clustering. **G:** Representative cortical neurons of Group 6 from the replicated population. Note the morphological similarity to Group 6 (See Figure 8) in the original clustering. Scale bars are 50μm.

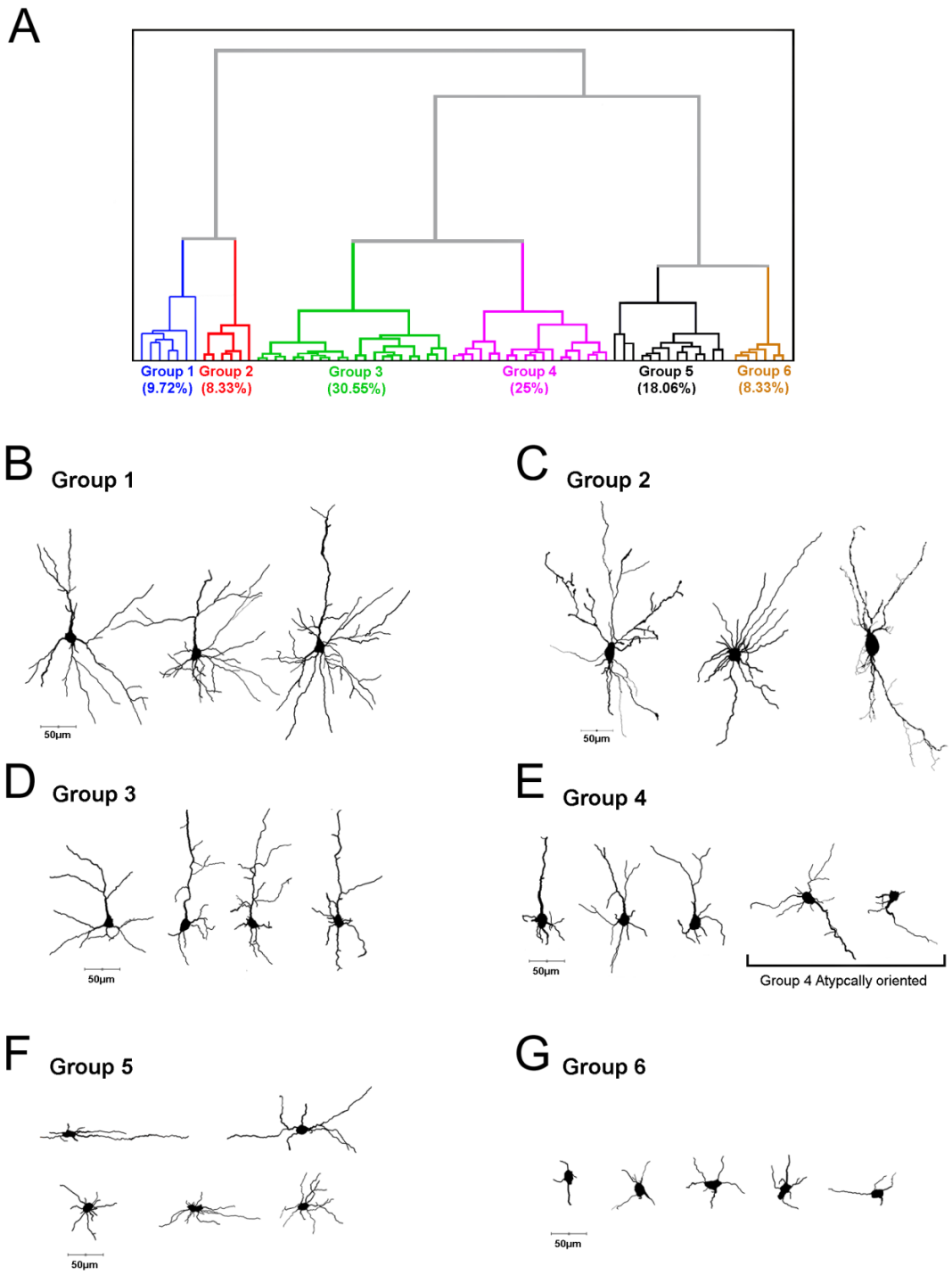

Figure 10. Laminar Location. **A:** Schematics of laminar location. Each component (cortical plate distance, distance from distal process to pia, and distance from cell body to white matter) was obtained for all neurons. **B:** *Relative distances (%) from soma to pia*. **C:** *Relative distances (%) from distal process to pia.* Center white lines represent numerical means while center black lines represent medians.

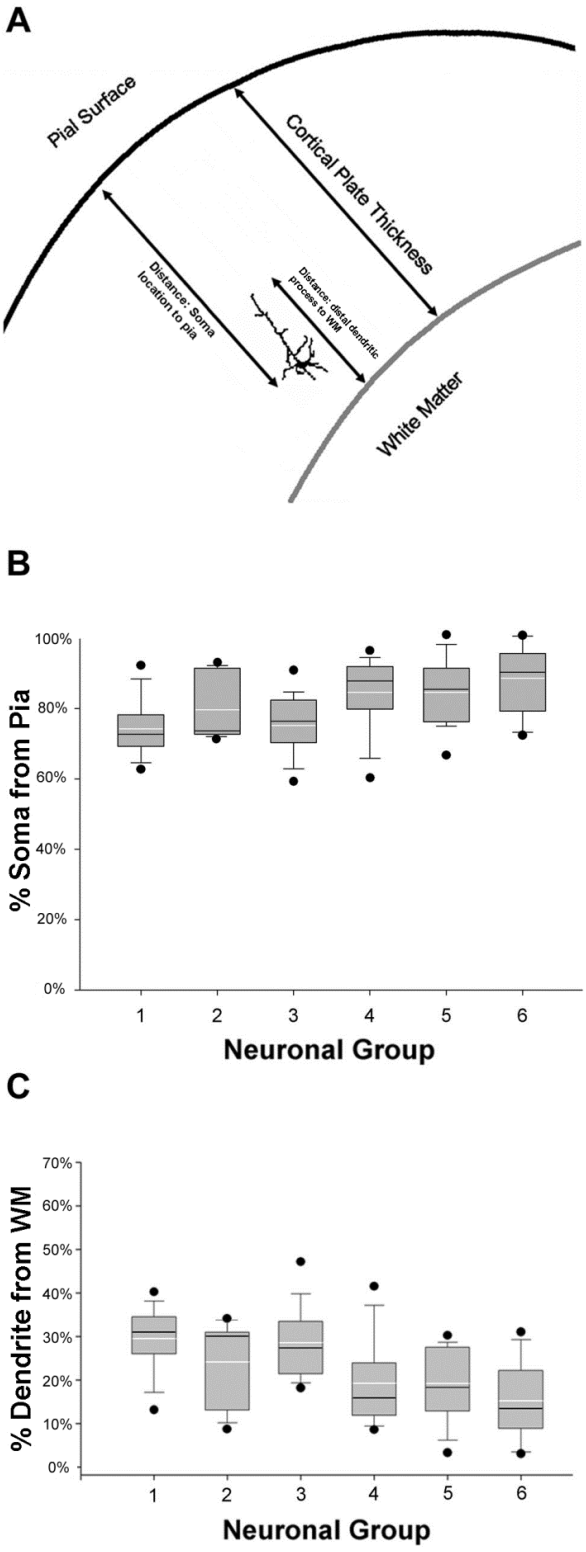

Figure 11. Sholl Analyses. **A:** Schematics of Sholl Analysis. Each increment of concentric sphere radii is 10μm. Total dendritic intersections, total dendritic spines, and total dendritic nodes were measured and analyzed. **B:** The number of dendritic intersections as a function of distance away from the soma (μm). **C:** The number of spines as a function of distance away from the soma (μm) for each neuronal group. **Inset:** The overall density of dendritic spines per 10μm of total dendritic length. **D:** The number of dendritic nodes as a function of distance away from the soma (μm) for each neuronal group. For all panels, error bars represent Standard Error of the Mean (SEM).

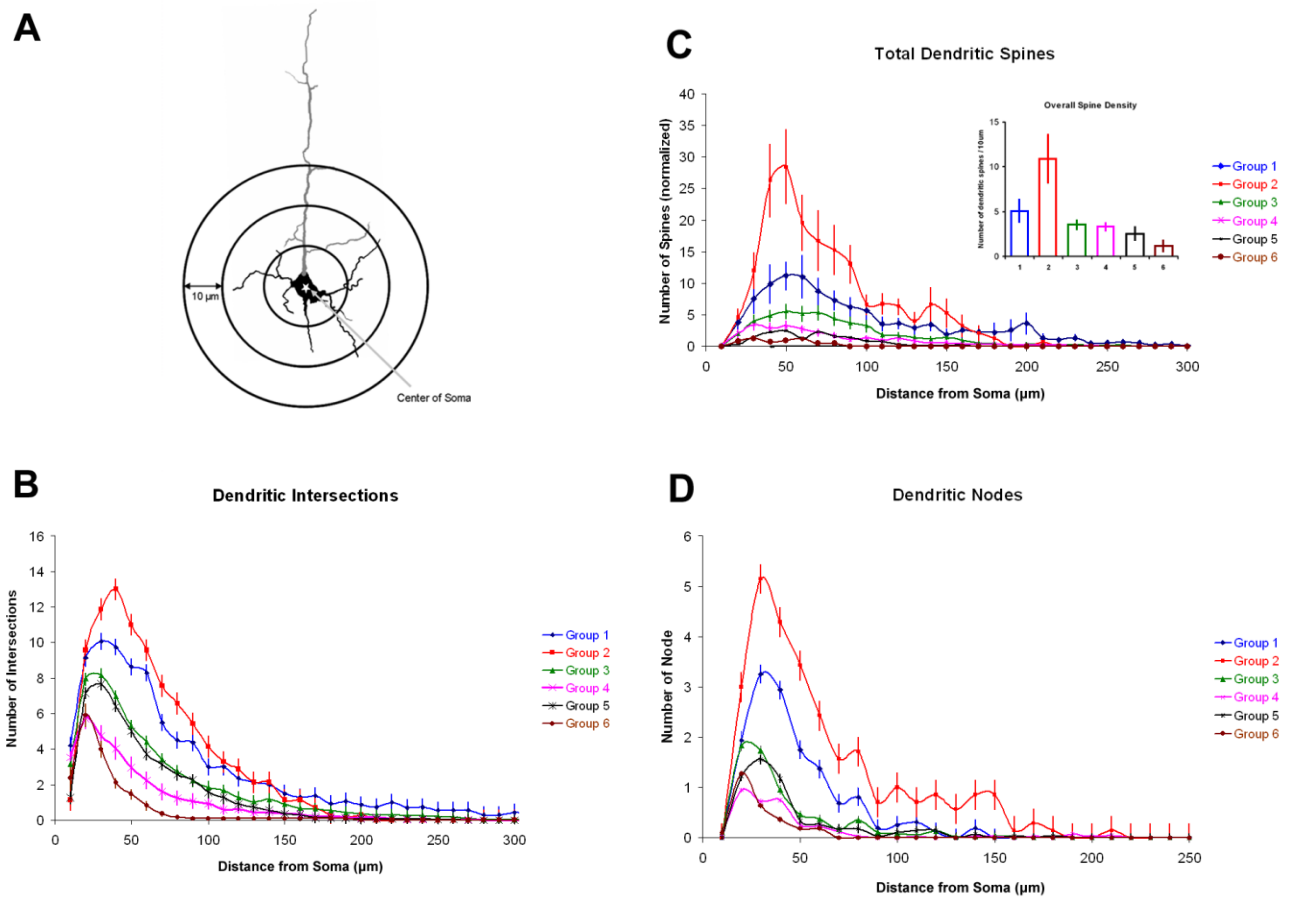

Figure 12. Polar plots of dendritic fanning pattern. **A:** Schematics of polarity. 0° represents the direction towards the pial surface, while 90° and 270° represents the direction towards lateral/inferior side and medial/superior side, respectively. **B-G:** Polar plots of dendritic pattern for each neuronal group. Theta axes depict length of dendrites (μm) while the radian depicts degree in angles (°) of the fanning pattern. Solid lines represent length of basilar dendrites while dotted lines represent length of apical dendrites. Atypically oriented neurons were excluded.

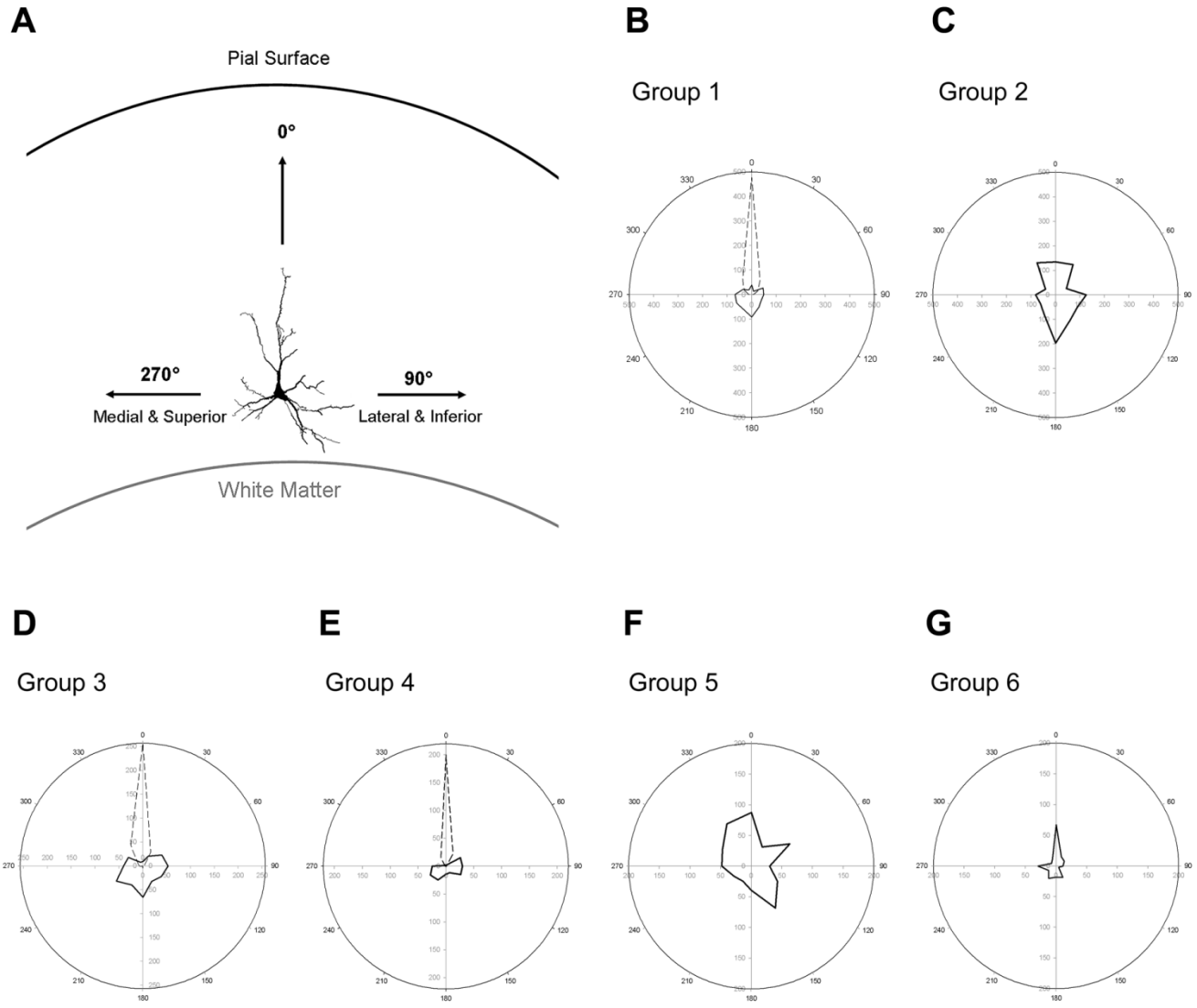

Figure 13. Representative reconstructed neurons. **A, B**: Reconstructed layer VI pyramidal neurons in the control P30 and sensory deprived P30, respectively. **C, D**: Reconstructed layer VI nonpyramidal neurons in the control P30 and sensory deprived P30, respectively. All scale bars: 50µm.

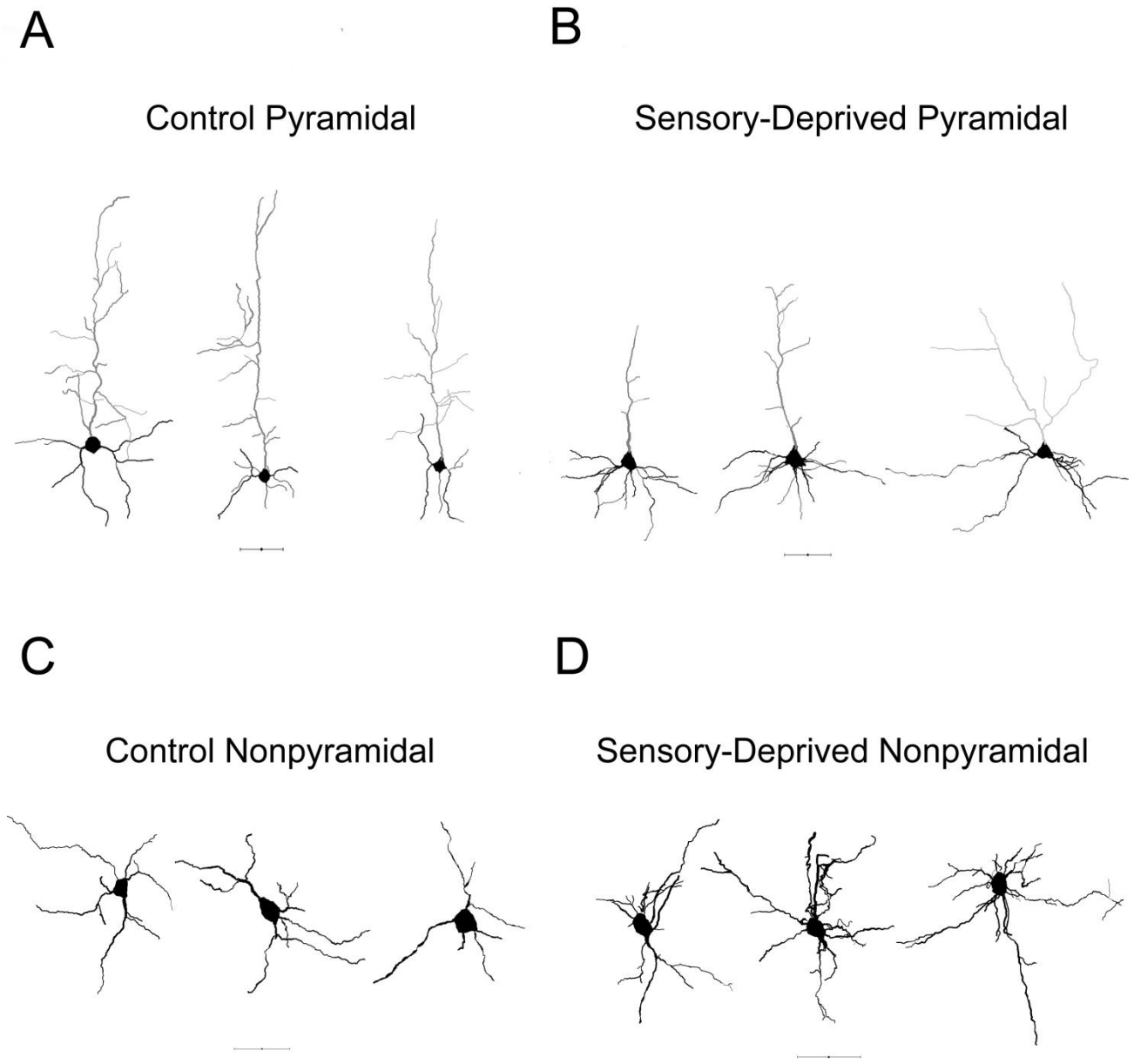

Figure 14. Effect of chronic sensory deprivation on dendritic parameters of layer VI non-pyramidal neurons. Dendritic morphometric variables in control vs. sensory deprived animals. Overall, dendritic parameters increased considerably (with the exception of *dendritic quantity*) following chronic sensory deprivation in developing animals, means and one standard error of the mean are plotted. Asterisks indicates statistical significance at $p<0.05$.

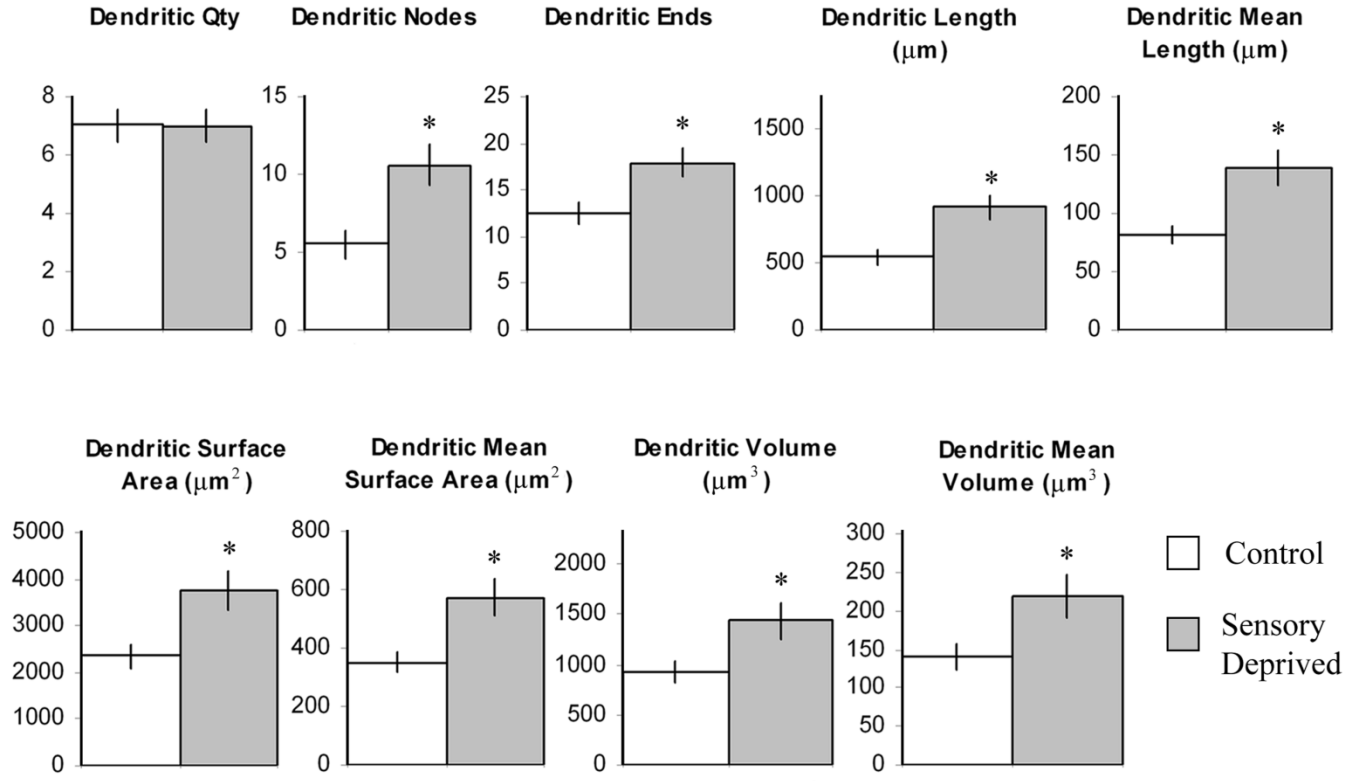

Figure 15. Sholl analyses of the dendrites in layer VI non-pyramidal neurons following chronic sensory deprivation. **A:** Mean number of dendritic intersections between 10μm concentric spheres in control versus sensory-deprived mice. Increased number of dendritic intersections in sensory-deprived relative to control mice was distributed mostly within the first 90μm, suggesting that the effect is relatively localized. **B:** Mean number of dendritic lengths between 10μm concentric spheres in control versus sensory-deprived mice. Similar to mean number of dendritic intersections, the increased dendritic length in sensory-deprived relative to control mice were distributed mostly within the first 110μm of the dendrite, indicating that the effect is localized. Error bars indicate standard error of the mean (SEM). Asterisks indicates statistical significance of posthoc tests (Tukey HSD) at individual levels ($p < 0.05$).

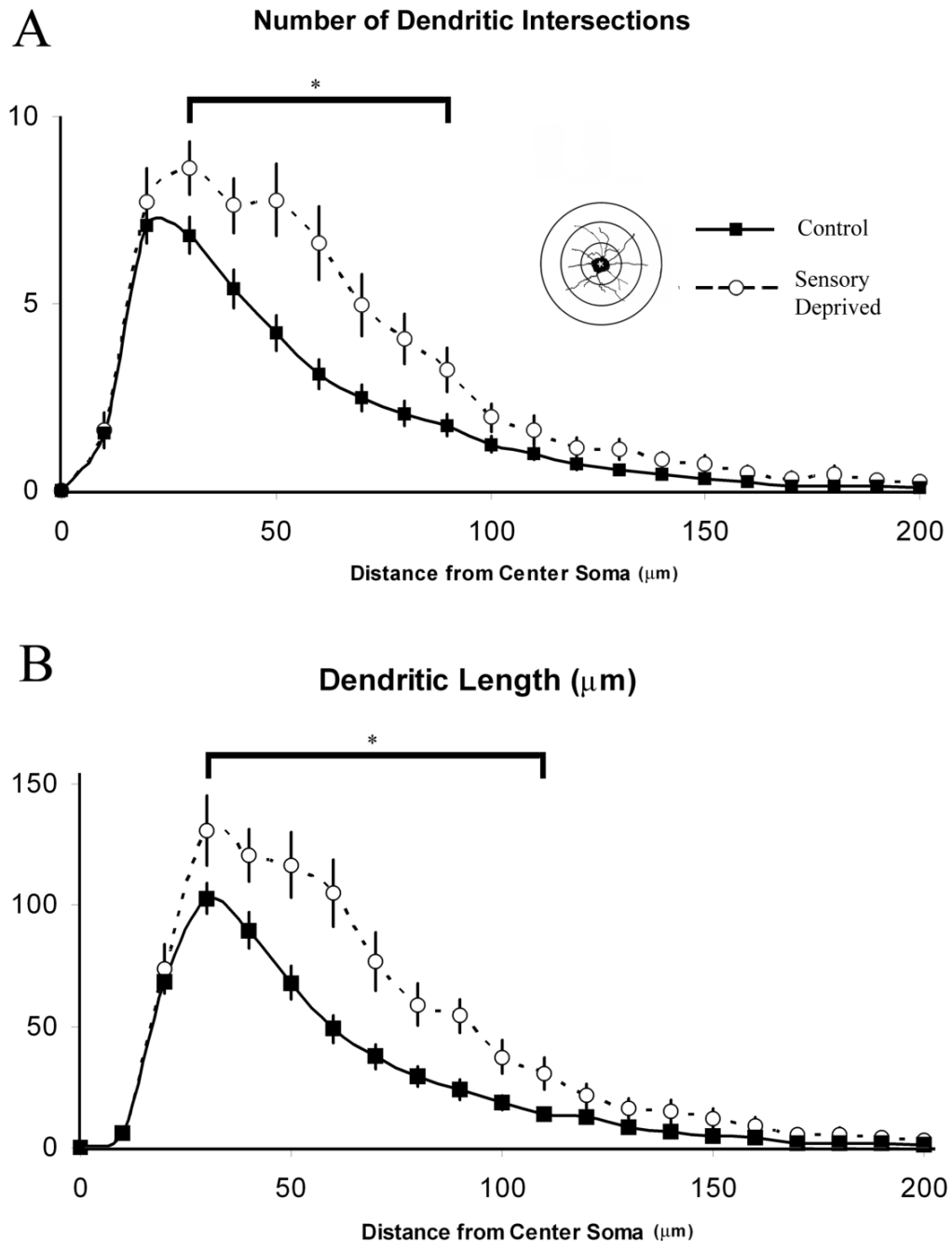

Figure 16. Effect of chronic sensory deprivation on apical dendritic parameters of layer VI pyramidal neurons. Apical dendritic morphometric variables in control vs. sensory deprived animals. Apical dendritic parameters showed decreased significantly (with the exception of *dendritic quantity and number of bi/trifurcations*) following chronic sensory deprivation in developing animals, means and one standard error of the mean are plotted. Asterisks indicates statistical significance at $p<0.05$.

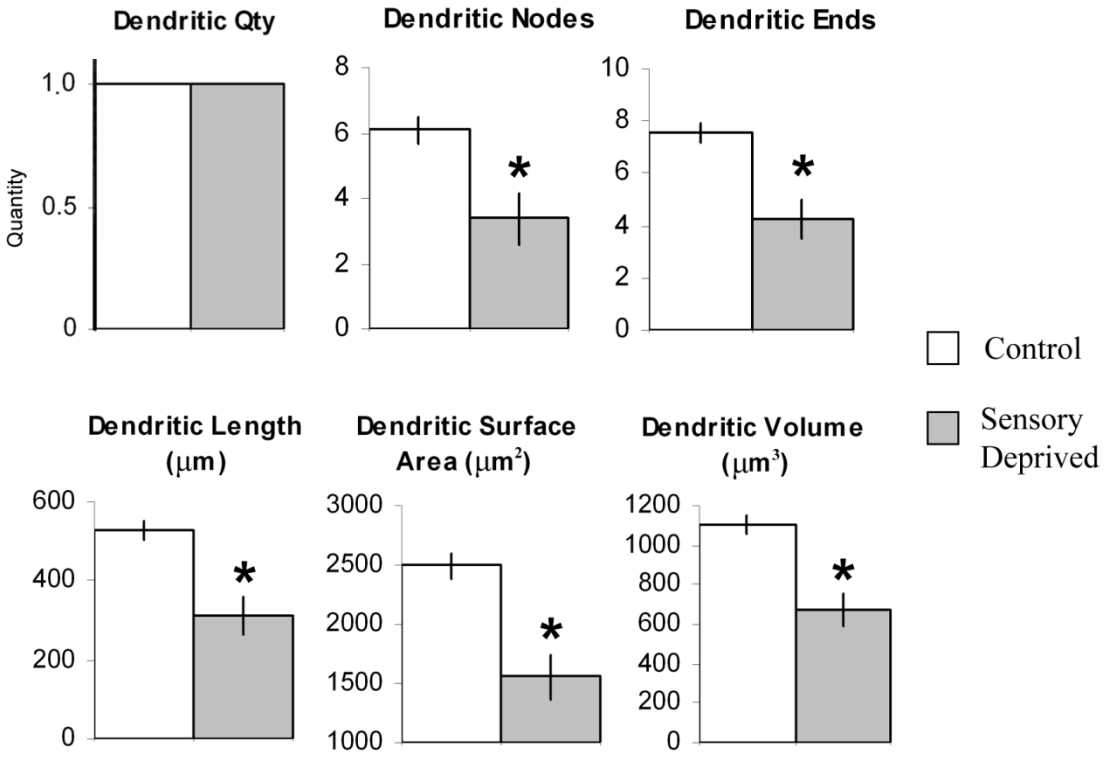

Figure 17. Sholl analyses of the apical dendrites in layer VI pyramidal neurons following chronic sensory deprivation. **A:** Mean number of apical dendritic intersections between 10μm concentric spheres in control versus sensory-deprived mice. The decreased number of dendritic intersections in sensory-deprived relative to control mice was distributed from 120μm to 180μm from the center of the soma, suggesting that the effect is relatively distal and might be outside of layer VI. **B:** Mean number of apical dendritic lengths between 10μm concentric spheres in control versus sensory-deprived mice. Similar to mean number of apical dendritic intersections, the decreased apical dendritic length in sensory-deprived relative to control mice was distributed mostly from 90μm to 190μm away from the soma. Error bars indicate standard error of the mean (SEM). Asterisks indicates statistical significance of posthoc tests (Fisher LSD) at individual levels ($p < 0.05$).

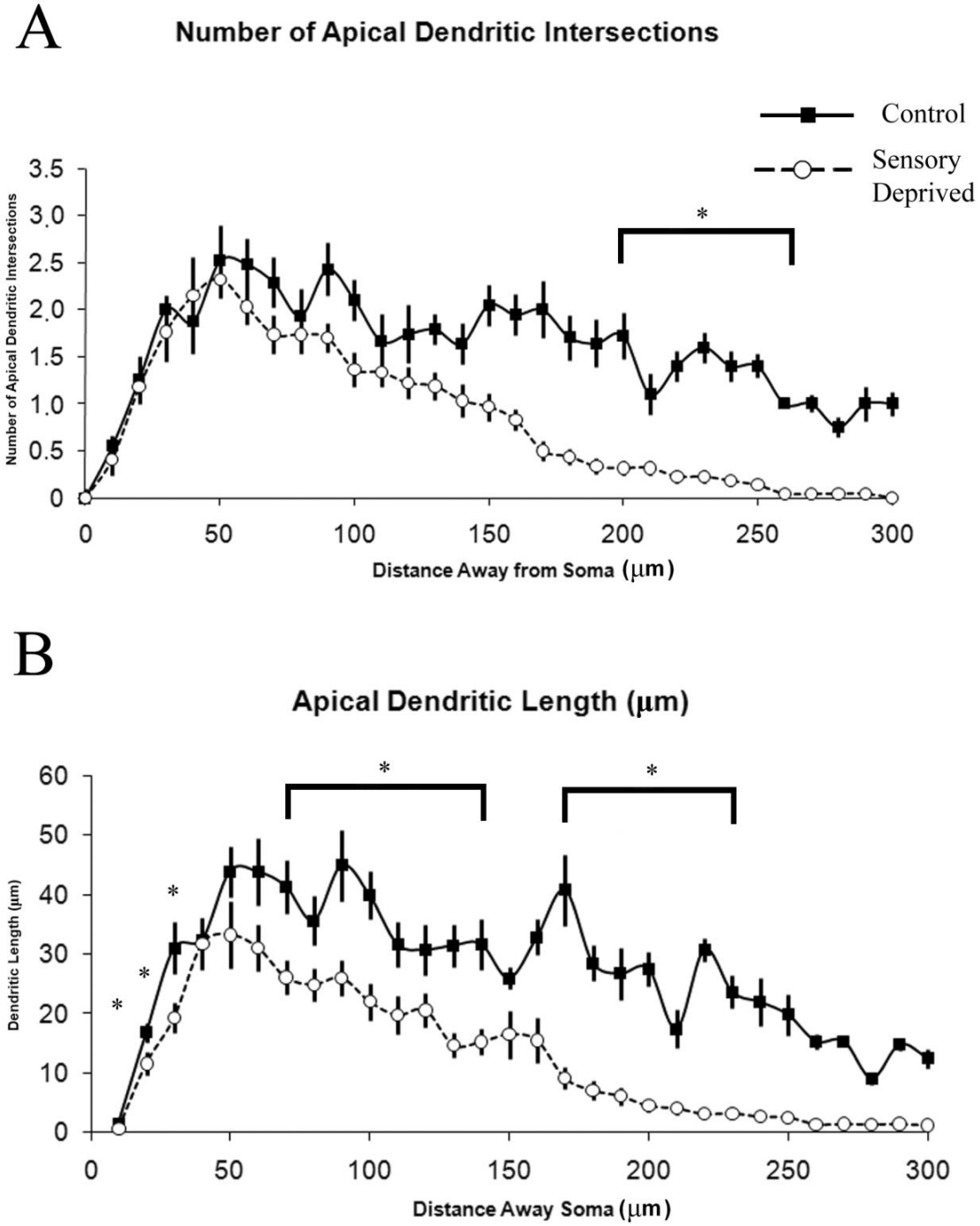

Figure 18. Effect of chronic sensory deprivation on basilar dendritic parameters of layer VI pyramidal neurons. Basilar dendritic morphometric variables in P30 control vs. sensory deprived animals. Basilar dendritic parameters exhibited an overall trend to increase significantly (including *dendritic nodes*, *dendritic ends*, and *dendritic length*) following chronic sensory deprivation in developing animals. Numerical means and one standard error of the mean (as error bars) are plotted. Asterisks indicates statistical significance at $p<0.05$.

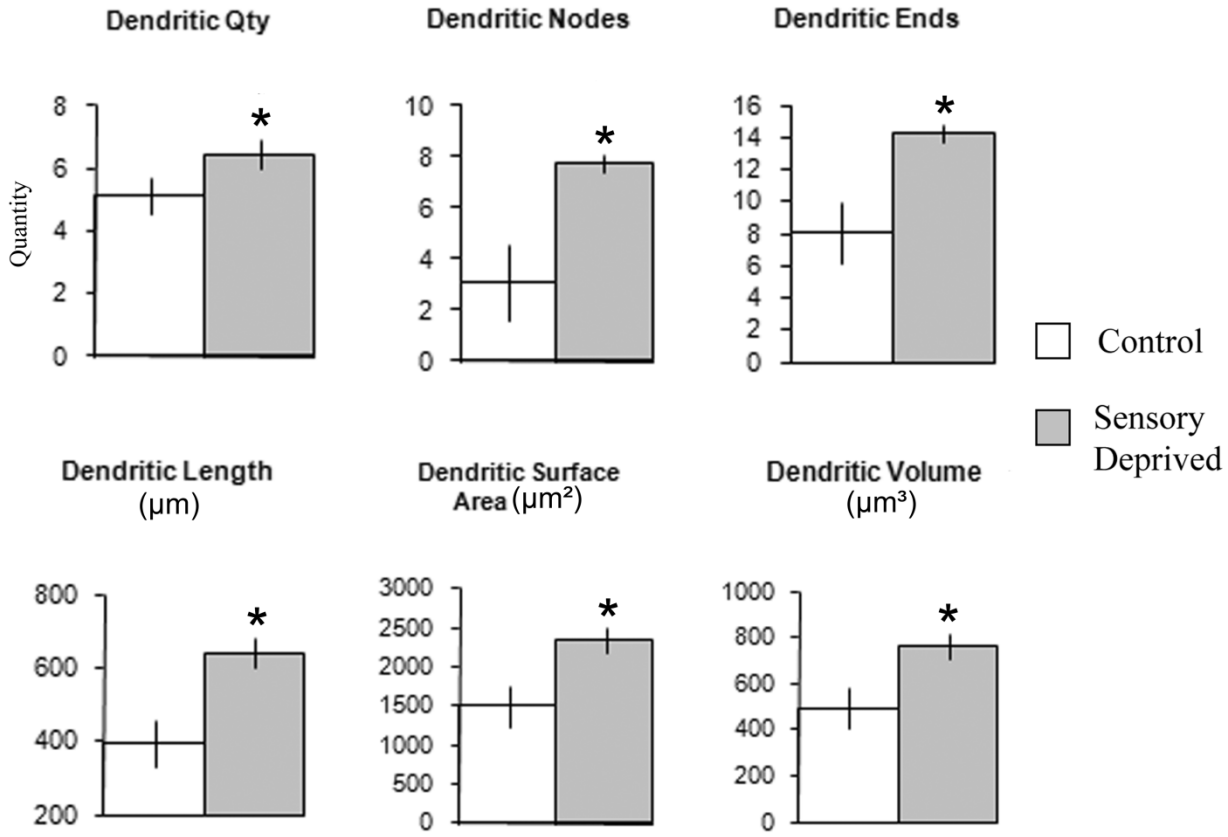

Figure 19. Sholl analyses of the basilar dendrites in layer pyramidal neurons following chronic sensory deprivation. **A:** Mean number of basilar dendritic intersections between 10μm concentric spheres in control versus sensory-deprived mice. The increased number of dendritic intersections in sensory-deprived relative to control mice was distributed from 20μm to 50μm away from the center of the soma, suggesting that the effect is relatively localized. **B:** Mean number of basilar dendritic lengths between 10μm concentric spheres in control versus sensory-deprived mice. Similar to mean number of basilar dendritic intersections, the decreased basilar dendritic length in sensory-deprived relative to control animals was distributed mostly from 30μm to 60μm away from the soma, indicating the localized effect of sensory deprivation on the development of basilar dendrites. Error bars indicate standard error of the mean (SEM). Asterisks indicates statistical significance of posthoc tests (Fisher LSD) at individual levels ($p < 0.05$).

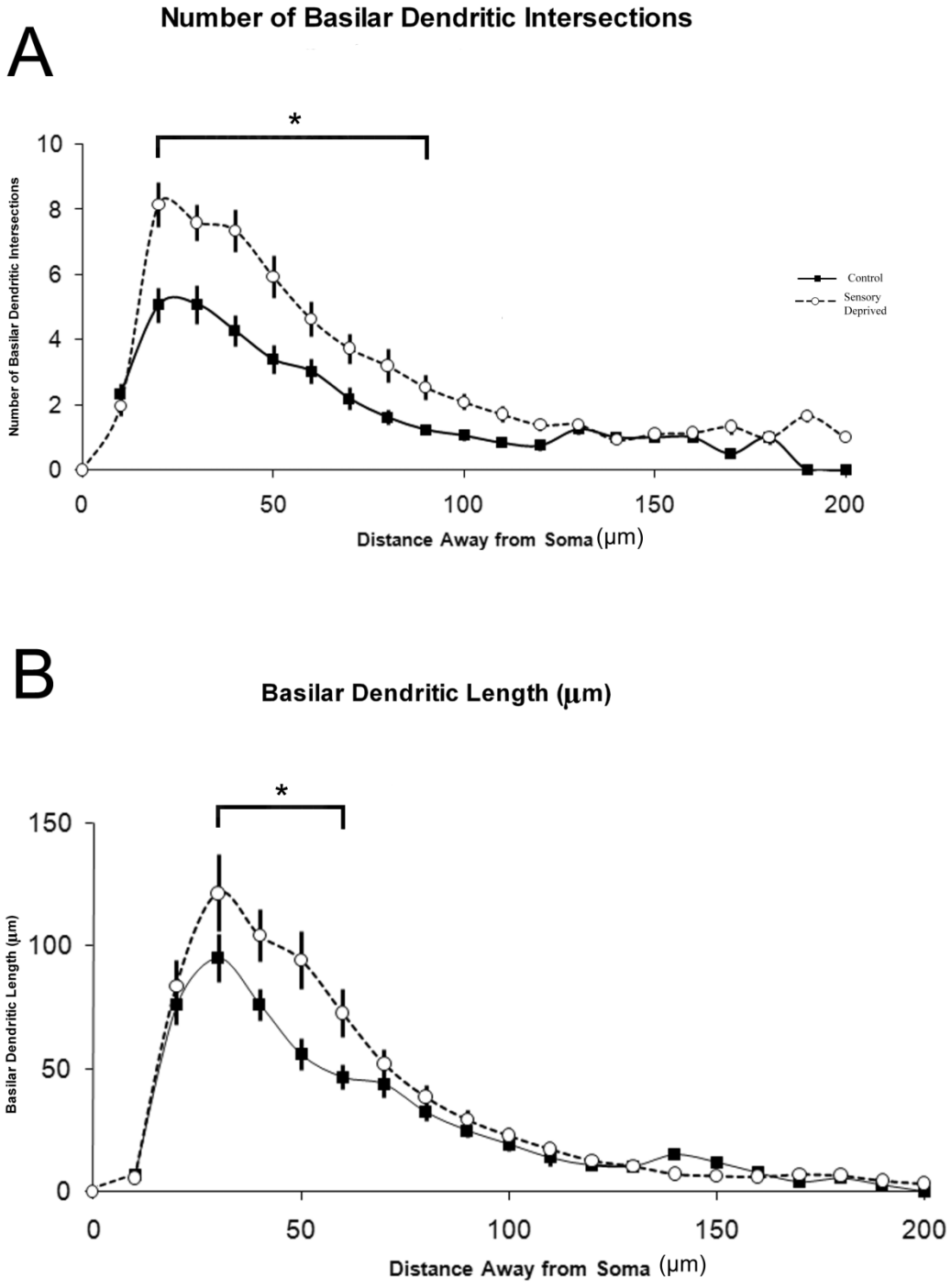

Figure 20. Morphological heterogeneity of dendritic protrusions. **A:** High magnification (100X) view of the dendritic shaft and protrusions in a Golgi-labeled cortical neuron. Scale bar: 2µm. **B:** Representative schematic drawing of the distinctive dendritic protrusions categorized and grouped into several morphological categories: branched, filopodia, stubby, lollipop-like spines, and thick-neck mushrooms. **C:** The numerical average showing the distance from the tip of the dendritic protrusion to the surface of the dendritic shaft by different protrusion categories. Error bars: one standard error of the mean (SEM). Asterisks represent statistically significances at $p<0.05$ (also see Table 5 for results of pair-wise comparison).

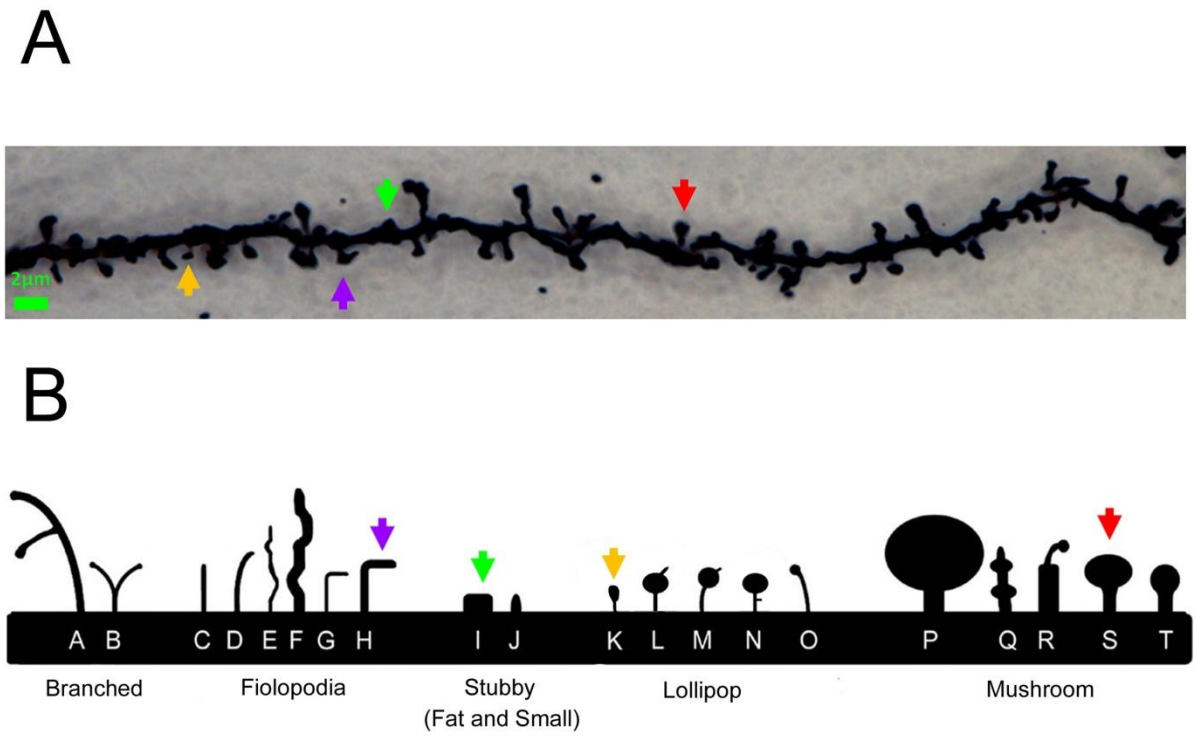

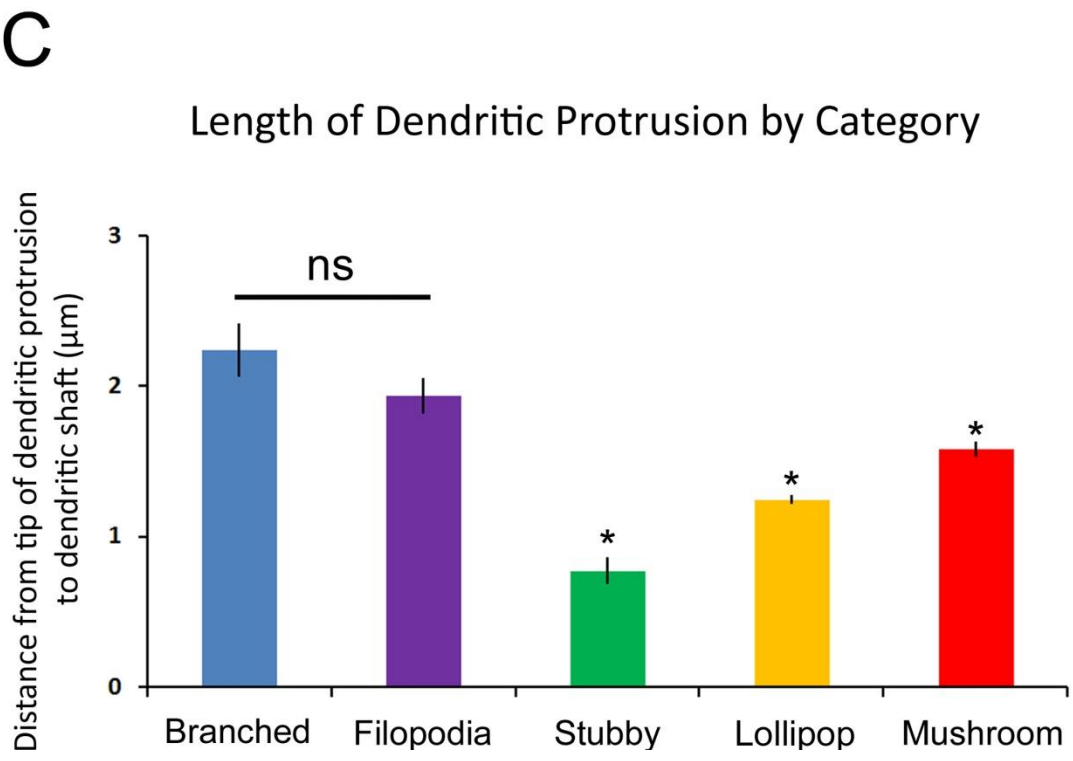

Figure 21. Density of dendritic protrusions in normal developing barrel cortex. **A:** Density of dendritic protrusions in basilar dedrites of layer IV and VI barrel cortical neurons. Note the overall trend in the steadily decreasing density of dendritic protrusions as the animals mature. **B,C:** Sholl analyses (density of dendritic protrusions) across various developmental ages. Note that for both layers IV and VI, the main portion of the disparity is in the proximal portion, rather than in the distal portion. Data points represents numerical averages with the error bars showing one SEM.

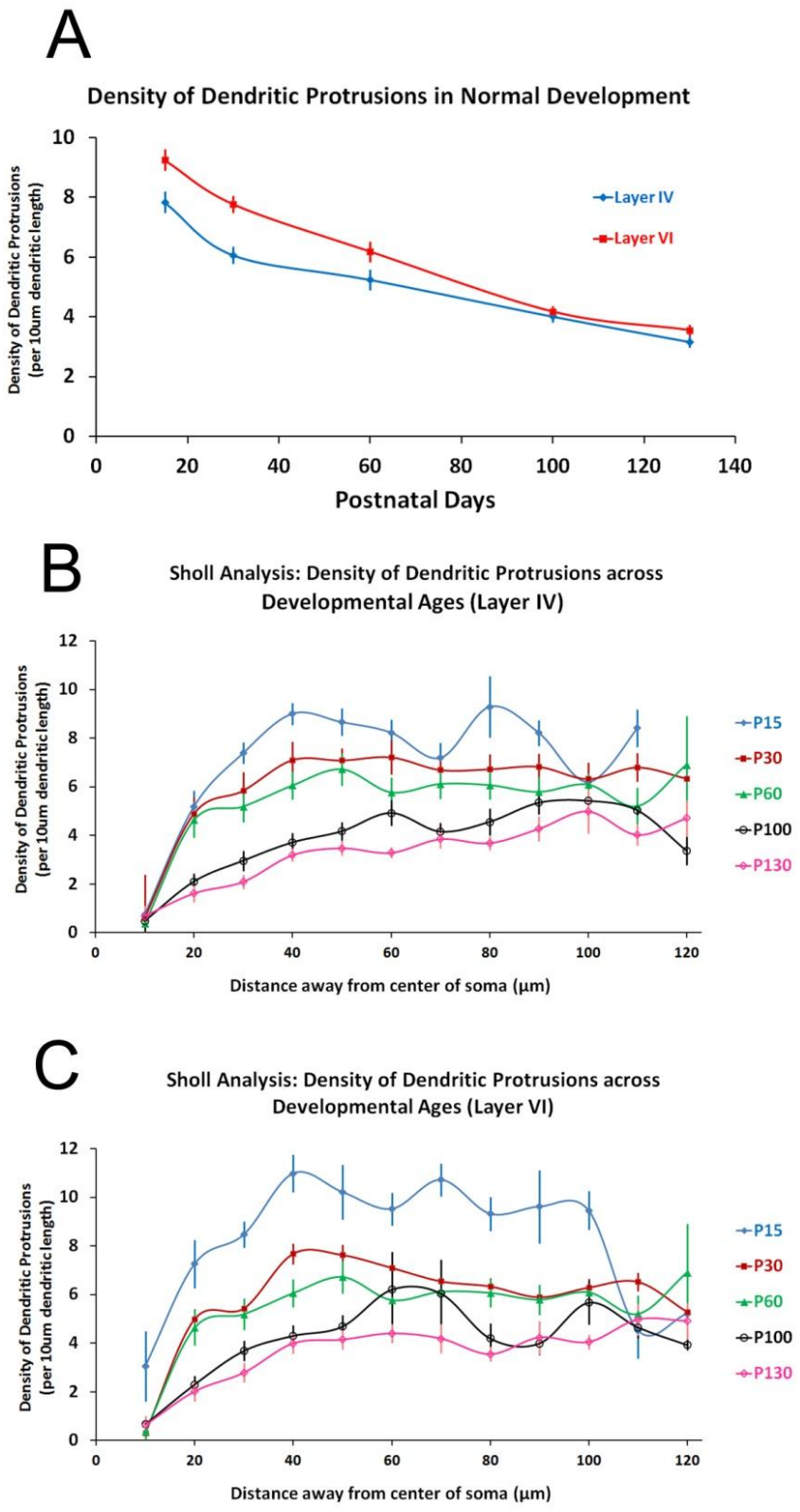

Figure 22. Estimated net loss of dendritic protrusion per developmental epoch. The estimated net loss of dendritic protrusions (see Methods [3]) is more rapid in the earlier periods of life for layer IV (A) and layer VI (B), compared to later periods of life. Asterisks indicate statistical significance ($p<0.05$) compared to epoch of P15-30. Data points represents sample mean with the error bars showing one SEM.

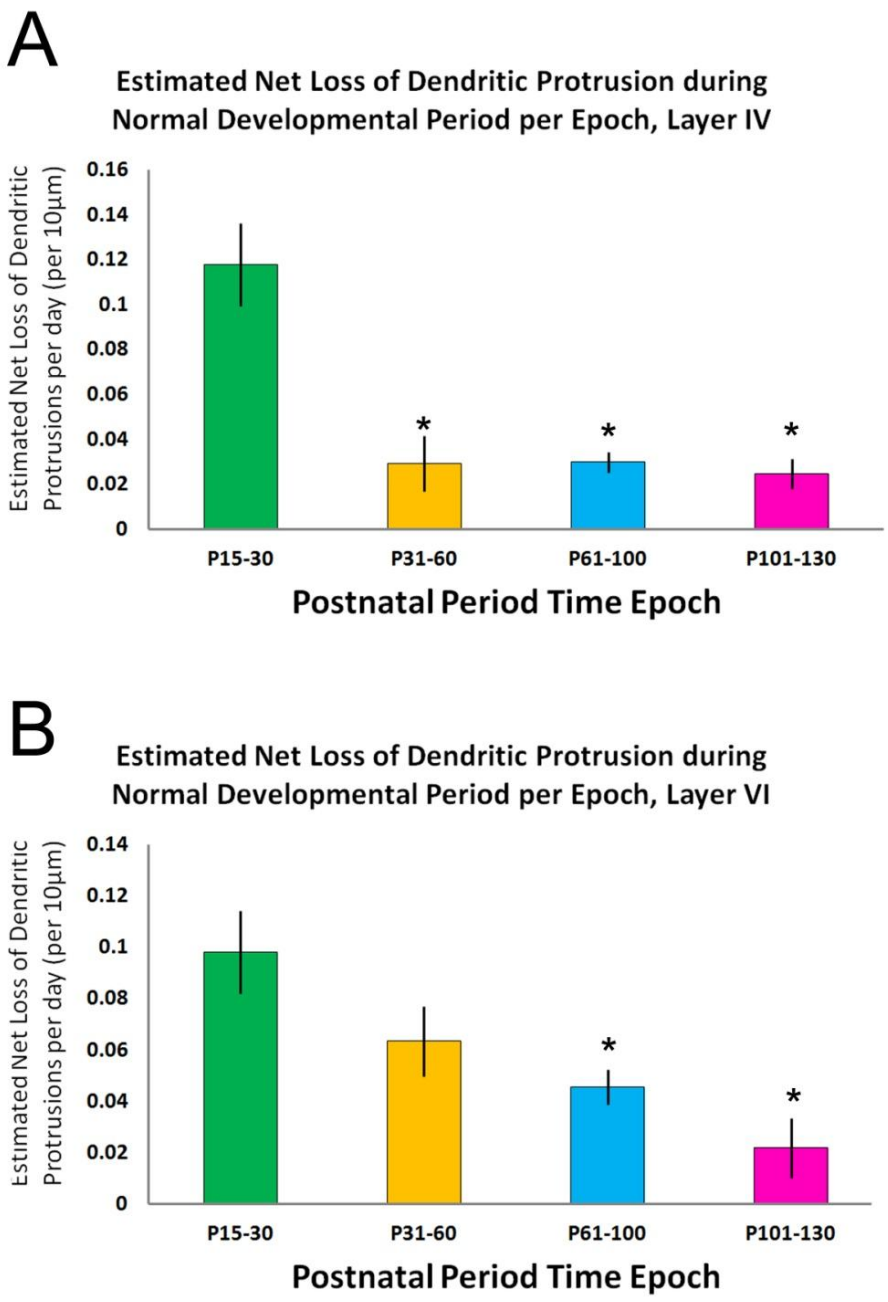

Figure 23. Morphologic distribution of dendritic protrusions across developmental life span in layer IV (A) and VI (B). The distribution of dendritic protrusions in their morphologies change significantly as the animals mature. While the distribution of branched, thin lollipops, and fat stubby did not vary significantly, the small stubby and filopodia protrusions steadily decreased as the animals mature, and the mushroom spines showed a stable increase as the animals reached adulthood. Data points represents sample mean with the error bars showing one SEM.

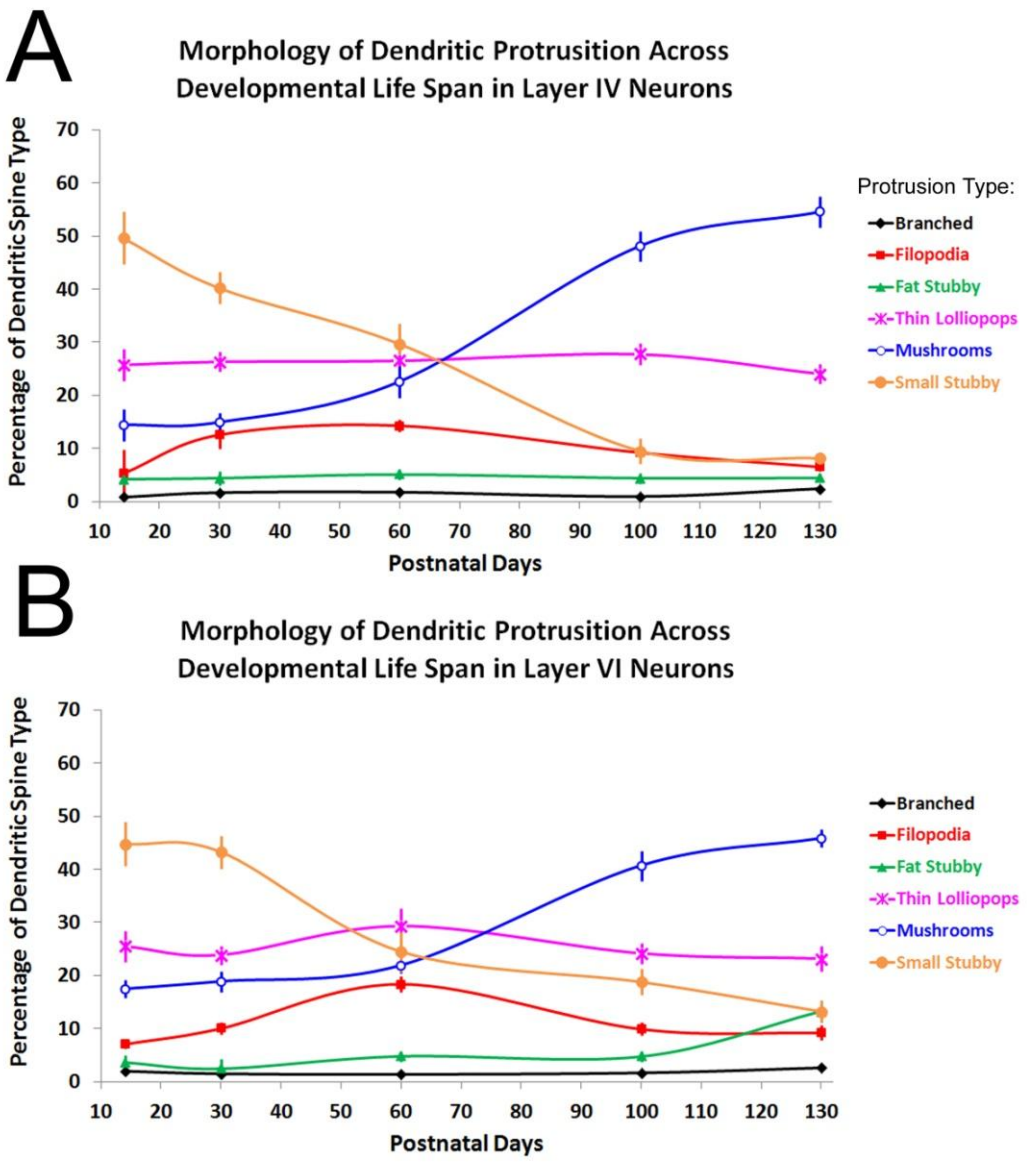

Figure 24. Layer-specific response of dendritic protrusions in barrel cortex to chronic sensory deprivation in neonatal mice. **A**: Following chronic sensory deprivation from P0-P30, the density of dendritic protrusions in layer IV barrel cortical neurons (basilar dendrite of pyrmidal cells) is significantly elevated in the deprived groups. **B:** Following chronic deprivation from P0-P30, the density of dendritic protrusion in layer VI is lower compared with the control counterparts. **C,D:** Chronic sensory deprivation from P0-P30 resulted in a distributional shift in the proportion of morphological classes in the dendritic protrusions. The response to deprivation varies depending on the morphological class and the layer investigated. Asterisks indicates statistical significance at $p<0.05$. Data points represents numerical averages with the error bars showing one SEM.

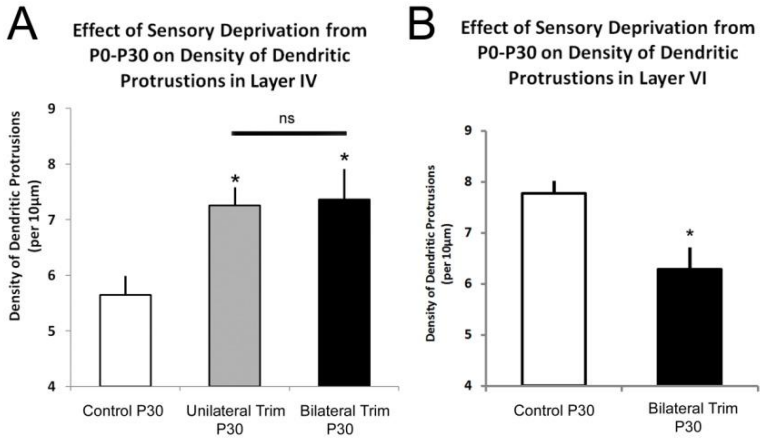

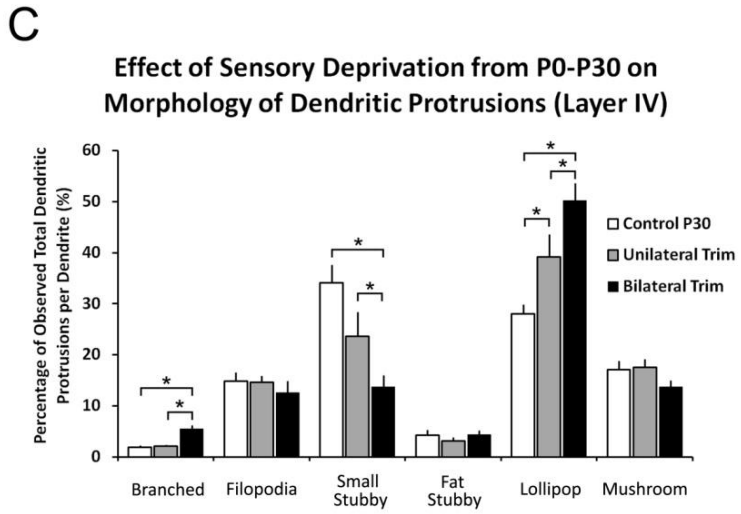

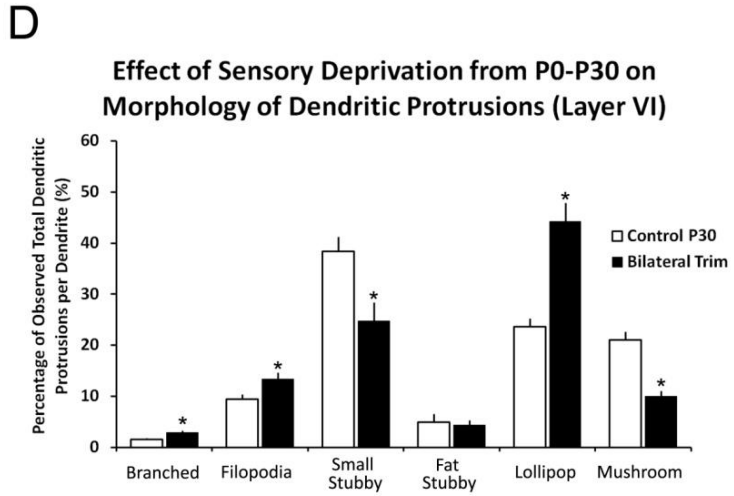

Figure 25. Layer-specific response of dendritic protrusions in barrel cortex following a period (P31-60) of sensory restoration. **A:** Following a period of sensation recovery, the density of dendritic protrusions in layer IV barrel cortical neurons (basilar dendrite of pyrmidal cells) remained significantly elevated compared to the previously deprived groups. **B:** However, the densities of dendritic protrusions in layer VI returned to comparable levels following sensory restoration. **C,D:** Prior sensory deprivation from P0-P30 resulted in a long-lasting repercussion in terms of the distributional shift in the proportion of morphological classes. The pattern of statistical significance remained similar to that of P0-P30 control vs. trimmed, suggesting that prior deprivation experience lingered until P60, even when sensation is restored. Asterisks indicates statistical significance at $p<0.05$. Data points represents numerical averages with the error bars showing one SEM.

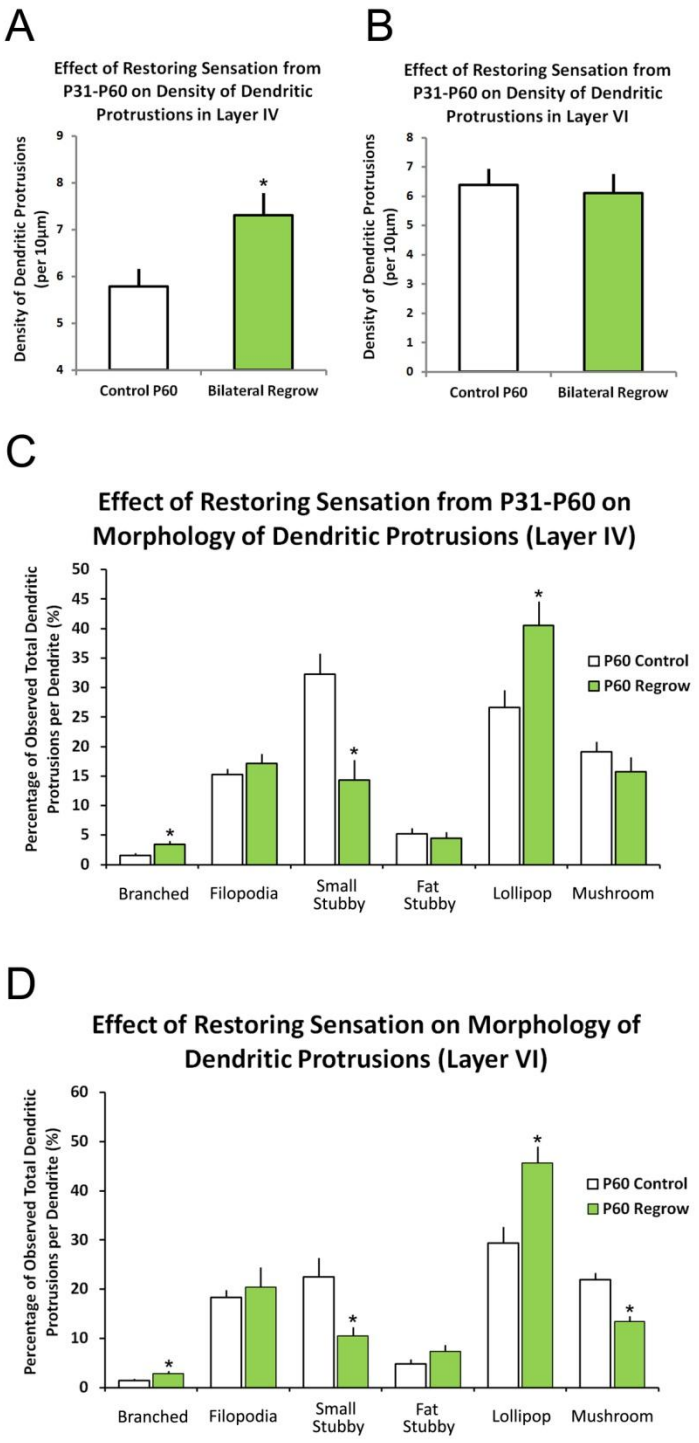

Figure 26. Effect of sensory deprivation from P100-130 on dendritic protrusions. The response to sensory deprivation in mature animals results in layer-specific responses. **A:** Chronic sensory deprivation via whisker trimming in mature animals leads to elevated density of dendritic protrusions in layer IV. **B:** Chronic sensory deprivation from P100-130, however, did not significantly influence the density of dendritic protrusions in layer VI. **C, D:** Chronic sensory deprivation from P100-130 resulted in notable distributional change in the morphology of dendritic protrusions. In both layers IV and VI, the small stubby and mushroom spines significantly decreased, while the proportion of lollipop spines increased. The other types of dendritic protrusions remained comparable. Asterisks indicates statistical significance at $p<0.05$. Data points represents numerical averages with the error bars showing one SEM.

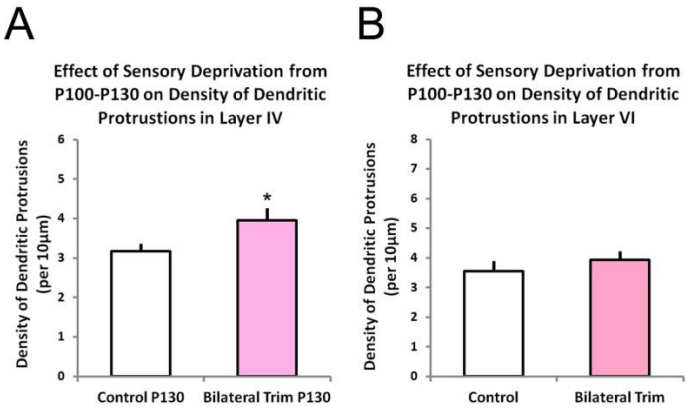

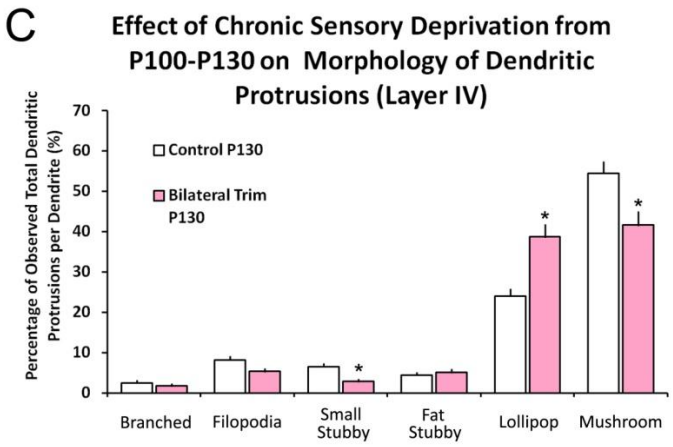

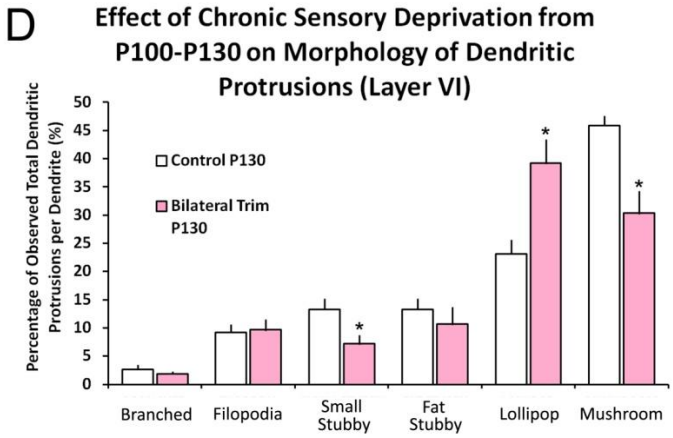

Figure 27. Effect of chronically blocking NMDA-R (from P0-30) on layers IV and VI dendritic protrusions. **A, B:** Chronically administering MK801 (a NMDA-R noncompetitive blocker) from birth to P30 resulted in significant elevation of dendritic protrusions in layers IV and VI, respectively. **C, D:** Chronically blocking NMDA-R from birth - P30 resulted in notable distributional change in the morphology of dendritic protrusions. In layer IV, the MK801-injected group showed significantly higher distributions of branched and filopodia, and lower distributions of small stubby type of protrusions. In layer VI, the MK801-injected group showed significantly higher distributions of branched, lollipop, and filopodia, with a paralleling decrease in the mushroom type of dendritic protrusions. Asterisks indicates statistical significance at $p<0.05$. Data points represents numerical averages with the error bars showing one SEM.

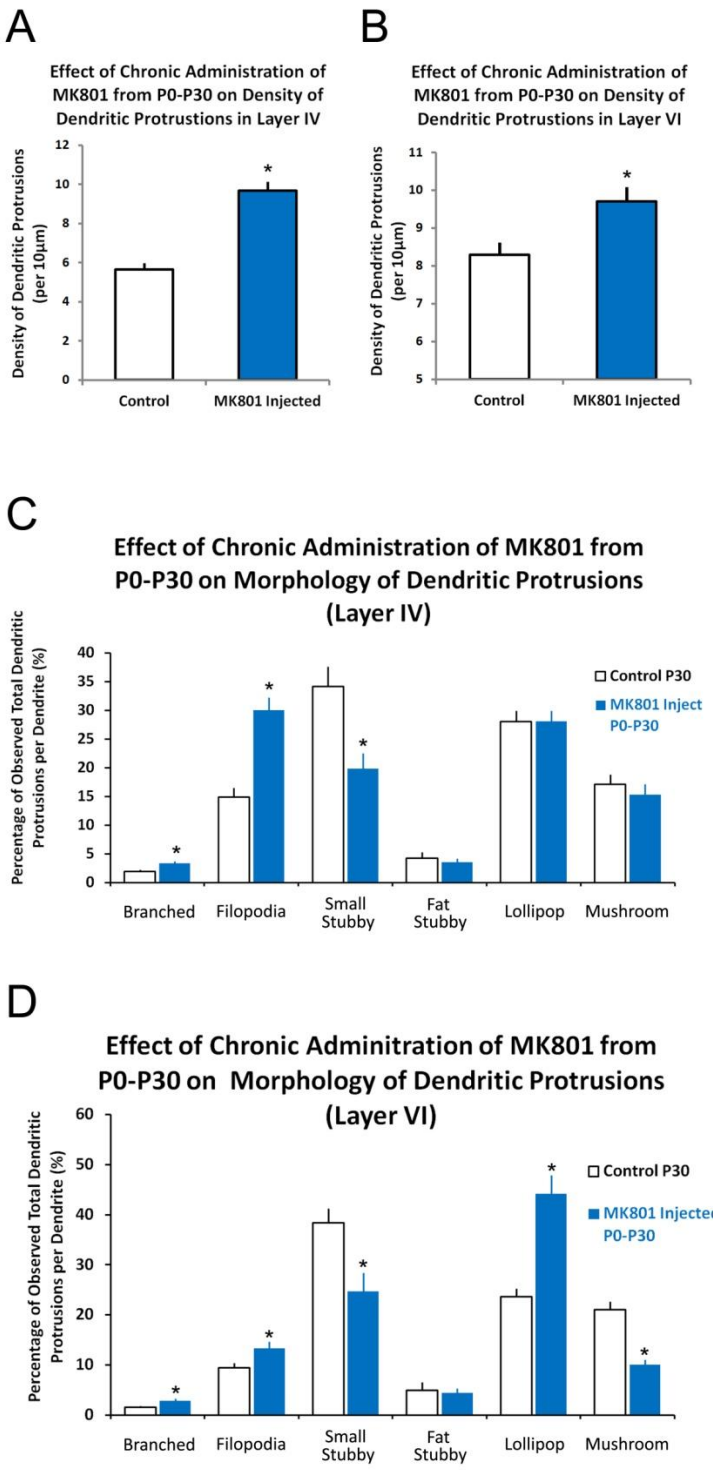

Figure 28. Unblocking NMDA-R activity from P31-60 results in partial recovery of dendritic protrusion phenotype. **A, B:** The density of dendritic protrusions, upon withdrawing MK801 from P31-60 after P0-30 blockade returned to comparable levels compared with age-matched control in both layers IV and VI, respectively. **C, D:** The distributional change in the morphology of dendritic protrusions in layers IV and VI. In layer IV, the branched and filopodia type of dendritic protrusions returned to comparable levels after withdrawing MK801, while the distribution of stubby spines remained lower, with possible compensatory increase in the mushroom type of spines. In layer VI, the branched, filopodia, and mushroom type of dendritic protrusions returned to comparable to that of control group, while the distribution of small stubby and lollipop spines showed compensated increase and decrease, respectively. Data points represents numerical averages with the error bars showing one SEM.

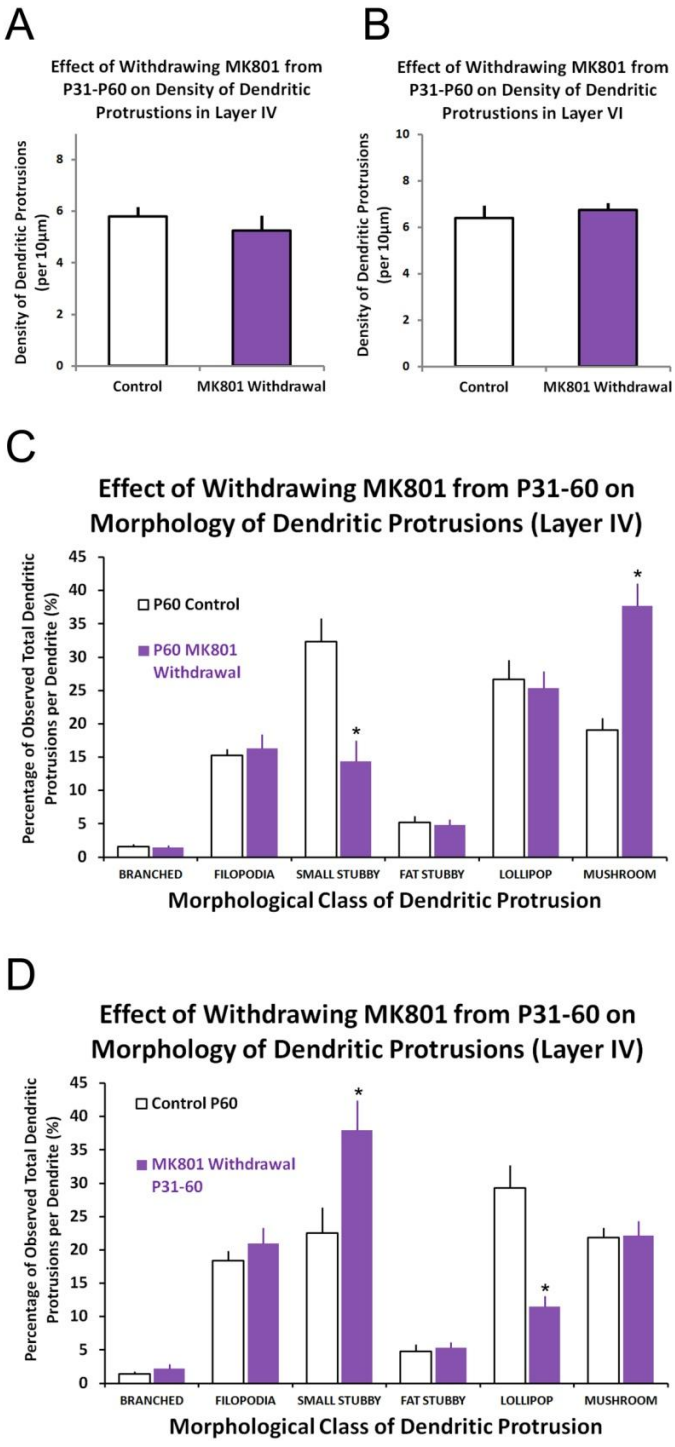

Figure 29. Tissue-type plasminogen activator immunoreactivity in the mouse barrel cortex. **A**: tPA (green, A_1) is expressed in the barrel cortex. Scale bar: 25µm. **B**: tPA-immunopositive (red) cells rarely colocalized with somatostatin-positive cells in the barrel cortex. Scale bar: 100µm. **C:** tPA-immunopositive (red) cells often colocalized with parvalbumin-positive cells in the barrel cortex. Scale bar: 20µm.

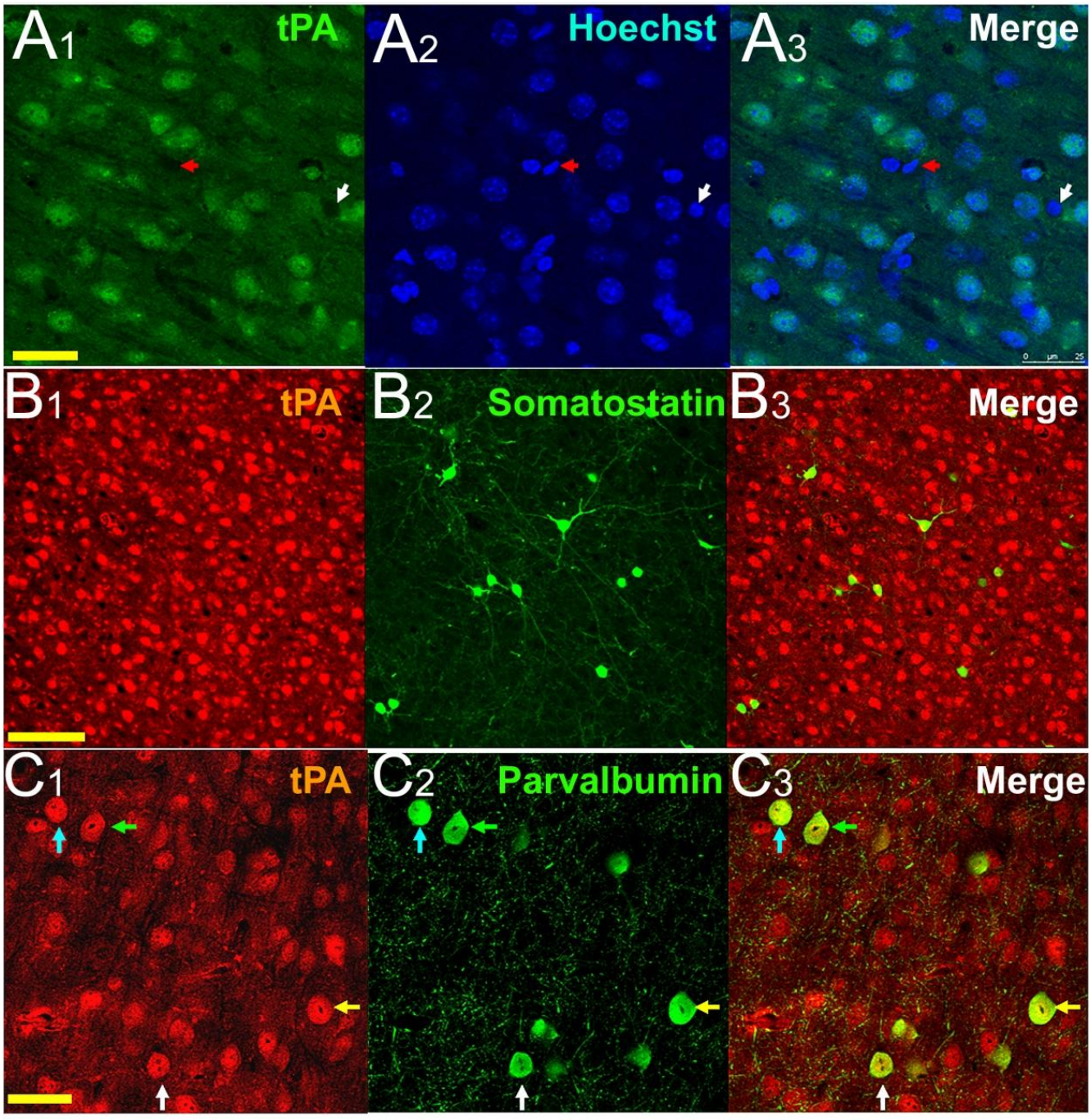

Figure 30. Sensory experience influences the expression of tPA. **A:** tPA-immunopositive cells in the barrel cortex of P30 control (A_1) and deprived (A_2) animals. B: tPA-immunopositive cells in the barrel cortex of P60 control (B_1) and regrow (B_2) animals. Scale bar: 250µm. **C:** The protein expression level of tPA is increased in all layers of barrel cortex following chronic sensory deprivation from P0-30. **D:** After a significant period of restoring sensation (whisker regrow), this elevated level of tPA remained in the regrow group compared with age-matched controls. Asterisks indicate statistical significance at $p<0.05$.

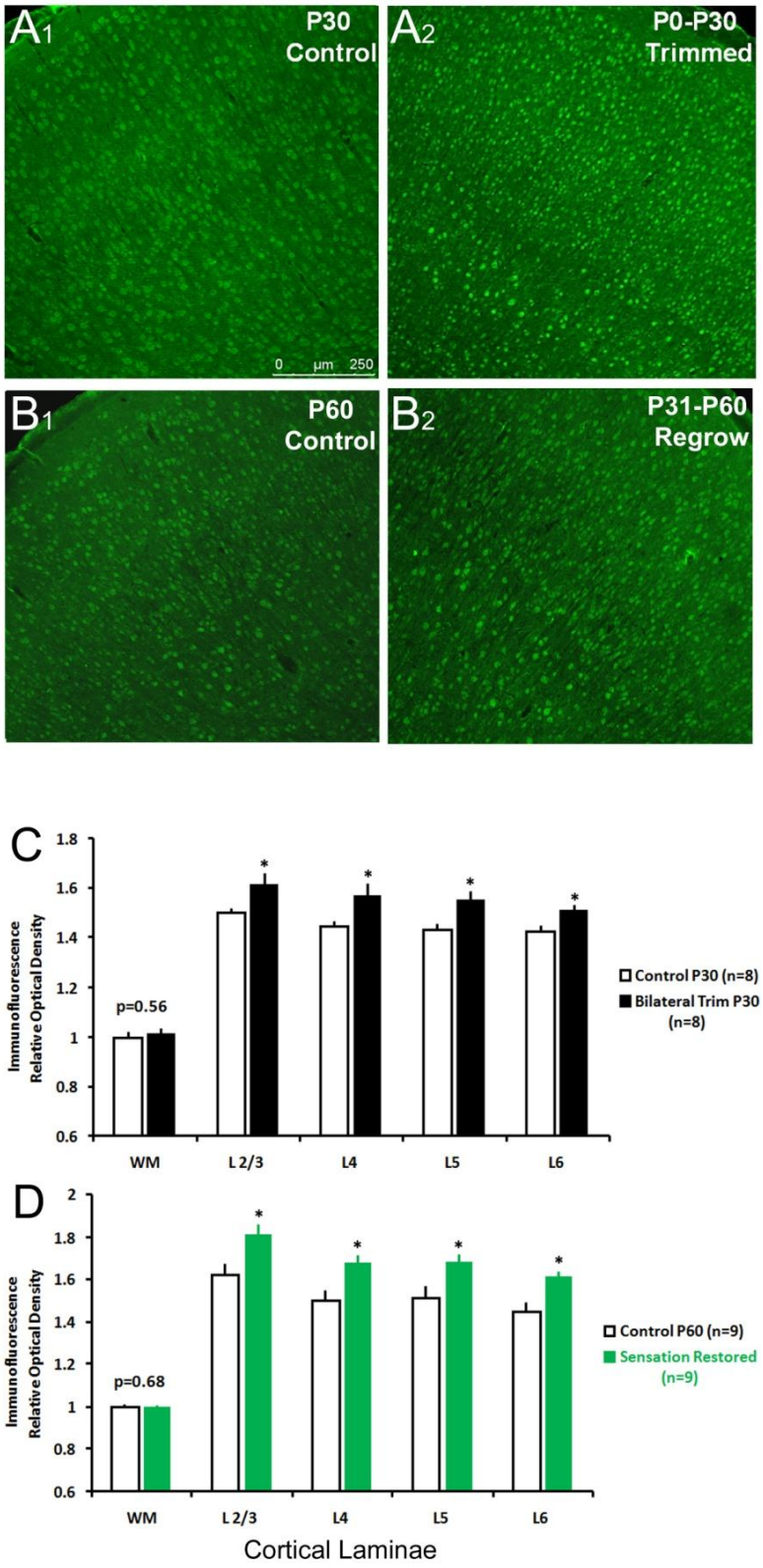

Figure 31. Proposed mechanisms to the changes in morphological categories of dendritic protrusions and the shift in balance of lemniscal thalamocortical / corticocortical connections. It is suggested that following chronic sensory deprivation, there is a significant decrease in the proportion of principal TCA presynaptic connection to the postsynaptic dendritic protrusion, resulting in shift in thalalmocortical / non-TCA connections.

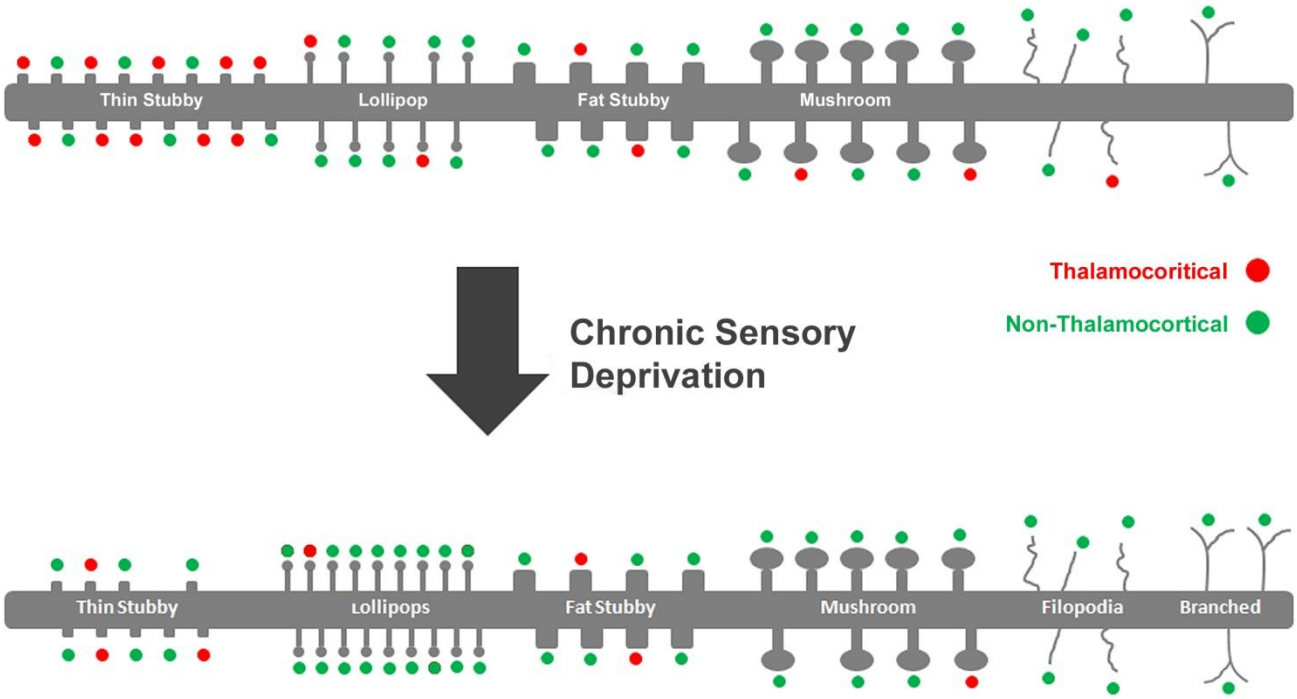

Figure 32. Cortical structural plasticity can occur at many levels of organization. **A:** Outline of the cerebral cortex in tangential section. Studies investigating the gross level of structural alteration (disappearance, shift, expansion, or shrinkage of somatotopic map) are well suited for this level of anatomical analysis. Adapted from Wijetunge et al., 2008. **B:** Schematic drawing showing a coronal plane of the barrel cortex. Studies investigating the regional relationship with barrels, such as cellular population distribution, dendritic and axonal pattern, and local functional circuitry are well suited for this level of analysis. Shaded light blue area represents the barrel region and the green circles represent cell bodies, the red axon represents a TCA originating from VPM synapasing onto both spiny stellate cells (black) and small pyramidal neurons (blue). Adapted from Wu et al., 2011. **C:** Schematic drawing of a pyramidal neuron. Studies investigating the neuronal morphology, as well as studies exploring their computational properties at the cellular level are well suited for this type of study. **D:** Representative tracing of an apical dendrite. Studies investigating the relationship between one dendrite and the proximity to somata, the geometric angular relationship to the cortex (or somata), and quantifications of dendritic protrusions are well suited at this level of analysis. Dendritic branches are numeric and color coded for clarity. Adapted from Chen et al., 2009. **E:** Schematic drawing a dendritic spine. Studies investigating anatomical evidence of learning and memory, as well as dendritic protrusion dynamics (motility, formation, elimination) are well suited for this level of analysis. The black arrow represents length from the head of spine to the surface of parent dendrite, the red arrow represents length of spine neck, the white arrow represents width of the dendritic neck and the yellow arrow represents the width of a spine head. Finally, the light blue arrows represent the surface area or volume of the spine head. Adapted from Dumitriu et al., 2010.

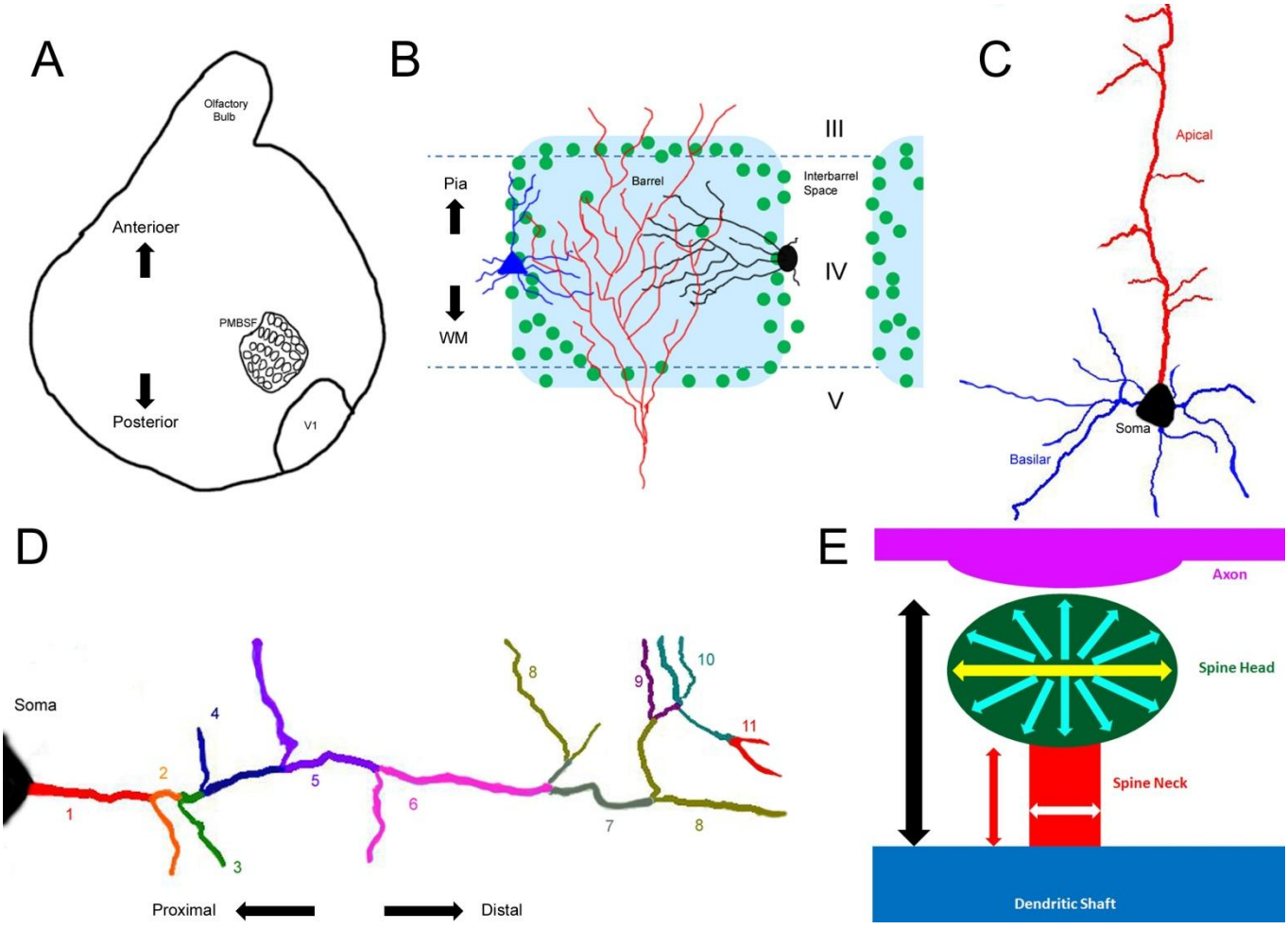

References

Andolina IM, Jones HE, Wang W, Sillito AM. (2007). Corticothalamic feedback enhances stimulus response precision in the visual system. *PNAS, 104(5):*1685-1690.

Araya, R., Jiang, J., Eisenthal, K.B., & Yuste, R. (2006). The spine neck filters membrane potentials. *PNAS, 103(47):* 17961-6.

Arellano JI, Espinosa A, Fairén A, Yuste R, DeFelipe J. (2007). Non-synaptic dendritic spines in neocortex. *Neuroscience, 145(2):* 464-9.

Bear MF, Huber KM, Warren ST. (2004). The mGluR theory of fragile X mental retardation. *Trends in Neurosciences, 27(7):* 370-7.

Bhatt DH, Zhang S, Gan WB. (2009). Dendritic Spine Dynamics. *Annual Review of Physiology, 71:* 261-82.

Bishop KM, Goudreau G, O'Leary DD. (2000). Regulation of area identity in the mammalian neocortex by Emx2 and Pax6. *Science, 288(5464):* 344-9.

Blakemore C, Cooper GG. (1970). Development of the brain depends on the visual environment. *Nature 228:* 477-8.

Blakemore, C., Van Sluyters, R.C. (1975). Innate and environmental factors in the development of the kitten's visual cortex. *Journal of Physiology, 248(3),* 663-716.

Briner A, De Roo M, Dayer A, Muller D, Kiss JZ, Vutskits L. (2010). Bilateral whisker trimming during early postnatal life impairs dendritic spine development in the mouse somatosensory barrel cortex. *Journal of Comparatively Neurology, 518(10):*1711-1723.

Brumberg JC, Pinto DJ, Simons DJ. (1999). Cortical columnar processing in the rat whisker-to-barrel system. *Journal of Neurophysiology,82(4):* 1808-17.

Brumberg JC, Hamzei-Sichani F, Yuste R. (2003). Morphological and physiological characterization of layer VI corticofugal neurons of mouse primary visual cortex. *Journal of Neurophysiology 89:* 2854-67.

Brumberg JC, Nowak LG, McCormick DA. (2000). Ionic mechanisms underlying repetitive high-frequency burst firing in supragranular cortical neurons. *Journal of Neuroscience, 20(13):*4829-43.

Bruno RM, Hahn TT, Wallace DJ, de Kock CP, Sakmann B. (2009). Sensory experience alters specific branches of individual corticocortical axons during development. *Journal of Neuroscience, 29(10):* 3172-3181.

Cardin JA, Palmer LA, Contreras D. (2005). Stimulus-dependent gamma (30-50 Hz) oscillations in simple and complex fast rhythmic bursting cells in primary visual cortex. *Journal of Neuroscience, 25(22):* 5339-50

Carvell GE, Simons DJ. (1996). Abnormal tactile experience early in life disrupts active touch. *Journal of Neuroscience, 16(8):*2750-2757.

Casanova MF, Trippe J 2nd. (2006). Regulatory mechanisms of cortical laminar development. *Brain Research Review, 51(1)*:72-84.

Catalano SM, Robertson RT, Killackey HP. (1991). Early ingrowth of thalamocortical afferents to the neocortex of the prenatal rat. *PNAS,* 88: 2999-3003.

Caviness VS Jr. (1982). Neocortical histogenesis in normal and reeler mice: a developmental study based upon [3H]thymidine autoradiography. *Brain Research, 256(3):*293-302.

Cauli B, Audinat E, Lambolez B, Angulo MC, Ropert N, Tsuzuki K, Hestrin S, Rossier J. (1997). Molecular and physiological diversity of cortical nonpyramidal cells. *Journal of Neuroscience, 17(10):*3894-906.

Cauli B, Porter JT, Tsuzuki K, Lambolez B, Rossier J, Quenet B, Audinat E. (2000). Classification of fusiform neocortical interneurons based on unsupervised clustering. *PNAS, 97:* 6144-49.

Chakrabarti S, Alloway KD. (2006). Differential origin of projections from SI barrel cortex to the whisker representations in SII and MI. *Journal of Comparative Neurology 498(5):* 624-36

Chen CC, Abrams S, Pinhas A, Brumberg JC. (2009). Morphological heterogeneity of layer VI neurons in mouse barrel cortex. *Journal of Comparative Neurology, 512(6):* 726-46.

Chen CC, Tam D, Brumberg JC. (2011). Sensory deprivation differentially impacts the dendritic development of pyramidal versus non-pyramidal neurons in layer 6 of mouse barrel cortex. *Brain Structure and Function,* [Epub ahead of print] PMID: 21861159

Chen ZL, Indyk JA, Strickland S. (2003). The hippocampal laminin matrix is dynamic and critical for neuronal survival. *Mol Biol Cell,* 14(7):2665-76.

Comery TA, Harris JB, Willems PJ, Oostra BA, Irwin SA, Weiler IJ, Greenough WT. (1997). Abnormal dendritic spines in fragile X knockout mice: maturation and pruning deficits. *PNAS, 94(10):* 5401-4.

Cook SC, Wellman CL. Chronic stress alters dendritic morphology in rat medial prefrontal cortex. J Neurobiol. 2004;60:236–248.

Corson J, Nahmani M, Lubarsky K, Badr N, Wright C, Erisir A. (2009). Sensory activity differentially modulates N-methyl-D-aspartate receptor subunits 2A and 2B in cortical layers. *Neuroscience, 163*(3):920-32.

Crick FC, Koch C. (2005). What is the function of the claustrum? Philosophical Transactions of the Royal Society of London, Series B: Biological Sciences 360(1458):1271-1279

Cruz-Martín A, Crespo M, Portera-Cailliau C. (2010) Delayed stabilization of dendritic spines in fragile X mice. *J Neuroscience,* 30(23):7793-803.

Dalva MB, Ghosh A, Shatz CJ. (1994). Independent control of dendritic and axonal form in the developing lateral geniculate nucleus. *Journal of Neuroscience, 14(6):* 3588-602.

Datwani A, Iwasato T, Itohara S, Erzurumlu RS. (2002). NMDA receptor-dependent pattern transfer from afferents to postsynaptic cells and dendritic differentiation in the barrel cortex. *Molecular Cell Neuroscience, 21(3):* 477-92.

Davis TL, Sterling P. (1979). Microcircuitry of cat visual cortex: classification of neuronsin layer IV of area 17, and identification of the patterns of lateral geniculate input. *Journal of Comparative Neurology 188:* 599–628.

Denton DA, McKinley MJ, Farrell M, Egan GF. (2009). The role of primordial emotions in the evolutionary origin of consciousness. *Consciousness and Cognition, 18(2):*500-514.

Diamond ME, Armstrong-James M, Ebner FF. (1992). Somatic sensory responses in the rostral section of the posterior group (POm) and in the ventral posterior medial nucleus (VPM) of the rat thalamus. *Journal of Comparative Neurology, 318(4):* 462-76.

Dumitriu D, Hao J, Hara Y, Kaufmann J, Janssen WG, Lou W, Rapp PR, Morrison JH. (2010). Selective changes in thin spine density and morphology in monkey prefrontal cortex correlate with aging-related cognitive impairment. *Journal of Neuroscience,* 30(22):7507-15.

Elston GN, Oga T, & Fujita I. (2009). Spinogenesis and pruning scale across functional hierarchies. *Journal of Neuroscience, 29(10):* 2371-3275.

Elston GN, Oga T, Okamoto T, Fujita I. (2010). Spinogenesis and pruning from early visual onset to adulthood: an intracellular injection study of layer III pyramidal cells in the ventral visual cortical pathway of the macaque monkey. *Cerebral Cortex, 20(6):* 1398-408.

Erzurumlu RS, Itohara S. (2000). Cortex-restricted disruption of NMDAR1 impairs neuronal patterns in the barrel cortex. *Nature, 406(6797):*726-31.

Fanselow EE, Richardson KA, Connors BW. (2008). Selective, state-dependent activation of somatostatin-expressing inhibitory interneurons in mouse neocortex. *Journal of Neurophysiology, 100(5):* 2640-52.

Feldman DE, Brecht M. (2005). Map plasticity in somatosensory cortex. Science 310(5749): 810-5.

Feldman D. (2009). Synaptic Mechanisms for Plasticity in Neocortex. *Annual Review of Neuroscience 32:* 33-55.

Ferrer I, Fabregues I, & Condom E. (1986). A Golgi study of the sixth layer of the cerebral cortex. II. The gyrencephalic brain of Carnivora, Artiodactyla and Primates. *Journal of Anatomy, 146:* 87-104.

Fiala JC, Feinberg M, Popov V, Harris KM. (1998). Synaptogenesis via dendritic filopodia in developing hippocampal area CA1. *Journal of Neuroscience, 18(21):* 8900-11.

Fiala JC & Harris KM. (2000). Dendrite structures. In Stuart G, Sprutson N, Hausser M (Eds.) Dendrites, 1-28. New York, NY: Oxford

Fox K, Wong RO. (2005). A comparison of experience-dependent plasticity in the visual and somatosensory systems. *Neuron, 48(3):* 465-477.

Fox K, Schlaggar BL, Glazewski S, O'Leary DD. (1996). Glutamate receptor blockade at cortical synapses disrupts development of thalamocortical and columnar organization in somatosensory cortex. *PNAS, 93(11):* 5584-9.

Fu M, Yu X, Lu J, Zuo Y. (2012). Repetitive motor learning induces coordinated formation of clustered dendritic spines in vivo. *Nature, 483*(7387):92-5

Fukuchi-Shimogori, T., and Grove, E.A. (2001). Neocortex patterning by the secreted signaling molecule FGF8. *Science 294,* 1071–1074.

Furtak SC, Moyer JR Jr, Brown TH. (2007). Morphology and ontogeny of rat perirhinal cortical neurons. *Journal of Comparative Neurology, 505(5)*: 493-510.

Gazzaley AH, Siegel SJ, Kordower JH, Mufson EJ, Morrison JH. (1996). Circuit-specific alterations of N-methyl-D-aspartate receptor subunit 1 in the dentate gyrus of aged monkeys. PNAS, 93(7):3121-5.

Glaser ME, Van der Loos H. (1981). Analysis of thick brain sections by obverse-reverse computer microscopy: application of a new, high clarity Golgi-Nissl stain. *Journal of Neuroscience Methods 4:* 117-125.

Goldstein EB. (2007). *Sensation and Perception,* 7th edition. Belmont, CA: Thomson/Wadsworth.

Gravanis I, Tsirka SE. (2005). Tissue plasminogen activator and glial function. *Glia, 49(2):* 177-83.

Hannan AJ, Blakemore C, Katsnelson A, Vitalis T, Huber KM, Bear M, Roder J, Kim D, Shin HS, Kind PC. (2001). PLC-beta1, activated via mGluRs, mediates activity-dependent differentiation in cerebral cortex. *Nature Neuroscience, 4(3):* 282-8.

Holtmaat A, Svoboda K. (2009). Experience-dependent structural synaptic plasticity in the mammalian brain. *Nat Rev Neuroscience,* 10(9):647-58

Hao JD, Rapp PR, Leffler AE, Leffler SR, Janssen WGM, Lou W, McKay H, Roberts JA, Wearne WL, Hof PR, & Morrison JH. (2006). Estrogen alters spine number and morphology in prefrontal cortex of aged female rhesus monkeys. *Journal of Neuroscience, 26(9):* 2671-2678.

Hardingham N, Wright N, Dachtler J, Fox K. (2008). Sensory deprivation unmasks a PKA-dependent synaptic plasticity mechanism that operates in parallel with CaMKII. *Neuron, 60(5):* 861-874.

Harvey, C.D., Yasuda, R., Zhong, G., & Svoboda, K. (2008). The spread of Ras activity triggered by activation of a single dendritic spine. *Science, 321(5885):* 136-40.

Hensch TK. (2005). Critical period mechanisms in developing visual cortex. Current *Topics in Developmental Biology; 69:*215-37.

Hickmott PW, Steen PA. (2005). Large-scale changes in dendritic structure during reorganization of adult somatosensory cortex. *Nature Neuroscience, 8(2):* 140-142.

Hof PR, de Vellis J, Nimchinsky EA, Kidd G, Cludia Luz, & Trapp BD. (2008). Cellular components of the nervous tissue, in Fundamental Neuroscience, 3rd edition: 41-58.

Hofer SB, Mrsic-Flogel TD, Bonhoeffer T, Hübener M. (2009). Experience leaves a lasting structural trace in cortical circuits. *Nature, 457* (7227): 313-7.

Holtmaat A, Svoboda K. (2009). Experience-dependent structural synaptic plasticity in the mammalian brain. *Nature Review Neuroscience. 10*(9):647-58.

Holtmaat AJ, Trachtenberg JT, Wilbrecht L, Shepherd GM, Zhang X, Knott GW, Svoboda K. (2005). Transient and persistent dendritic spines in the neocortex in vivo. *Neuron, 45(2):* 279-91.

Huang L, Pallas SL. (2001). NMDA antagonists in the superior colliculus prevent developmental plasticity but not visual transmission or map compression. *Journal of Neurophysiology, 86*(3):1179-94.

Hubel, D.H., Wiesel, T.N., & LeVay, S. (1979). Plasticity of ocular dominance columns in monkey striate cortex. *Philos Trans R Soc Lond B Biol Sciences, (278)961*: 377-409.

Hubel DH, Wiesel TN. (1959). Receptive fields of single neurons in the cat's striate cortex. *Journal of Physiology, 148:* 574-91.

Hubel DH, Wiesel TN. (1969). Anatomical demonstration of columns in the monkey striate cortex. *Nature, 221:* 747-750.

Hubel DH, Wiesel TN. (1972). Laminar and columnar distribution of geniculo-cortical fibers in the macaque monkey. *Journal of Comparative Neurology, 146:* 421-450.

Hubel DH, Wiesel TN, Stryker MP. (1978). Anatomical demonstration of orientation columns in macaque monkey. *Journal of Comparative Neurology, 177:* 361-379.

Imig TJ, and Adrian HO. (1977). Binaural columns in the primary field (AI) of cat auditory cortex. *Brain Research, 138:* 241-257.

Inan M, Lu HC, Albright MJ, She WC, Crair MC. (2006). Barrel map development relies on protein kinase A regulatory subunit II beta-mediated cAMP signaling. *Journal of Neuroscience, 26(16):* 4338-49.

Irwin SA, Galvez R, Greenough WT. (2000). Dendritic spine structural anomalies in Fragile-X mental retardation syndrome. *Cerebral Cortex, 10:*1038-44.

Irwin SA, Idupulapati M, Gilbert ME, Harris JB, Chakravarti AB, Rogers EJ, Crisostomo RA, Larsen BP, Mehta A, Alcantara CJ, Patel B, Swain RA, Weiler IJ, Oostra BA, Greenough WT. (2002). Dendritic spine and dendritic field characteristics of layer V pyramidal neurons in the visual cortex of fragile-X knockout mice. *American Journal of Medical Genetics, 111(2):*140-6.

Iwasato T, Datwani A, Wolf AM, Nishiyama H, Taguchi Y, Tonegawa S, Knöpfel T, Jones EG. (1975). Varieties and distribution of non-pyramidal cells in the somatic sensory cortex of the squirrel monkey. *Journal of Comparative Neurology, 160(2):* 205-67.

Jiao Y, Zhang C, Yanagawa Y, Sun QQ. (2006) Major effects of sensory experiences on the neocortical inhibitory circuits. *Journal of Neuroscience*, 26(34):8691-701.

Kalb RG. (1994). Regulation of motor neuron dendrite growth by NMDA receptor activation. *Development, 120(11):* 3063-71.

Katz LC. (1987). Local circuitry of identified projection neurons in cat visual cortex brain slices. *Journal of Neuroscience 7(4):* 1223-49.

Karagiannis A, Gallopin T, Dávid C, Battaglia D, Geoffroy H, Rossier J, Hillman EM, Staiger JF, Cauli B. (2009). Classification of NPY-expressing neocortical interneurons. *Journal of Neuroscience, 29(11):* 3642-59

Killackey HP, Koralek KA, Chiaia NL, Rhodes RW. (1989). Laminar and areal differences in the origin of the subcortical projection neurons of the rat somatosensory cortex. *Journal of Comparative Neurology,282(3):* 428-45.

Kleinfeld D, Ahissar E, Diamond ME. (2006). Active sensation: insights from the rodent vibrissa sensorimotor system. *Current Opinion in Neurobiology,* 16(4):435-44.

Kossel AH, Williams CV, Schweizer M, Kater SB. (1997). Afferent innervation influences the development of dendritic branches and spines via both activity-dependent and non-activity-dependent mechanisms. *Journal of Neuroscience, 17(16):* 6314-24.

Kossut M, Hand PJ, Greenberg J, Hand CL. (1988). Single vibrissal cortical column in SI cortex of rat and its alterations in neonatal and adult vibrissa-deafferented animals: a quantitative 2DG study. *Journal of Neurophysiology, 60(2):* 829-52.

Kozorovitskiy Y, Gross CG, Kopil C, Battaglia L, McBreen M, Stranahan AM, Gould E. (2005). Experience induces structural and biochemical changes in the adult primate brain. *PNAS,* 102(48):17478-82

Le Roux P, Behar S, Higgins D, Charette M. (1999). OP-1 enhances dendritic growth from cerebral cortical neurons in vitro. *Experimental Neurology, 160(1):* 151-63.

Leergaard TB, Alloway KD, Pham TA, Bolstad I, Hoffer ZS, Pettersen C, Bjaalie JG. (2004). Three-dimensional topography of corticopontine projections from rat sensorimotor cortex: comparisons with corticostriatal projections reveal diverse integrative organization. *Journal of Comparative Neurology, 478(3):* 306-22.

Lee S, Hjerling-Leffler J, Zagha E, Fishell G, Rudy B. (2010). The largest group of superficial neocortical GABAergic interneurons expresses ionotropic serotonin receptors. *Journal of Neuroscience, 30(50):* 16796-808.

Lee SH, Land PW, Simons DJ. (2007). Layer- and cell-type-specific effects of neonatal whisker-trimming in adult rat barrel cortex. *Journal of Neurophysiology,* 97(6):4380-5.

Lendvai B, Stern EA, Chen B, Svoboda K. (2000). Experience-dependent plasticity of dendritic spines in the developing rat barrel cortex in vivo. Nature, 404(6780):876-81.

Lewis DA, Lund JS. (1990). Heterogeneity of chandelier neurons in monkey neocortex: Corticotropin-releasing factor-and parvalbumin-immunoreactive populations. *Journal of Comparative Neurology, 293(4):* 599-615.

Lorente de Nó R. (1949). Cerebral cortex: architecture, intracortical connections, motor projections. Physiology of the nervous system. New York: Oxford University Press. 288-330.

López-Aranda MF, López-Téllez JF, Navarro-Lobato I, Masmudi-Martín M, Gutiérrez A, Khan ZU. (2009). Role of layer VI of V2 visual cortex in object-recognition memory. *Science, 325(5936):*87-89.

Lu S. M., Lin R.C.S. (1992) Thalamic afferents of the rat barrel cortex: A light- and electron-microscopic study using phaseolous vulgaris leucoagglutinin as an anterograde tracer. *Somatosens. Mot. Res.* 10:1–16.

Lund JS, Holbach SM, Chung WW. (1991). Postnatal development of thalamic recipient neurons in the monkey striate cortex: II. Influence of afferent driving on spine acquisition and dendritic growth of layer IVC spiny stellate neurons. *Journal of Comparative Neurology, 309(1):* 129-40.

Majewska AK, Newton JR, Sur M. (2006). Remodeling of synaptic structure in sensory cortical areas in vivo. *Journal of Neuroscience, 26(11):* 3021-9.

Mallamaci A, Muzio L, Chan CH, Parnavelas J, Boncinelli E. (2000). Area identity shifts in the early cerebral cortex of Emx2-/- mutant mice. *Nature Neuroscience, 3(7):* 679-86.

Malenka RC, Nicoll RA. (1993). NMDA-receptor-dependent synaptic plasticity: multiple forms and mechanisms. *Trends Neuroscience 16,* (12):521-7.

Mao T, Kusefoglu D, Hooks BM, Huber D, Petreanu L, Svoboda K. (2011). Long-range neuronal circuits underlying the interaction between sensory and motor cortex. *Neuron, 72(1):* 111-23.

Maravall M, Koh IY, Lindquist WB, Svoboda K. (2004). Experience-dependent changes in basal dendritic branching of layer 2/3 pyramidal neurons during a critical period for developmental plasticity in rat barrel cortex. *Cerebral Cortex, 14(6):* 655-664.

Martin JH. (2003). Neuroanatomy: Text and Atlas, 3rd edition. New York: McGraw-Hill.

Mataga N, Nagai N, Hensch TK. (2002). Permissive proteolytic activity for visual cortical plasticity. *PNAS, 99(11):* 7717-21.

Mataga N, Mizuguchi Y, Hensch TK. (2004). Experience-dependent pruning of dendritic spines in visual cortex by tissue plasminogen activator. *Neuron, 44(6):* 1031-41.

Maya Vetencourt JF, Sale A, Viegi A, Baroncelli L, De Pasquale R, O'Leary OF, Castrén E, Maffei L. (2008). The antidepressant fluoxetine restores plasticity in the adult visual cortex. *Science, 320*(5874):385-8.

McAllister AK, Katz LC, Lo DC. (1996). Neurotrophin regulation of cortical dendritic growth requires activity. *Neuron, 17(6):* 1057-64.

McRae PA, Rocco MM, Kelly G, Brumberg JC, Matthews RT (2007) Sensory deprivation alters aggrecan and perineuronal net expression in the mouse barrel cortex. *J Neuroscience 27(20):* 5405-5413.

Mendizabal-Zubiaga JL, Reblet C, Bueno-Lopez JL. (2007). The Underside of the cerebral cortex: layer V/VI spiny inverted neurons. *Journal of Anatomy 211(2):* 223-36.

Merzenich, M.M., Nelson, R.J., Stryker, M.P., Cynader, M.S., Schoppmann, A., & Zook, J.M. (1984). Somatosensory cortical map changes following digit amputation in adult monkeys. *Journal of Comparative Neurology, 224(4),* 591-695.

Merzenich, MM, Knight PL, and Roth GL. (1975). Representation of cochlea within primary auditory cortex in the cat, *J Neurophysiol, 38:* 231-249.

Middlebrooks JC, Dykes RW, Merzenich MM. (1980). Binaural response-specific bands in primary auditory cortex (A1) of the cat: topographical organization orthogonal to isofrequency contours. *Brain Research, 181:* 31-48.

Miller M, Peters A. (1981). Maturation of rat visual cortex. II. A combined Golgi-electron microscope study of pyramidal neurons. *Journal of Comparative Neurology, 203(4):* 555-73.

Molyneaux BJ, Arlotta P, Menezes JR, Macklis JD. (2007). Neuronal subtype specification in the cerebral cortex. *Nature Review Neuroscience 8(6):* 427-37.

Mountcastle VB. (1957). Modality and topographic properties of single neurons of cat's somatic sensory cortex. *Journal of Neurophysiology, 20(4):* 408-34.

Ngo-Anh TJ, Bloodgood BL, Lin M, Sabatini BL, Maylie J, Adelman JP. (2005). SK channels and NMDA receptors form a Ca2+-mediated feedback loop in dendritic spines. *Nature Neuroscience, 8*(5):642-9.

Niblock MM, Brunso-Bechtold JK, Riddle DR. (2000). Insulin-like growth factor I stimulates dendritic growth in primary somatosensory cortex. *Journal of Neuroscience, 20(11):* 4165-76.

Oray S, Majewska A, Sur M. (2004). Dendritic spine dynamics are regulated by monocular deprivation and extracellular matrix degradation. *Neuron, 44(6):* 1021-30.

Pan F, Gan WB. (2009). Two-photon imaging of dendritic spine development in the mouse cortex. *Developmental Neurobiology, 68(6):* 771-8.

Peters A, Jones EG., eds. (1984). *Cellular components of the cerebral cortex.* Vol. 1. Plenum, New York.

Petersen, CCH. (2007). The functional organization of the barrel cortex. *Neuron 56:* 339-54

Pizzorusso T, Medini P, Berardi N, Chierzi S, Fawcett JW, Maffei L. (2002). Reactivation of ocular dominance plasticity in the adult visual cortex. Science, 298(5596):1248-51.

Prescott TJ, Mitchinson B, Grant RA. (2011). Vibrissal behavior and function. Scholarpedia, 6(10):6642.

Prieto JJ, & Winer JA. (1999). Layer VI in cat primary auditory cortex: Golgi study and sublaminar origins of projection neurons. *Journal of Comparative Neurology 404:* 332-358.

Polleux F, Morrow T, Ghosh A. (2000). Semaphorin 3A is a chemoattractant for cortical apical dendrites. *Nature, 404(6778):* 567-73.

Popescu MV, Ebner FF. (2010). Neonatal sensory deprivation and the development of cortical function: Unilateral and bilateral sensory deprivation result in different functional outcomes. *Journal of Neurophysiology, 104(1)* 98-107.

Radley JJ, Rocher AB, Rodrigeuz A, Ehlenberger DB, Dammann M, McEwen BS, Morrison JH, Wearne SL, & Hof PR. (2008). Repeated stress alters dendritic spine morphology in the rat medial prefrontal cortex. *Journal of Comparative Neurology, 507:* 1141-50.

Rakic P. (2009). Evolution of the neocortex: a perspective from developmental biology. *Nature Reviews Neuroscience, 10(10):* 724-735.

Ramón-Moliner E. (1970). The Golgi-Cox technique. In Nauta WJH and Ebbesson SOE (eds.), Contemporary Methods in Neuroanatomy. New York: Springer.

Ramos RL, Tam DM, & Brumberg JC. (2008). Physiology and morphology of callosal projection neurons in mouse. *Neuroscience 153(3):* 654-63.

Rice DS, Curran T. (2001). Role of the reelin signaling pathway in central nervous system development. *Annual Review of Neuroscience, 24:*1005-39.

Richardson RJ, Blundon JA, Bayazitov IT, Zakharenko SS. (2009). Connectivity patterns revealed by mapping of active inputs on dendrites of thalamorecipient neurons in the auditory cortex. *Journal of Neuroscience, 29*(20):6406-17.

Rocco MM, & Brumberg JC. (2007). The sensorimotor slice. *Journal of Neuroscience Methods, 162(1-2):* 139-47.

Rocha M, Sur M. (1995). Rapid acquisition of dendritic spines by visual thalamic neurons after blockade of N-methyl-D-aspartate receptors. *PNAS, 92(17):* 8026-30.

Sala C, Cambianica I, Rossi F. (2008). Molecular mechanisms of dendritic spine development and maintenance. *Acta Neurobiol Exp. 68(2):* 289-304.

She WC, Quairaux C, Albright MJ, Wang YC, Sanchez ED, Chang PS, Welker E, & Lu HC. (2009). Roles of mGluR5 in synaptic function and plasticity of the mouse thalamocortical pathway. *European Journal of Neuroscience, 29(7):* 1379-1396.

Sherman SM and Guillery RW. (2002). The role of the thalamus in the flow of information to the cortex. *Philosophical Transactions of the Royal Society of London, Series B: Biological Sciences 357(1428):* 1695-1708.

Shoykhet M, Land PW, Simons DJ. (2005). Whisker trimming begun at birth or on postnatal day 12 affects excitatory and inhibitory receptive fields of layer IV barrel neurons. *Journal of Neurophysiology, 94*(6):3987-95.

Sholl DA. (1956). The organization of the cerebral cortex. New York:John Wiley Press

Simons DJ, Land PW. (1987). Early experience of tactile stimulation influences organization of somatic sensory cortex. *Nature, 326(6114):* 694-697.

Somogyi, P, Kisvarday ZF, Martin KAC, Whitteridge D. (1983). Synaptic connections of morphologically identified and physiologically characterized large basket cells in the striate cortex of cat. *Neuroscience, 10(2):* 261-294.

Solecki DJ, Liu XL, Tomoda T, Fang Y, Hatten ME. (2001). Activated Notch2 signaling inhibits differentiation of cerebellar granule neuron precursors by maintaining proliferation. *Neuron, 31(4):*557-68.

Sur M, Rubenstein JLR. (2005). Patterning and Plasticity of the Cerebral Cortex. *Science, 310(5749):* 805-810.

Tailby C, Wright LL, Metha AB, Calford MB. (2005). Activity-dependent maintenance and growth of dendrites in adult cortex. *PNAS, 102(12):* 4631-4636.

Takasaki C, Okada R, Mitani A, Fukaya M, Yamasaki M, Fujihara Y, Shirakawa T,

Tanaka K, Watanabe M. (2008). Glutamate transporters regulate lesion-induced plasticity in the developing somatosensory cortex. *Journal of Neuroscience, 28(19):* 4995-5006.

Takahashi H, Sekino Y, Tanaka S, Mizui T, Kishi S, Shrao T. (2003). Drebrin-dependent actin clustering in dendritic filopodia governs synaptic targeting of postsynaptic density-95 and dendritic spine morphogeneis. *Journal of Neuroscience, 23:* 6586-6595.

Tamas G, Buhl EH, Lorincz A, Somogyi P. (2000). Proximally targeted GABAergic synapses and gap junctions synchronize cortical interneurons. *Nature Neuroscience 3:* 366-71.

Tang Y, Jassen WGM, Hao JD, Roberts JA, McKay H, Lasley B, Allen PB, Greengard P,

Rapp PR, Kordower JH, Hof PR, and Morrison JH. (2004). Estrogen replacement increases spinophilin-immunoreactive spine number in the prefrontal cortex of female rhesus monkeys. *Cerebral Cortex, 14:*215-223.

Thomson AM. (2010). Neocortical layer VI, a review. *Frontiers and Neuroanatomy, 4:* 1-14.

Tombol T. (1984) Layer VI cells. Cellular components of the cerebral cortex. New York: Plenum Press.

Trachtenberg JT, Chen BE, Knott GW, Feng G, Sanes JR, Welker E, Svoboda K. (2002). Long-term in vivo imaging of experience-dependent synaptic plasticity in adult cortex. *Nature, 420(6917):* 788-94.

Tsiola A, Hamzei-Sichani F, Peterlin Z, Yuste R. (2003). Quantitative morphologic classification of layer 5 neurons from mouse primary visual cortex. *Journal of Comparative Neurology, 461(4):* 415-28

Tunturi AR. (1950). Physiological determination of the arrangement of the afferent connections to the middle ectosylvian auditory area in the dog. *American Journal of Physiology, 162:* 489-502.

Van der Loos H, Woolsey TA. (1973). Somatosensory cortex: structural alterations following early injury to sense organs. *Science, 179(71):* 395-8.

Van Brederode JF, Snyder GL. (1992). A comparison of the electrophysiological properties of morphologically identified cells in layer 5B and 6 of the rat neocortex. *Neuroscience 50(2):* 315-37.

Valverde F. Golgi atlas of the postnatal mouse. Austria: Springer-Verlay/Wein, (1998).

Ward, JH Jr. (1963). Hierarchical grouping to optimize an objective function. *Journal of American Statistical Association 58:* 236-244.

Washbourne P, Dityatev A, Scheiffele P, Biederer T, Weiner JA, Christopherson KS, El-Husseini A. (2004). Cell adhesion molecules in synapse formation. *Journal of Neuroscience, 24*(42):9244-9.

Weller WL, Johnson JI. (1975). Barrels in cerebral cortex altered by receptor disruption in newborn, but not in five-day-old mice (Cricetidoe and Muridae). Brain Research, 83(3):504-8.

White EL. (1989). Cortical Circuits, Synaptic organization of the Cerebral Cortex, Structure, Function, and Theory. Boston, MA: Birkhauser,

Wijetunge LS, Till SM, Gillingwater TH, Ingham CA, Kind PC. (2008). mGluR5 regulates glutamate-dependent development of the mouse somatosensory cortex. *Journal of Neuroscience, 28(49):*13028-37.

Wimmer VC, Broser PJ, Kuner T, Bruno RM. (2010). Experience-induced plasticity of thalamocortical axons in both juveniles and adults. Journal of Comparative Neurology, *15;518(22):* 4629-48.

Woolley CS, Gould E, Frankfurt M, McEwen BS. (1990). Naturally occurring fluctuation in dendritic spine density on adult hippocampal pyramidal neurons. *Journal of Neuroscience, 10(12):* 4035-9.

Woolsey, T.A., & Van der Loos, H. (1973). Somatosensory cortex: structural alterations following early injury to sense organs. *Science, 179(71),* 395-8.

Woolsey TA, Van der Loos H. (1970). The structural organization of layer IV in the somatosensory region (SI) of mouse cerebral cortex. The description of a cortical field composed of discrete cytoarchitectonic units. *Brain Research, 17(2):*205-42.

Woolsey TA, Wann JR.Areal changes in mouse cortical barrels following vibrissal damage at different postnatal ages. Journal of Comparative Neurology, 170(1):53-66.

Wu CS, Ballester-Rosado, Lu HC. (2011). What can we get from 'barrels': the rodent barrel cortex as a model for studying the establish of neural circuits. *European Journal of Neuroscience,* 34, 1663-76.

Xu X, Callaway EM. (2009). Laminar specificity of functional input to distinct types of inhibitory cortical neurons. *Journal of Neuroscience, 29(1):* 70-85.

Yang CR, Seanmens JK, and Gorelova N. (1996). Electrophysiological and morphological properties of layer V-VI principal pyramidal cells in rat prefrontal cortex in vivo. *Journal of Neuroscience (16):* 1904-21.

Yang G, Pan F, Gan WB. (2009). Stably maintained dendritic spines are associated with lifelong memories. *Nature,* 462(7275):920-4.

Yuste R, Bonfoeffer T. (2004). Genesis of dendritic spine: Insights from ultrastructural and imaging studies. *Nature Neuroscience Reviews, 5(1):* 24-34.

Zheng S, Yin ZQ, Zeng YX. (2008). Developmental profile of tissue plasminogen activator in postnatal Long Evans rat visual cortex. *Molecular Vision, 14:* 975-82.

Zhong W, Feder JN, Jiang MM, Jan LY, Jan YN. (1996). Asymmetric localization of a mammalian numb homolog during mouse cortical neurogenesis. *Neuron, 17(1):*43-53.

Zhu Y, Li H, Zhou L, Wu JY, Rao Y. (1999). Cellular and molecular guidance of GABAergic neuronal migration from an extracortical origin to the neocortex. *Neuron, 23(3):* 473-85.

Zuo Yi, Lin A, Chang P, Gan WB. (2005). Development of long-term dendritic spine stability in diverse regions of cerebral cortex. *Neuron, 46:* 181-189.

Zuo Y, Yang G, Kwon E, Gan WB. (2005). Long-term sensory deprivation prevents dendritic spine loss in primary somatosensory cortex. *Nature, 436(7048):* 261-5.